LBL-32304
UC-000

Lawrence Berkeley Laboratory
UNIVERSITY OF CALIFORNIA

Trapping the M_1 and M_2 Substates of Bacteriorhodopsin for Electron Diffraction Studies

G.A. Perkins
(Ph.D. Thesis)

May 1992

Donner Laboratory

Biology & Medicine Division

Prepared for the U.S. Department of Energy under Contract Number DE-AC03-76SF00098

DISCLAIMER

LBL-32304
UC-000

Trapping the M_1 and M_2 Substates of Bacteriorhodopsin for Electron Diffraction Studies

Guy A. Perkins
Ph.D. Thesis

Department of Biophysics
University of California

and

Life Sciences Division
Lawrence Berkeley Laboratory
University of California
Berkeley, California 94720

May 1992

This work was supported by the National Institutes of Health under Project No. JM36884, and by the Office of Health and Environmental Research of the U.S. Department of Energy under Contract No. DE-AC03-76SF00098.

Trapping the M_1 and M_2 Substates of Bacteriorhodopsin for Electron Diffraction Studies

by

Guy A. Perkins

Abstract

Visible and Fourier transform infrared (FTIR) absorption spectroscopies are used to observe protein conformational changes occuring during the bacteriorhodopsin photocycle. Spectroscopic measurements which define the conditions under which bacteriorhodopsin can be isolated and trapped in two distinct substates of the M intermediate of the photocycle, M_1 and M_2, are described. A protocol that can be used for high-resolution electron diffraction studies is presented that will trap glucose-embedded purple membrane in the M_1 and M_2 substates at greater than 90 % concentration. It was discovered that glucose alone does not provide a fully hydrated environment for bacteriorhodopsin. Equilibration of glucose-embedded samples at high humidity can result in a physical state that is demonstrably closer to the native, fully hydrated state. An extension of the C-T Model of bacteriorhodopsin functionality (Fodor et al., 1988; Mathies et al., 1991) is proposed based on FTIR results and guided by published spectra from resonance Raman and FTIR work.

TABLE OF CONTENTS

Acknowledgements

This dissertation is dedicated to my wife, Dale, for her support, understanding and patience.

I express my heartfelt gratitude to my advisor, Dr. Robert Glaeser, who has supported me in my research endeavors despite my shortcomings. His invaluable advice has made it possible to complete this work. The initial suggestion that led to this work grew out of discussions with Dr. Richard Mathies. Helpful ideas about the significance of the data have been gained from discussions by either myself or Dr. Glaeser with Dr. Janos Lanyi and Dr. Kenneth Rothschild. I also wish to thank Drs. Robert Glaeser, Richard Mathies and David Cole for their critical reading of this manuscript and for the suggested improvements.

Dr. Ed Berry's, Rick Burkard's and Ed Liu's expertise and help contributed to the success of my spectroscopic work. Gratitude is tendered to Ken Downing, Bing Jap, Tom Earnest, Peter Walian, Bong-Gyoon Han, Li-Shar Huang, Charles Chang, Paula Flicker and Santosh Sikerwar for their help and for the many hours of stimulating discussion. I acknowledge the generosity of Dr. Herb Strauss, Wes Burrows and the Chemistry Department for the loan of an infrared cryostat and for allowing me to use the teaching lab's spectrometer. Special thanks go to Perkin Elmer for the gift of the upgrade board for the 1600 spectrometer and to Edmundo Angeles for assistance with the interface.

Finally, I would like to thank my mother, father, brother and sister for their encouragement, teachings and example. I give thanks to God for creating this world and for inspiring men and women of science in their endeavors to probe its wonders.

Chapter 1

INTRODUCTION[1]

A Brief Review of What is Known About the Structure and Function of Bacteriorhodopsin

This dissertation describes spectroscopic measurements which define the conditions under which the bacteriorhodopsin (bR) molecule can be trapped in two distinct substates of the M-state intermediate of the photocycle. A short review of bR structure and function will first be presented to help understand why further structural studies on these structurally distinct substates represent an important step in understanding the molecular mechanism by which bR uses light energy to pump charged species across the cell membrane. More extensive reviews have been published elsewhere (Henderson, 1977; Ovchinnikov et al., 1979; Birge, 1990; Mathies et al., 1987; Rothschild, 1988; Stoeckenius et al., 1979; Stoeckenius & Bogomolni, 1982; Mathies et al., 1991).

Bacteriorhodopsin (bR) is the only protein found in the purple membrane (PM) of the archaebacterium, *Halobacterium halobium,* which thrives in bodies of water with a high salt concentration. The bacterium grows PM under anaerobic conditions. By pumping charge across the membrane, bR generates an electrochemical gradient that

---

[1]ABBREVIATIONS: bR, bacteriorhodopsin; FTIR, Fourier transform infrared; IR, infrared; PM, purple membrane; UV, ultraviolet; EM, electron microscope.

drives ATP synthesis and other metabolic processes when oxygen becomes too depleted to generate ATP via oxidative phosphorylation (Birge, 1990). In vivo, PM forms 2-D crystalline patches, packed into a hexagonal (p3) lattice, of ~ 0.5 micrometer diameter (largest observed) that are composed of proteins and lipids in a 3:1 ratio (Oesterhelt & Stoeckenius, 1971). BR has also been crystallized in an orthorhombic ($p2_12_1$) lattice. BR is a single polypeptide, MW ~ 26,534, consisting of 248 amino acids surrounding a retinal chromophore (Khorana et al., 1979). The primary structure of bR was first determined by sequencing the protein (Khorana et al., 1979; Ovchinnikov et al., 1979) and later confirmed by sequencing the gene which encodes the apoprotein (Dunn et al., 1981). Utilizing hydrophobicity profiles, Engelman et al. (1980) discovered that there are seven regions of hydrophobic amino acids approximately 20 residues long that were postulated to be seven alpha helices which span the membrane. Seven transmembrane rods were first noticed by Henderson and Unwin (1975) who constructed a three-dimensional map of bR at 7 Å resolution using electron crystallographic techniques.

BR uses light as the primary source of energy to actively transport charge (protons or hydroxyl ions) against an electrochemical gradient. Nearly all bR papers surveyed state that the species bR pumps are protons. At low pH, bR can pump chloride ions (Der et al., 1989). BR's ability to pump Cl^- and its close sequence homology to halorhodopsin, a known Cl^- pump found in the same bacterium as bR, make one consider the alternative that bR

pumps OH^-. Structural studies of bR's intermediates may resolve the question of which species is transported across the membrane.

The chromophore in bR is retinal. Retinal is covalently attached to lys-216 via a protonated Schiff base (Huang et al., 1982). Neutron diffraction (Heyn et al., 1988) and linear dichroism studies (Lin & Mathies, 1989) have helped to determine the position and orientation of the chromophore. When no actinic light is incident on purple membrane, bR relaxes to the dark-adapted state. It was shown that the chromophore population of dark-adapted bR consists of a 2:1 mixture of 13-cis:all-trans retinal (Scherrer et al., 1989). BR containing the 13-cis retinal has an absorbance maximum at 555 nm, while bR containing the all-trans retinal has an absorbance maximum at 568 nm. Even though dark-adapted bR progresses through a photocycle, the light-adapted bR (all-trans retinal) is the functionally active state. The protonation and isomerization states of bR's retinal were determined by comparing the vibrational spectra of bR and its intermediates with spectra of known isomers of retinal and its Schiff bases (Curry et al., 1985).

The primary step in the photocycle is a trans to cis isomerization around the $C_{13}=C_{14}$ double bond. The configuration of the chromophore at the various intermediates of the photocycle has been determined by Mathies and co-workers (e.g. see Smith et al., 1985; Mathies et al., 1991). Other major changes occur in the chromophore during the photocycle. These include deprotonation of the Schiff base, reprotonation of the Schiff base, and re-

isomerization to the all-trans configuration. The purple color of the membrane is due to the "opsin shift" (Nakanishi et al., 1980) caused by the interactions between various protein and retinal moieties. Most of the contribution to the opsin shift has been attributed to the interaction of the 6-s-trans retinal (as opposed to the 6-s-cis retinal in solution) with the residues of the retinal binding pocket in bR and the weak Schiff base hydrogen bond with protein "counterions" (Harbison et al., 1985; Lugtenberg et al., 1986). The protonated Schiff base linkage to lys-216 also contributes to the opsin shift. Recently, it was shown that Asp-85 is one of the key residues which regulate the color of bR (Subramaniam et al., 1990).

A model of bR structure has been constructed from a 3-D electron density map that exhibits 3.5 Å resolution parallel to the membrane plane and 10 Å resolution perpendicular to the membrane plane (Henderson et al., 1990). Because of lower resolution in the perpendicular direction (caused by fewer good images at high tilt), side-chain position and orientation were not determined for non-aromatic residues. This model confirms the initial conclusion that BR has seven transmembrane alpha-helices that extend across the membrane roughly perpendicular to its plane (Henderson, 1977). Perhaps the most interesting feature of this model is the determination of residues forming the pocket for the retinal. The residues are identified as Asp-85, 96, 115 and 212, Trp-86, 182 and 189, Arg-82, Tyr-185 and Pro-186. Asp-85, Asp-96 and Asp-212 are crucial for ion pumping (Mogi et al., 1988). Site-directed mutagenesis studies further show that substitutions of the other

pocket residues affect pumping efficiency and/or the chromophore (Khorana, 1988). Although the proximity of residues to the Schiff base is known, the postulated hydrogen-bonding and salt-bridge interactions have not yet been determined.

It is thought that the bR photocycle consists of five (perhaps six) intermediates (Xie et al., 1987; Ames & Mathies, 1990; Varo & Lanyi, 1990). The photointermediates can be identified by their visible absorption maximum. The nomenclature for established intermediates assigns a single letter to each intermediate. The first intermediate formed after bR absorbs a photon to initiate the photocycle is called K. [An earlier short-lived intermediate, J, is sometimes included in the photocycle (Sharkov et al., 1985; Mathies et al., 1988; Pollard et al., 1990). Femtosecond resonance Raman spectroscopy was used to identify J (Mathies et al., 1988). J and the femtosecond dynamics occuring in bR are discussed at length by Mathies et al. (1991).] Following intermediates are designated, L, M, N, and O. Time-resolved resonance Raman spectroscopy gives the simplest photocycle scheme that accurately fits the kinetic data (Ames & Mathies, 1990). Vibrational spectroscopy has the advantage over optical spectroscopy in that the bR intermediates have more distinctive peaks. The overlap of peaks in visible absorption spectra means that the kinetic analysis is not global. When referring to spectroscopic methodology, a "global" analysis means that the absorbance peaks present in a spectrum can be observed separately from each other. Visible absorption spectroscopy of bR and its intermediates requires spectral decomposition in order to separate

the peak absorbances (Varo & Lanyi, 1991). For a clean decomposition, reasonable assumptions were made concerning non-negative absorption, smooth spectra and peak shapes similar to rhodopsin-type pigments . Even though resonance Raman spectroscopy is global, while visible spectroscopy is not, both support almost identical photocycle schemes. A sequential model that allows back-reactions is as follows (Mathies et al., 1991),

$$bR_{568} \xrightarrow{h\nu} K \rightleftharpoons L \rightleftharpoons M^{t} \rightarrow M^{c} \rightleftharpoons N^{-} \rightleftharpoons N \rightleftharpoons O \rightarrow bR_{568}.$$

M^{t} and M^{c} are also named M_1 and M_2, respectively (Kalisky et al., 1981; Varo & Lanyi, 1990).

Spectroscopic studies have provided information on important intermediates in the bR photocycle. Fully hydrated M has a lifetime of ~ 5 - 10 ms at 16.5 °C (Braiman et al., 1991). The Schiff base is deprotonated (Lewis et al., 1974). Infrared spectroscopy has provided information concerning the protonation states of carboxyl and tyrosine sidechains at distinct points in the photocycle (Engelhard et al., 1985; Rothschild et al., 1986; Dollinger et al., 1986; Roepe et al., 1987). FTIR spectroscopy demonstrates that both Asp-85 and Asp-96 are protonated in the M intermediate (Gerwert et al., 1990). The L - M transition sees the transfer of a proton from the Schiff base to Asp-85. Before N is formed, the proton on Asp-96 is transferred to the Schiff base. This model, derived from FTIR studies, is supported by point mutation studies. When Asn replaces Asp-96, M decay and the associated proton movement is slowed by

two orders of magnitude (Holz et al., 1989). There may be other aspartic acids and/or tyrosines that change their protonation states as bR progresses through M, N and O (Braiman et al., 1988; Gerwert et al., 1989).

Evidence of protein conformational changes in the bR photocycle has been gathered from UV-Visible spectroscopy. It is reasonable that bR's visible spectrum should be sensitive to selected tertiary structural changes. For example, because of its interaction with the binding pocket, the retinal of bR has a spectrum that is red-shifted significantly from the spectra of model compounds (Nakanishi et al., 1980). The existence of photocycle intermediates having different absorption spectra and reaction rates that are temperature-dependent indicate distinct bR conformations (Lozier et al., 1975). The fact that hydroxylamine reacts with the retinal much more readily when bR is cycling through its intermediates indicates the existence of conformational states that allow access to the protein interior that are closed with quiescent bR (Becher et al., 1978). M, trapped at -96 °C, returns to light-adapted bR upon absorbing photons. Yet, this pathway is blocked at liquid nitrogen temperature. This is most easily explained if a conformational change cannot occur at the lower energies available at liquid nitrogen temperature (Hurley et al., 1978).

Little is yet known about the magnitude of protein conformational changes which must occur during the bR photocycle. The importance of conformational changes with respect to the

mechanism of active transport is best understood within the framework of the "C-T Model" of bR functionality (Fodor et al., 1988). The logic of this model becomes clear when one realizes that the retinal doesn't change configuration between L, M and N, thus eliminating models which rely on retinal isomerization alone to explain transport. The C-T Model is a proposed two-state protein conformational switch that allows the connectivity of the release and uptake channels to be altered. The absorption of a photon and the subsequent isomerization of the retinal chromophore from all-trans to 13-cis starts a series of pKa shifts, free energy loss and gain from steric repulsion and electrostatic interactions, proton transfer and protein conformational changes that result in charge being transported across the PM against an electrochemical potential (Mathies et al., 1991). The key feature of the T - C transition is the mechanism by which the Schiff base donates a proton to Asp-85 (L - M_1) and then accepts another proton from Asp-96 (M_2 - N). The shift to the C conformation is most likely to occur between M_1 and M_2 (Ormos, 1991). Movement of residues may also be needed to allow water, both on the surface and inside the protein, to organize around newly exposed hydrophobic areas of the protein. The C-T Model elegantly describes why charge transport occurs in bR. Certainly, bR runs through more conformations than the two described in the model as it converts light energy to chemical energy. I believe that only when the structure of the protein moiety of bR_{568} and the key photocycle intermediates are "known" on the atomic scale (i.e. a reasonable model of the positions of all residues with their side chains is accepted) can the mechanism of charge

transport be understood. This is an exciting motivation for future structural work on bR.

The extent of protein conformational changes in bR as it cycles through its intermediates remains a matter for debate. A discussion of the experimental evidence supporting a large conformational change upon M formation and refuting evidence is made available by Glaeser et al. (1986). Recent work provides evidence that the conformational switch from T to C could be rather large (Muller et al., 1991). It is unlikely that spectroscopy or neutron and x-ray diffraction of stacked PM patches will ever delineate just how large this conformational transition is. From these mainstays of physical chemistry, however, we receive hints that the tertiary structural change is significant. The fact that the M peak is quite blue-shifted (412 nm) from light-adapted bR (568 nm) does not in itself require that the extent of residue movement in M be very large. UV spectra (Becher et al., 1978), FTIR difference spectra (Braiman et al. 1987) and neutron diffraction on bR_{568} and M, on the other hand, can be interpreted in terms of major conformational changes. The neutron diffraction measurements made by Dencher et al. (1989), of course, do not distinguish between tilting of alpha-helices and movements of several residues within the helices. A time-resolved x-ray diffraction study of M and bR_{568} (resting state) (Koch et al., 1991; Nakasako et al., 1992) indicates greater conformational changes in M than previously believed (Glaeser et al., 1986). Recent X-ray diffraction studies show an intensity change of ~ 9 % between M and bR_{568} (Koch et al., 1991).

Statement of the Main Question

The principal question that motivates the work undertaken in this dissertation is, "What is the mechanism of ion transport in bacteriorhodopsin?" To answer this question, three-dimensional (3-D) difference Fourier maps should be created for important intermediates in the bR photocycle. These maps could show displacements of specific residues at the atomic level which must happen if bR translocates ions across the purple membrane. To aid in the interpretation of the 3-D difference Fourier maps, spectroscopic results from the published literature of bR can be used. The complementary information from electron microscopy and spectroscopy will provide the means by which the molecular strategy of active ion transport, using light energy captured by the covalently attached retinal, is understood.

Why study the structure and function of bR? Understanding how bR's structure enables it to function not only will establish paradigms of active ion transport, but it will also enable comparisons to be made with other membrane proteins proposed to have seven transmembrane helices. Secondary structure models have indicated that the following receptors may have seven transmembrane helices: visual receptors, adrenergic receptors, acetylcholine and muscarinic receptors, neural peptide receptors, and yeast pheromone receptors (Khorana, 1988).

An analysis of spectroscopic results and difference Fourier maps of bR and key photocycle intermediates is expected to answer these questions:

1. How is energy coupled between specific amino acid residues and the retinal in its (strained) configurations?

2. What is the identity of the ion that is actively transported across purple membrane? Conventional wisdom holds that the pumped species is a proton. But, the possibility that bR pumps hydroxyl ions has not been ruled out.

3. How does bR solve the "Born energy problem" (Glaeser & Jap, 1984)? That is, how is the photonic energy partitioned by the protein in order to move an ion from an aqueous solution into the low-dielectric-constant environment of the protein or lipid bilayer? The energy barrier is great, roughly 40 kcal per ion.

4. How large is the conformational change between bR in the T conformation and bR in the C conformation? A likely place to hunt for an answer to this question is in the difference Fourier maps of M_1 and M_2 with resting-state bR.

The ultimate goal of this project is to collect 3-D diffraction intensity data for the M_1 and M_2 substates at atomic resolution. The diffraction data, coupled with phase information from the molecular

model (Henderson et al., 1990) should give difference Fourier maps that can detect movements of individual amino acid residues. This is important since the extent of protein conformational changes that occur when charge is pumped across the membrane remains controversial.

The new insights gained by answering the questions posed here may have broader relevance in formulating paradigms of active ion transport and bioenergetics.

What This Thesis Work Contributes to Answering the Principal Question

The aim of this work is to establish the protocol by which both M_1 and M_2 can be studied using high-resolution electron diffraction to calculate difference Fourier maps (Glaeser et al., 1986; Ceska & Henderson, 1990). Recently, a procedure was reported that describes the means whereby bR can be trapped in either the M_1 or the M_2 state (Ormos, 1991). The conformational marker bands in the Amide I region of the IR, M - bR difference spectrum differ markedly between M_1 and M_2 (There is some N present with M_2.). Even though a protocol was followed that should give a high percentage of M, at least at 240 K, the actual percent M formed in the work of Ormos (1991) was undetermined, and could not be determined from FTIR difference spectra.

By coupling FTIR spectroscopy with visible spectroscopy, I show that M_1 and M_2 can be "trapped", both at 90 % or greater concentration. Since the absorbance peak of M (412 nm) lies in the visible spectrum far removed from the peaks of other intermediates, (all 550 nm or higher) it is straightforward to determine the concentration of M. Visible spectroscopy cannot differentiate between M_1 and M_2, of course, since both have a peak at 412 nm, but FTIR difference spectroscopy can (Ormos, 1991). For spectroscopic studies, it is not crucial to form a high percentage of M. However, difference Fourier maps require a high level of specimen conformational homogeneity because every bR molecule in the crystal that is not in the M conformation adds noise to the map.

Chapter 2

VISIBLE SPECTROSCOPY METHODOLOGY

Introduction

In this chapter, the methods used for specimen preparation are discussed. A description of the optical spectroscopy protocol is also included. A technique for trapping the M intermediate at low temperatures is presented. The instruments used required calibration, which is discussed in detail. At the end of this chapter is a novel section called, "Things That Can Go Wrong", that describes the errors made and learning experiences derived from having done the experiments described in this chapter and the following two chapters. The purpose of this section is to provide warnings for those in the lab who will follow me and may want to extend the results presented in this dissertation.

By way of background, I discuss various ways by which the M intermediate can be formed at high concentrations. The amount of bR that can be trapped in the M state can approach 100 %. There have been several distinct protocols for forming ~ 100 % M described in the literature. Most protocols rely on thin films of PM. The method used by Becher et al. (1978), however, is unique in that PM in the aqueous phase was suspended in 67 % (v/v) glycerol before the temperature was lowered to -40 °C. The high concentration of

glycerol prevents specimen cracking at low temperature. A small cell pathlength was needed to bring the optical density down to a "noise-free" range. High pH (to increase the yield of M) and low temperature (to slow M decay) were used to record the visible spectrum of M. When PM is exposed to molecules possessing guanidinium groups, specifically guanidine and arginine, M decay is slowed (Kalisky et al., 1981; Nakasako et al., 1989; and Siebert et al., 1982). Dencher et al. (1989) report that M is generated for a time long enough to "trap" it at 5 - 7 °C due to a combination of guanidine and high pH. Guanidine slows M decay by two to three orders of magnitude. If the specimen is then rapidly cooled to -180 °C, M is trapped for days. Koch et al. (1991) are able to form 100 % M with mutant bR. Greater than 90 % M can be trapped by shining intense light on a thin film of glucose-embedded PM and then rapidly plunging the specimen in liquid nitrogen (Glaeser et al., 1986). A similar percentage of M can be trapped by slowly cooling the thin film under continuous illumination.

Materials and Methods

Specimen Preparation

PM sheets were isolated and purified from *Halobacterium halobium* strain ET1001 according to the protocol of Oesterhelt & Stoeckenius (1974). All samples contained 10 mM MOPS buffer adjusted to pH 6.7 so as to be in the pH range of largest photovoltage response (Varo & Kesthelyi, 1983).

Glucose-embedded samples were prepared for optical spectroscopy in a 1:4 (w/w) ratio of glucose to PM, a ratio typical for specimens prepared on electron microscope grids. Sodium azide (.03 %) was present in the glucose and PM solutions to avoid bacterial contamination. A buffered PM and glucose solution was deposited on a mylar film that had been smoothed with filter paper on a glass coverslip. The sample was placed in an oven at 313 K, until nearly all the water had evaporated (Glaeser et al., 1986). Evaporation at this warm temperature helped to produce films with fairly uniform thickness. The applied sample volume, the concentrations of PM and glucose in the aqueous phase and the contact area over which the PM drop was spread on the mylar were chosen such that the dried film of PM embedded in glucose had an optical density close to 1 A.U. The optical density was chosen to be less than 1 A.U. to avoid the noise inherent in spectra where too little light is transmitted.

Afterwards, samples were equilibrated for at least 24 hours in an atmosphere of constant relative humidity controlled by saturated salt solutions (Korenstein & Hess, 1977b; Kalisky et al., 1981; Korenstein & Hess, 1977a; Varo & Lanyi, 1991; Varo & Keszthelyi, 1983; and Lazarev & Terpugov, 1980). Since glucose deliquesces at relative humidities above 85 %, hydration of PM and glucose samples was accomplished in the atmosphere of a saturated ammonium sulfate solution which equilibrates at 81 % relative humidity in a closed container. A reservoir of distilled water in a closed chamber

gave 100 % relative humidity. Dehydrated samples were prepared by exposing the glucose-embedded PM films to either four hours of high vacuum (microTorr range) (Korenstein & Hess, 1977b; and Lazarev & Terpugov, 1980) or drying in the oven for three or more hours. After the specimen was hydrated (dehydrated) a cover film of mylar was placed on the specimen. Samples of glucose without PM were prepared as described in the protocol above.

By using saturated salt solutions with different relative humidities, I discovered a bound on functional relative humidities for specimen hydration. The deliquescence point of glucose is known to be 85 %. But, the deliquescence point of a glucose and PM mixture is unknown. An attempt was made to hydrate glucose-embedded PM specimens at the highest humidity that did not produce a "runny" sample. A saturated ammonium sulfate solution, relative humidity of 81 %, hydrates specimens without causing the PM and glucose to run off the mylar when the support film is placed in the cryostat. The level of hydration attained by the specimen is 34 % (water mass to sample mass). Other groups hydrate their PM samples to an even higher level, e.g. 50 - 70 % water by weight (Braiman et al., 1987). Specifically, Pfefferle et al. (1991) demonstrate that they can trap close to 100 % M at 230 K, a temperature close to the range I use, with what they describe as "humidified" PM, which consists of 50 % water by weight. I endeavored to bring the hydration level of my specimens above 34 % by utilizing a saturated salt solution that furnishes a higher relative humidity. A saturated sodium carbonate solution gives a relative humidity of 87 %. Specimens hydrated at

87 % relative humidity become too "runny" to use. Clearly, 87 % is too high and there is no point to going below 81 % if the goal is to raise the specimen hydration level as high as practicable.

Cracks appearing in dried specimens proved to be a valuable morphological test for weeding candidate specimens for spectroscopical use as well as helped to determine an optimal drying time. It was observed that the specimen became cracked, especially around the edges, if it was dried too long in the oven. This is not to be confused with the cracking that occurs when glucose-embedded PM is dried on a hydrophobic surface, e.g. a CaF_2 window. Only samples that were not cracked exhibited the behavior characteristic of hydrated samples discussed in this work.

Instrument Description and Calibration

Visible spectroscopy experiments were performed with an Aminco spectrophotometer (response time of 165 ms) with a homemade cryostat that cooled the specimen to the desired temperature with a steady flow of cold nitrogen gas (See Figure 2.1). It was determined that 45 minutes was a sufficient time to stabilize the specimen temperature. Since mylar absorbs strongly below 320 nm, UV experiments were not performed.

The bR was light-adapted at room temperature for 30 seconds with focused light from a 100 W Mercury Arc lamp passing through a heat filter and a 530 nm high-pass filter. Initially, I used a 250 W

Figure 2.1 Photographs of the instruments used for the visible absorption experiments taken from different angles. The top photograph shows the positions of instruments relative to each other, looking towards the Mercury Arc lamp. The first Fresnel lens was positioned close to the Mercury Arc lamp. The ensemble of second Fresnel lens and yellow, high-pass filter was positioned close to the cryostat entrance window, as shown in the bottom photograph. A Zenith PC interfaces the Aminco spectrophotometer and is shown (with a color monitor) in the upper-right-hand corner of the top photograph. The liquid nitrogen Dewar is just outside of the picture to the bottom; a black hose leads from the Dewar to the cryostat, as pictured. A strip chart recorder, used to record the absorbance as a function of time, is shown just to the left of the spectrophotometer. The photomultiplier tube is pictured hanging next to the strip chart recorder. This is its position when actinic light from the Mercury Arc lamp enters the cryostat window. For scanning, the photomultiplier tube is attached immediately to the left of the cryostat.

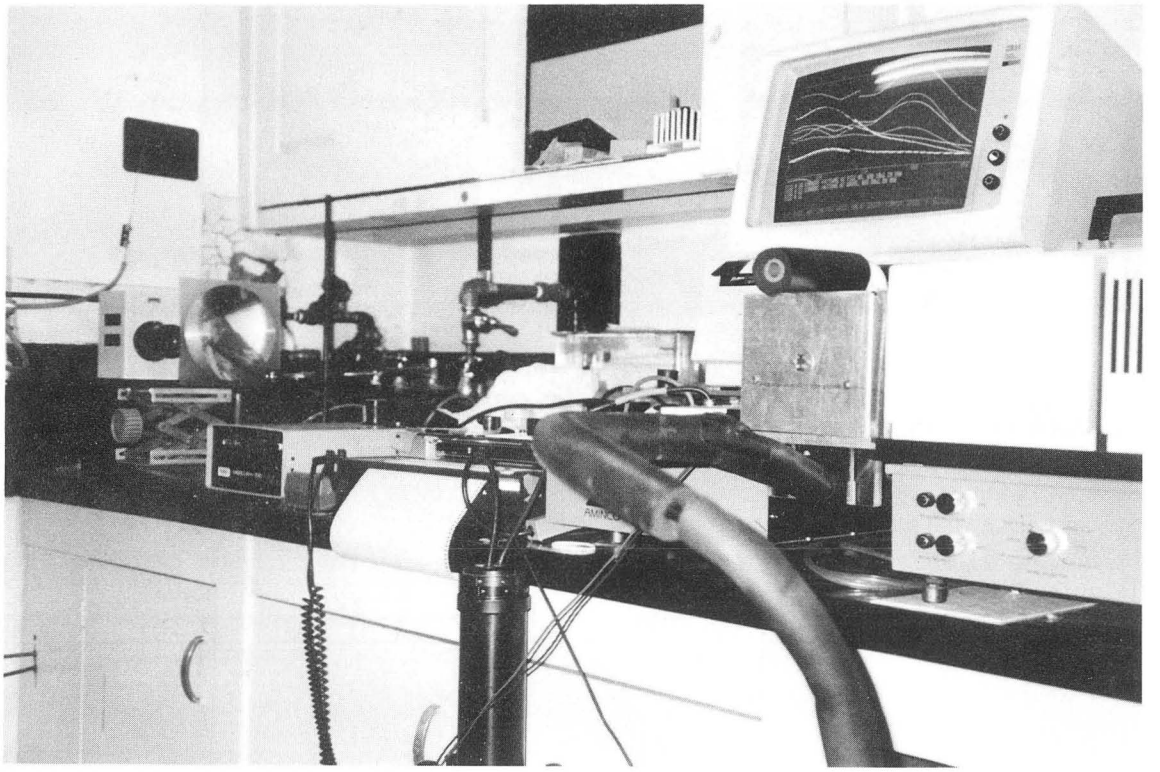

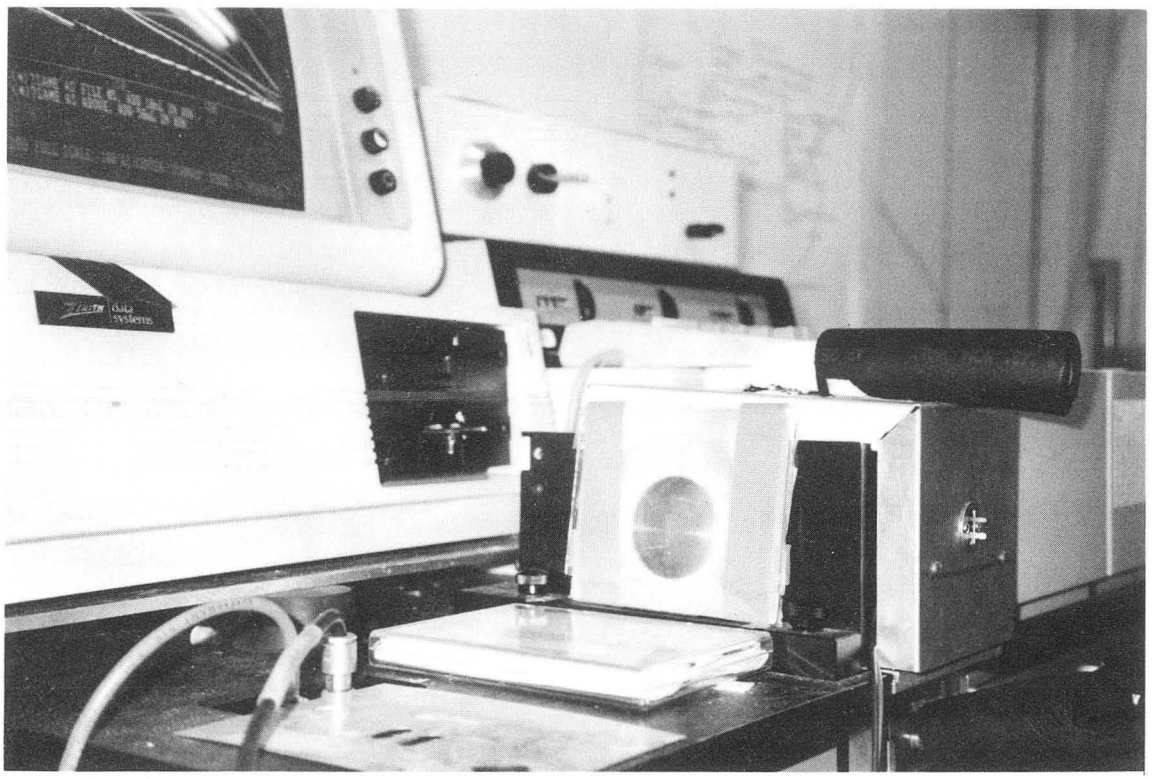
data
systems

projector lamp. However, the mercury lamp could be focused to a smaller, hence more intense, illumination spot. The relative light intensity for the two actinic sources I used was measured with a photodiode connected to a voltmeter. The diode was placed in two positions: at the light source and at the specimen plane. It was verified that the light intensity was not high enough to saturate the photodiode by increasing the illumination spot size at the specimen plane and recording the change in voltage. In this way, it was shown that the photodiode response was still linear. The relative intensities, given in millivolts are,

	Source	Specimen
250 W Projector lamp	640	600
100 W Mercury arc lamp	572	668

The Projector lamp is stronger at the source, but the Mercury lamp could be focused to a much smaller area (~ 4 times less than the projector). Clearly, the Mercury lamp, used for later experiments has more intense light on the specimen. Also, whereas the projector lamp emits white light, the mercury lamp emits strong bands of intensity in the visible region passed by the filter. (See Figure 2.1.)

Illumination of samples "in place" in the cryostat was carried out by removing the photomultiplier tube of the Aminco, and by bringing in the light through the "measurement window" of the cryostat. The illumination beam was further focused by means of

Figure 2.2 The relative spectral output of a 100 W Mercury arc lamp. Taken from D. Taylor & D. Salmon, *Basic Fluorescence Microscopy* in Methods in Cell Biology, Vol. 29 (1989) Ed. by Y. Wang & D. Taylor, pp. 207-237.

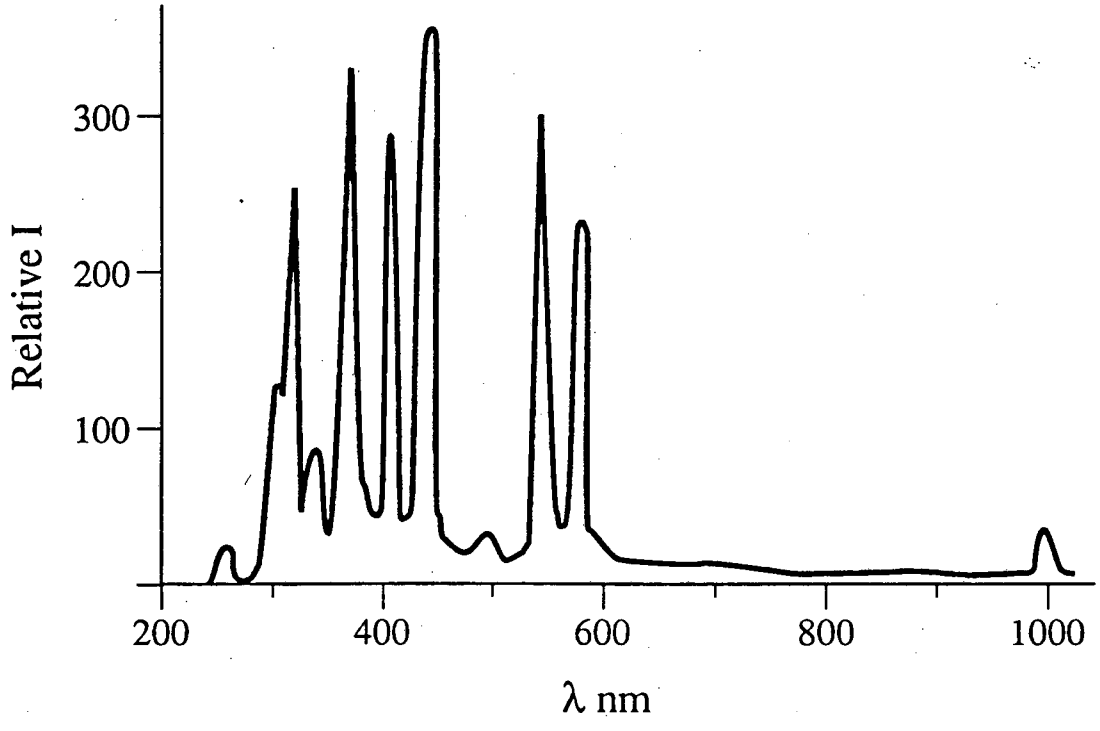

XBL 921-4643

two Fresnel lenses. A neutral density filter was used to reduce the light intensity in order to align the beam onto the specimen without eye damage. Blue light is filtered out as it induces the M to bR reaction (Kalisky et al., 1981). Care is taken to avoid exposure of the sample to intense light as it leads to water release and concomitant artificial structural alterations in bR (Dencher et al., 1989). Reference spectra were taken of light-adapted samples that had been cooled in the dark. Excitation of the bR photocycle was then initiated with the same actinic optics as used for light adaptation. It was necessary to rehydrate the specimen after each session of measurements. A photodiode connected to a voltmeter was used to assure that the actinic light intensity was reproducible in all experiments. The exciting light was terminated before scanning. The kinetics of M decay at lowered temperatures were fit with 2 or 3 exponentials (Korenstein & Hess, 1977b) using the program EXPFIT (Berry, unpublished work).

Does the most intense light source produce the most conversion to M? A problem often encountered with FTIR studies of M is finding an actinic light source strong enough to convert a high percent of light-adapted bR to M (Earnest et al., 1986). Conversely, if the light intensity is too high and/or the length of exposure is too long, then the risk of bleaching and dehydration is increased (Glaeser, personal communication). Furthermore, at low temperature, the L to M transition may have slowed relative to 20 °C. As a result, L may absorb a photon and back-react to bR_{568}. If this is the case, lower light intensity for a longer period of time might give more

conversion to M than does high intensity. The possibilities being as they are, the adequacy of a light source is tested by trial and error. With the optics I use, greater than 90 % M can be formed at low temperature; the light source was adequate.

Initially, a 550 nm high-pass filter was used to prevent any photoexcitation of the 412 nm intermediate. However, one of the larger intensity bands of the mercury arc lamp is centered at ~ 550 nm. (See Figure 2.1.) hence a different high-pass filter was needed. An old filter was found to have a useful 520 nm cut-off and was subsequently used to obtain the best visible and FTIR spectra.

The Aminco spectrophotometer calibration was checked by using its deuterium UV lamp. Deuterium's alpha and beta lines have been measured to 7 significant figures (Urey et al., 1932). (The Aminco records 5 significant figures.) and are,

Alpha	656.1000	nm
Beta	486.0000	nm.

Empirically, I found that for the Aminco I use, the alpha and beta lines measured,

Alpha	655.35	nm
Beta	485.25	nm.

Both alpha and beta lines measure 0.75 nm low. Thus, it is seen that the Aminco measures 0.75 nm low. The assumption can be made that all recorded, visible wavelengths will be off by this amount. Since the discrepancy was less than 1.0 nm, no changes to the calibration were deemed necessary.

Temperature calibration was required between the specimen and the cooling mechanism. An analog Variac controls the heating element fitted to the liquid nitrogen Dewar. Thermocouple wires were connected on one end to a digicator that reads degrees Celsius and the other end was soldered to the brass specimen holder. The digicator was calibrated at three known temperatures:

An ice bath set the digicator at 0 °C;

A stirred solid-liquid mixture of dry ice and acetone at its melting point, -78 °C (CRC Handbook of Chemistry & Physics, p. D-177);

Water at 21 °C, monitored by a thermometer.

Since the digicator is precise to 0.5 °C, all temperature measurements had the same precision. Variac settings and equilibrium specimen temperatures are as follows.

Variac	Specimen Temperature (°C)
34.25	-14

The higher temperature is stable for ~half-an-hour, while the lower temperature is stable for one hour. As the liquid nitrogen Dewar emptied, the Variac settings needed to be raised in order to keep the temperature constant. The reason is that over time, less and less of the heating element was immersed in the liquid, making the heating less efficient. As the nitrogen gas was boiled off, it was further heated by the exposed portion of the element.

Estimating M Concentration

Two methods were used to estimate the percentage of M formed at low temperature, based upon the reversible depletion (bleaching) of species that absorb in the 500 nm to 650 nm range. At 20 °C the light-adapted absorption maximum is at 568 nm. At -40 °C, the maximum shifts to 573 nm (Becher et al., 1978). For the temperature range used in my studies, 240 K to 260 K, the peak absorbance is found at 572 nm. The first method involves recording spectra from 570 nm to 750 nm. Two scans are needed to find the extent to which M is formed. The first scan is taken in the dark. This spectrum provides values for the peak absorbance of bR_{568} at the desired temperature (after having cooled the specimen in the dark) and the baseline absorbance (where bR does not absorb). Since the baseline is specimen-dependent, I established the baseline for any given specimen by interpolation of the absorbance measurements made at high wavelength. A reference 100 % bR absorbance, A_{ref}, is

then calculated by subtracting the baseline from the peak. The second scan starts after the actinic light has been terminated and runs through 750 nm. The disappearance of the 572 nm peak is a measure of the amount of M formed. Figure 2.2 shows how the percent M formed is determined. The amount of non-M present, ΔA, is determined by subtracting the baseline absorbance in the second scan from the lowered 572 nm absorbance in the same scan. At times, the baseline in the second scan is offset from the baseline in the first scan. Among other factors that may cause an offset in the baseline, the change in absorbance peaks from 572 nm to 412 nm, upon M formation, is accompanied by a change in the refractive index at long wavelength, which may cause a change in reflectance. Hence, the baseline is offset. The % M is then determined by,

$$\% \text{ M} = (1-\Delta A/A_{ref}) \times 100.$$

The calculation applied to the spectra shown in Figure 2.2 gives a value of 90 % M. This estimate is conservative. It underestimates the percent M formed for two reasons. First, it takes ~ 8 seconds to replace the photomultiplier tube and start the scan after ceasing to shine light on the specimen, during which time M is decaying. Second, at 570 nm there is a small tail to the 412 nm peak. (See Glaeser et al., 1986; Figure 1). The sum of both effects account for an estimate that can be 10 % or more low.

It is possible to estimate the % M by starting the scan at 380 nm instead of 570 nm by knowing the time interval between when

Figure 2.3 Visible absorption spectra of bR. Scans started at 570 nm and progressed to 750 nm. The dashed trace represents the light-adapted bR spectrum at 20 °C. The solid trace represents the light-adapted bR spectrum at 260 K. The specimen was cooled in the dark. The dotted trace represents the conversion of bR to M at 260 K, after actinic light illuminated the specimen for 30 seconds. By starting the scan at 570 nm, only half of the absorbance peak is recorded. The two variables used in the calculation of the percent M formed, A_{ref} and ΔA, are labelled.

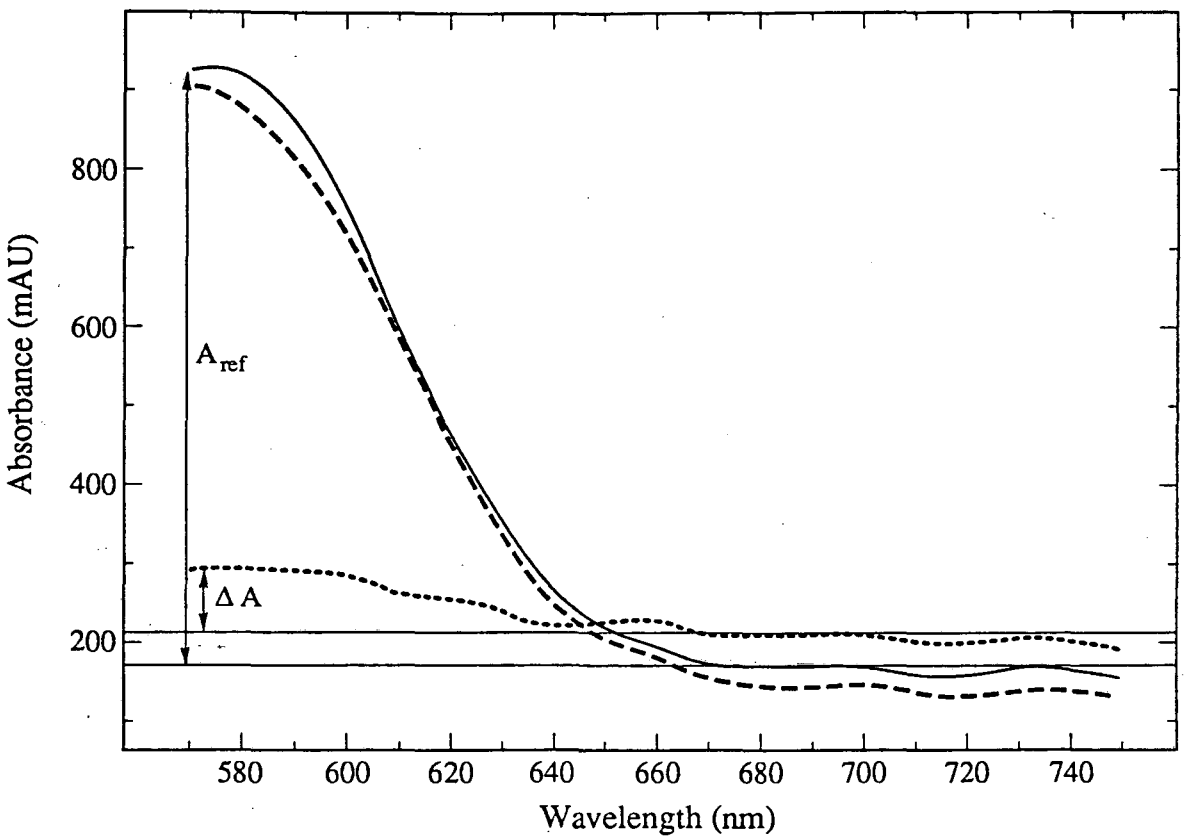
Absorbance (mAU)
800
600
400
200
A_{ref}
ΔA
580
600
620
640
660
680
700
720
740
Wavelength (nm)

XBL 921-4641

the scan starts and when 572 nm is reached. The previously measured parameters for M decay kinetics are then used to extrapolate the absorbance to time = 0. This method was rarely used as it adds an extra level of possible errors due to the inaccuracies inherent in fitting the decay curve with 2 or 3 exponentials. It does serve, however, to show that, indeed, M is formed since the scan runs through 412 nm. Spectra of this type will be shown in Chapter 3.

The second method to estimate the percentage of M formed involves recording the absorbance at a fixed wavelength (in this case, 572 nm) as a function of time. This not only allows the % M to be determined, but also serves for kinetic studies of M decay. At the desired temperature, before light excitation, the absorbance is read at both 572 nm and at the high-wavelength baseline. Immediately after light excitation, the absorbance is again read at 572 nm. For the studies of M formation (as opposed to M decay studies, i.e. my kinetic studies) it is important to quickly record the baseline, once the 572 nm absorbance is recorded, because as M decays to bR, the baseline, offset when M forms, will also "decay" to the bR baseline. The percent M is calculated per the equation two paragraphs ago.

For all stock solutions of PM, SDS-PAGE was used to test the homogeneity of bR. The C-terminus of bR has a stretch of some 20 amino acids which extend out of the membrane on the cytoplasmic side (Henderson et al., 1990). If care is not taken during the steps of protein purification and storage, this 20-amino acid-long stretch

may be clipped, ie. a peptide bond is cleaved and the C-terminal stretch dissociates from the main protein (Jap, private communication). If there is a significant population of clipped bR, as well as unclipped bR, then there will be two distinct bands in the electrophoresis gel, since the MW of the clipped and unclipped bR differ enough to get band separation. The Pharmacia Phastgel system with coomassie blue staining is used for SDS-PAGE. One lambda of sample is run on each column. In order to detect bands, a minimum of 30 ng/microliter per band is needed. Figure 2.3 shows that with a bR concentration of 400 ng/microliter only one band per lane is observed. Identical results were obtained for all stock PM solutions. Thus, my PM was homogeneous to better than 90 %. Of course, from these gels, I cannot tell if my PM stock is nearly all clipped, or nearly all unclipped. However, I know that my PM is not clipped because clipped bR aggregates horribly, and my PM patches remained suspended in distilled water under a force of one g.

"THINGS THAT CAN GO WRONG"

It was discovered that the cold nitrogen gas not only cooled the specimen and purged the cryostat so that water would not condense on the sample or the two "measurement windows", as desired, but it also dehydrated the specimen over the period of several hours. Newly made specimens that exhibited a high percentage of M would show much less M the following day. Nitrogen gas has been used to dry PM samples (Rothschild & Clark, 1979a). Clearly, little water, if any, remained after such drying (Rothschild & Clark, 1979a, see

Figure 2.4 SDS-PAGE gel with [bR] = 400 ng/microliter samples in lanes 3 and 5. Samples were taken from different stock solutions of PM. Only one band per lane was observed. The purity of samples was determined to be greater than 90 %.

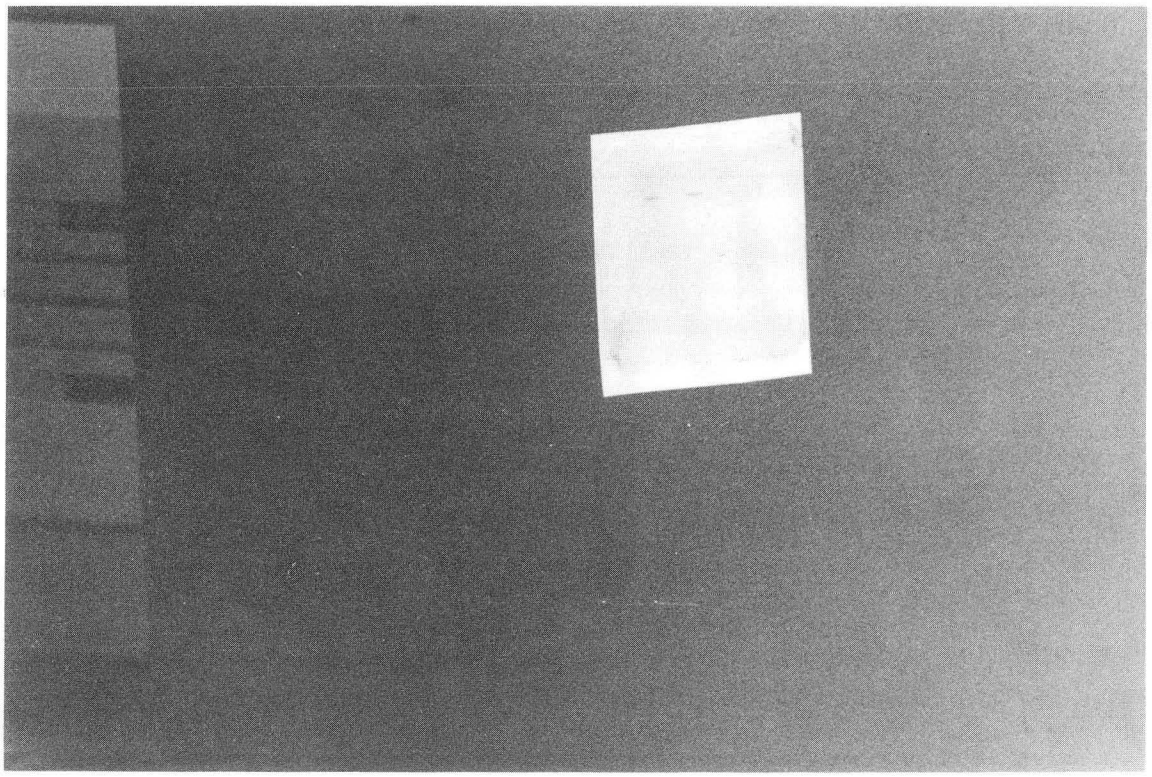

Figure 2). The ability to form M in glucose-preserved PM specimens, however, diminished noticeably only after ~3 hours under these conditions. I attribute this observation to two factors. First, the specimen was sandwiched between two mylar films, leaving the possibility of water loss only around the edges. Second, the presence of glucose retards water loss. After each day's experiment, I found it necessary to rehydrate my specimens overnight.

An attempt was made to subtract the contribution of the mylar Fraunhofer fringes from the PM spectrum. A single sheet of very thin (~10 micrometer thick) mylar was placed in the specimen holder and a baseline was taken. The sheet of mylar was replaced with a glucose-embedded PM specimen and a scan was recorded. The Fraunhofer fringes did not disappear, as hoped, but instead increased in amplitude. The same procedure was tried with two mylar sheets with the same result. (See Figure 2.4.) The fringes, most notably in the range 380 nm to 460 nm, exhibit amplitudes more than double those in Figure 2.5. Using hindsight, I see that the fringes depend on the thickness of the mylar sheets and the spacer (i.e. specimen) and that it is unreasonable to expect that the thickness will be uniform. This being the case, the reference sample position was left empty for all visible spectroscopy experiments.

The Aminco is sensitive to vibrations and minor jarrings. I was perplexed to observe that most of my spectra at the beginning contained random spikes that could not possibly be related to the PM

Figure 2.5 Visible absorption spectrum of light-adapted bR taken at 20 °C. The baseline was taken from double mylar sheets placed in the reference slot of the spectrophotometer. The peak absorbance was at 567 nm.

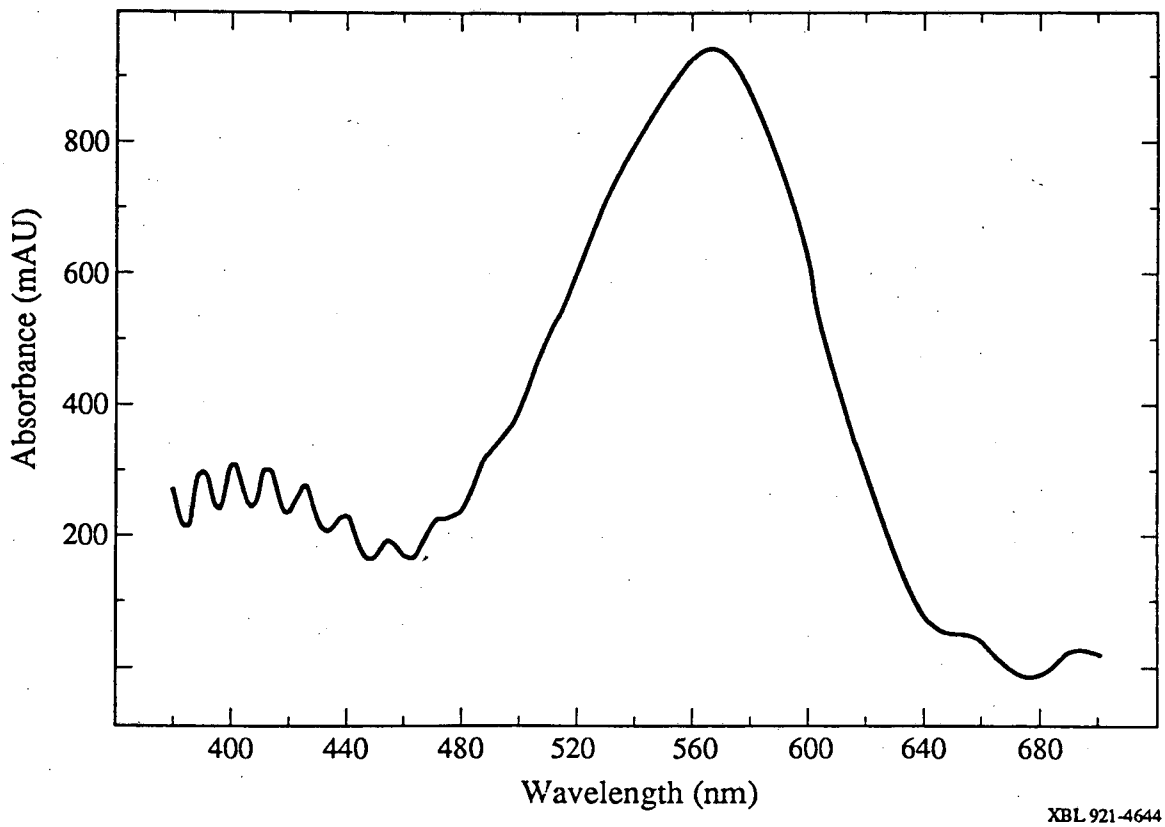
Absorbance (mAU)
800
600
400
200
400
440
480
520
560
600
640
680
Wavelength (nm)
XBL 921-4644

spectrum. The Aminco sits on a lab bench and while the scan was running, I did not touch it. I discovered, though, that seating myself or walking around caused these spikes. As a test, I stood in place during the scan except when the spectrophotometer was scanning between 540 and 585 nm. Figure 2.5 shows the results. The trace is smooth except during the portion of the scan when there was movement in the room. For subsequent scans, I limited my movement; the problem was alleviated.

The time that the specimen spent in the oven was minimized in order to avoid any irreversible denaturation due to "overcooking". It was discovered that some samples of glucose-embedded PM that had been dried for several hours at 40 °C would not form M at low temperature even after hydrating at 81% relative humidity for 24 hours or longer. From this experience, I included in the protocol the stricture that the specimen is to be dried only to the point that a thin coat of water is still visible on the surface. For a final optical density of ~0.5 A.U., this meant drying for ~30 minutes. For an optical density of ~1.0 A.U., this required no more than an hour of drying time. Subsequently, all specimens exhibited 90 % or greater M when "trapped" at low temperature.

While 99 % M was "trapped" at 240 K, only 80 % M could be "trapped" at 260 K with the optics initially employed. A stronger light source might give a higher percentage of M at 260 K. To maximize the light intensity incident on the specimen, I modified the holder so that all of the light striking the Fresnel lens/filter

Figure 2.6 Visible absorption spectrum of light-adapted bR recorded at 20 °C. The reference sample position was left empty. Movement in the room during the time when the Aminco spectrophotometer scanned from 540 nm to 585 nm caused the noisy changes in the measured absorbance over that interval.

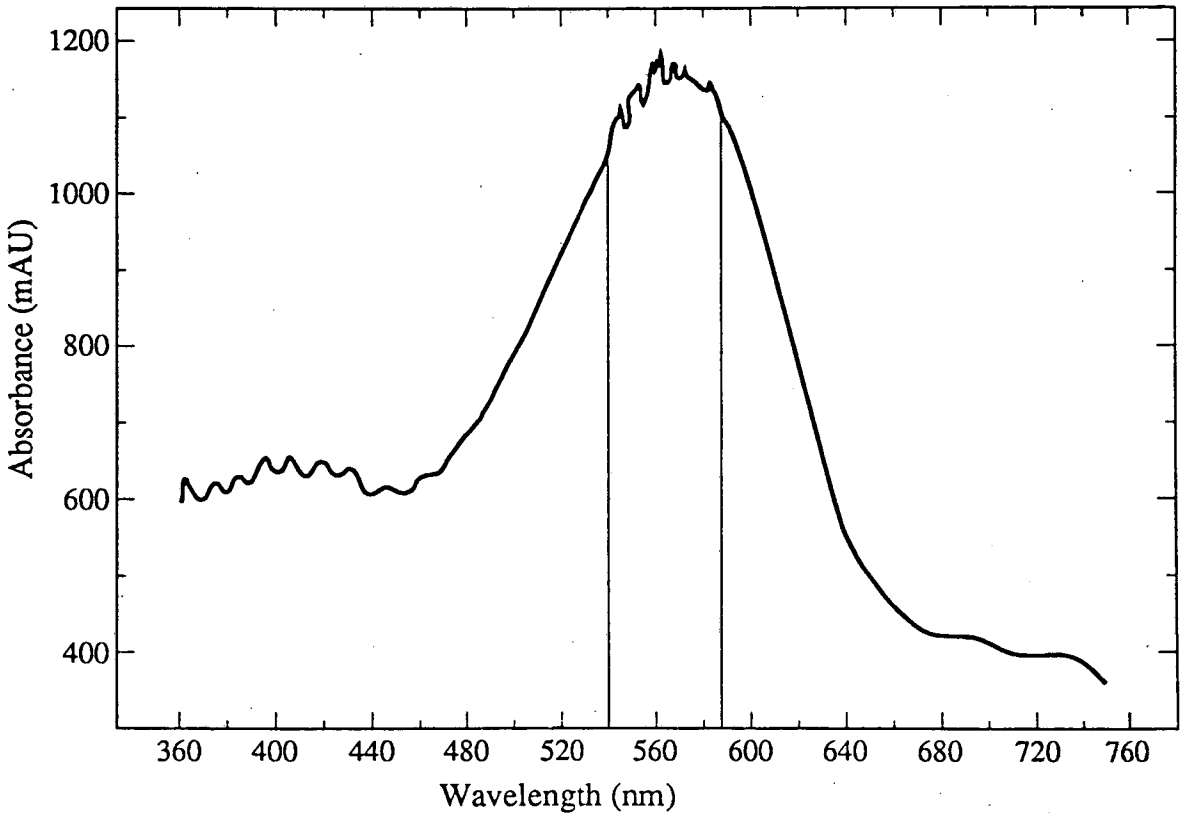
1200
1000
800
600
400
Absorbance (mAU)
360
400
440
480
520
560
600
640
680
720
760
Wavelength (nm)

XBL 921-4639

arrangement was transmitted. Before, tape had obstructed a portion of the light. I found that with this new arrangement, approximately 97 % M could be "trapped" at 260 K.

Chapter 3[2]

THE NECESSITY OF HYDRATING GLUCOSE-EMBEDDED SAMPLES

Introduction

It has been demonstrated that one can obtain *in vacuo* preservation of unstained membrane protein specimens to resolutions close to interatomic spacings by replacing their natural aqueous environment with another material which has similar chemical and physical properties, but is non-volatile. For example, glucose-embedded samples of purple membrane, isolated from *Halobacterium halobium*, have been used to obtain a complete data set of electron diffraction patterns, extending to 2.9 Å resolution, for bacteriorhodopsin (bR) (Ceska and Henderson, 1990). Examples of other compounds used to preserve membrane proteins are trehalose for the case of PhoE porin from *E. coli* (Jap et al., 1990), and tannin for the case of light-harvesting complex from pea (Kühlbrandt & Wang, 1991).

While it is true that glucose does preserve bR *in vacuo*, as judged by preservation of crystallinity in purple membrane, it also can mildly dehydrate the protein. Sugars are osmotically active solutes and perturbants that can extract water away from bR. Although glucose is not nearly as effective as sucrose in extracting the internal water molecules required for the M_2 - N reaction inside

---

[2]Parts of this chapter and the Materials and Methods section of the previous chapter are included in a manuscript submitted to the *J. of Microscopy*.

the protein (Cao et al., 1991), one should be cautious in assuming that glucose embedment results in the preservation of a completely native, hydrated state for biological macromolecules.

BR does not function properly in dehydrated, thin films of PM. By analyzing bR's photoelectric signal, Varo & Keszthelyi (1983) report that at low humidities, bR ceases to pump charge across the membrane. Most likely, the Schiff base proton that is donated to Asp-85 upon L decay is returned to the Schiff base during M decay since the forward steps in the photocycle, N and O, are blocked. That is, the back reaction of M to bR_{568} is traversed without a net charge translocation. The hypothesis that the M to N reaction is blocked as a result of protein dehydration is supported by Cao et al. (1991) who found that water is required for a proton to be transfered from Asp-96 to the Schiff base (Gerwert et al., 1989). It is possible that one or more of the four water molecules reported to be near the Schiff base of bR (Papadopoulos et al., 1989) aids this proton transfer. Even though key steps are blocked in dehydrated bR, dehydration may not affect peptide hydrogen bonds (Lazarev & Terpugov, 1980).

Spectroscopy provides numerous examples of the hydration requirements of thin films of purple membrane in order to approximate the photocycle kinetics and spectra characteristic of purple membrane in an aqueous medium; a decrease in specimen hydration results in perturbed spectra and kinetics. The lifetime of the M-state intermediate in the bR photocycle can be increased substantially by decreasing the relative humidity as well as the

temperature (Kalisky et al., 1981; Braiman et al., 1987; Varo & Kesthelyi, 1983; Lazarev & Terpugov, 1980; and Cao et al., 1991). Braiman et al. (1987) have also reported that the presence of liquid water is necessary in order to observe protein backbone alterations that accompany M formation. Spectral shifts in the visible and infrared regions occur when thin purple membrane preparations are equilibrated at low relative humidity (Lazarev & Terpugov, 1980). Resonance Raman spectroscopy provides evidence that the chromophores of a population of dehydrated, light-adapted bR are predominantly 13-cis (Alshuth et al., 1984), whereas hydrated, light-adapted bR has an all-trans chromophore. These various spectroscopies serve as useful diagnostics to qualitatively probe the level of hydration in purple membrane samples.

The amount of water that is present in a thin film, after drying or after equilibration at a given relative humidity, can be measured directly by weighing the sample and comparing the measured weight to the calculated weight of the organic solutes. I utilize such gravimetric studies of water uptake in thin films of glucose-embedded purple membrane to show that air-drying at ambient humidity, as in the usual technique of electron microscope specimen preparation, can leave very little water present. The high vacuum of the electron microscope can even further reduce the amount of water in a glucose-embedded biological specimen. After incubating thin films of purple membrane embedded in glucose in a humidity controlled atmosphere, I show that the percent water uptake is reproducible.

In addition, I report that the aberrant bR photocycle behavior observed for dehydrated glucose-embedded purple membrane is effectively reversed when the samples are hydrated at a relative humidity just below the deliquescence point of glucose. Under these conditions, the water content is 34 % by weight. Furthermore I find that only with well-hydrated, glucose-embedded purple membrane specimens can one obtain close to 100 % M formation in samples that have been first cooled to 240 to 260 K.

Materials and Methods: Gravimetric

Gravimetric studies of the water content in the specimens were made possible by first carefully measuring the mass of glucose and PM in aqueous solution. PM mass in solution was estimated from the absorbance at 568 nm using the value A = 2.35 for a concentration of 1.0 mg/ml. The final concentration of glucose in the aqueous solution was 2.17 % by weight, which was four times the concentration of PM. A 2 ml sample was placed on a glass slide and the water was evaporated in an oven set at 40 °C. After equilibrating at a controlled relative humidity, the specimens were weighed with a Beckmann digital balance displaying 1 mg precision. "Total" dehydration of the sample was accomplished by two means. The first involved drying the specimen in the oven for a time much longer than needed to evaporate water initially from the aqueous sample. The second involved exposure of the specimen to a high vacuum for four hours. Exposing the specimen for longer than four

hours resulted in no further decrease in weight. The experiment of equilibrating at various humidities and weighing was repeated four to twelve times to assure reproducibility of the measurements.

Results and Discussion

Characteristics of Dehydrated & Hydrated Specimens

When films of purple membrane and glucose were prepared under ambient temperature and humidity, visible spectroscopy revealed that in some samples the M intermediate could be quite long-lived at room temperature. In this case the 568 nm absorbance peak, which is characteristic of well-hydrated, light-adapted bR at room temperature, shifts toward 560 nm, which is characteristic of a 67:33 population of all-trans and 13-cis bR chromophores (Scherrer et al., 1989). This observation is consistent with the report by Alshuth et al. (1984) that the population of 13-cis bR is greatly increased in dehydrated purple membrane samples. Figure 3.1 displays a spectrum, recorded at room temperature, of glucose-embedded PM prepared under ambient humidity and illuminated with light at the intensity and duration used to light-adapt bR. However, the absorbance peak is at 560 nm, instead of 568 nm. It is known that when PM films become dehydrated, bR's absorbance maximum shifts from 568 nm to 560 nm (Korenstein & Hess, 1977a; see Figure 2). I conclude that the specimen used to record the spectrum of figure 3.1 must have been dehydrated. Figure 3.2 shows results with a thin film of glucose-embedded purple membrane that had been

Figure 3.1 Light-adapted bR visible absorption spectrum recorded at 20 °C. The vertical line to the right of the absorbance peak indicates 568 nm. The absorbance peak lies at 560 nm. The glucose-embedded PM specimen was prepared under ambient humidity.

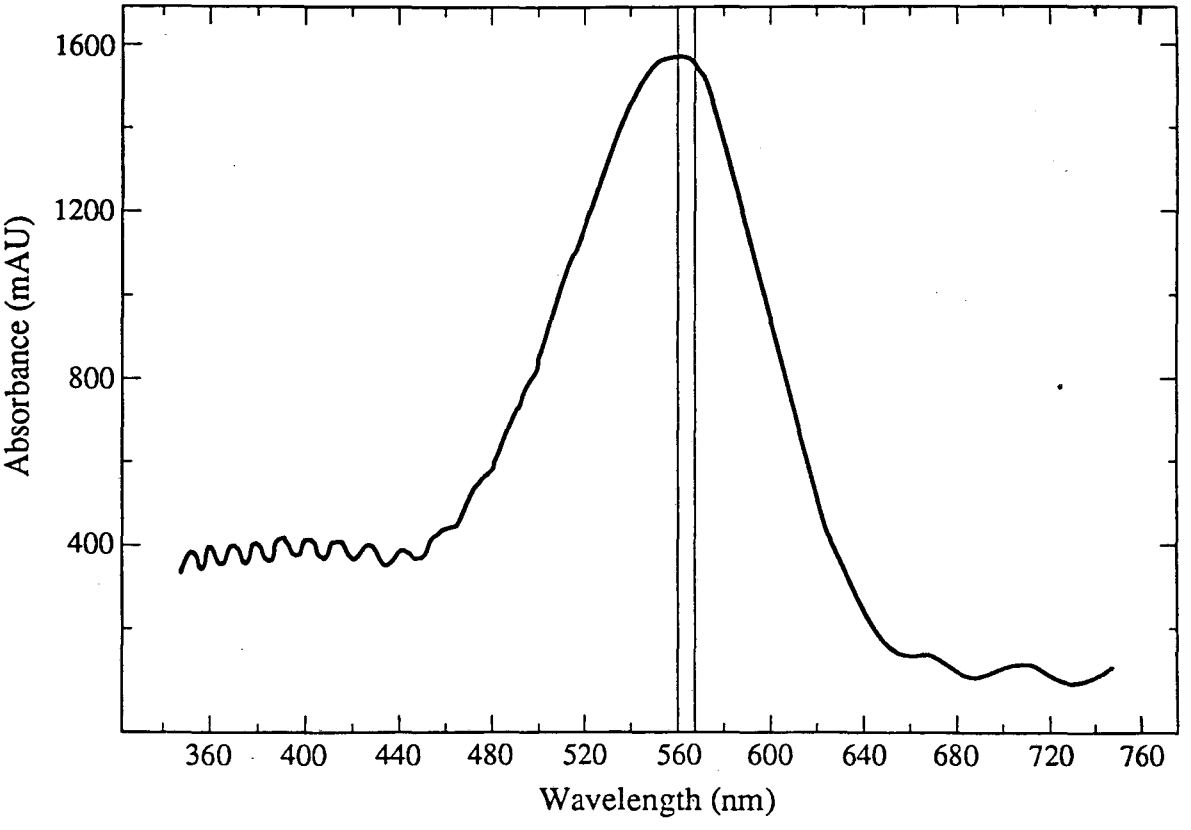
1600
1200
800
400
Absorbance (mAU)
360
400
440
480
520
560
600
640
680
720
760
Wavelength (nm)

XBL 921-4640

Figure 3.2 Room temperature visible absorption spectra of glucose-embedded PM prepared at ambient humidity. Scan time is 1.44 nm/s. Scans start at 380 nm and end at 700 nm. Scans were started 8 seconds after cessation of the actinic light. Heavy trace is light-adapted PM. Light trace is the spectrum after 20 seconds of intense actinic light. M has a peak absorbance at 412 nm. The interference fringes, most notable between 380 and 460 nm are caused by the mylar support film.

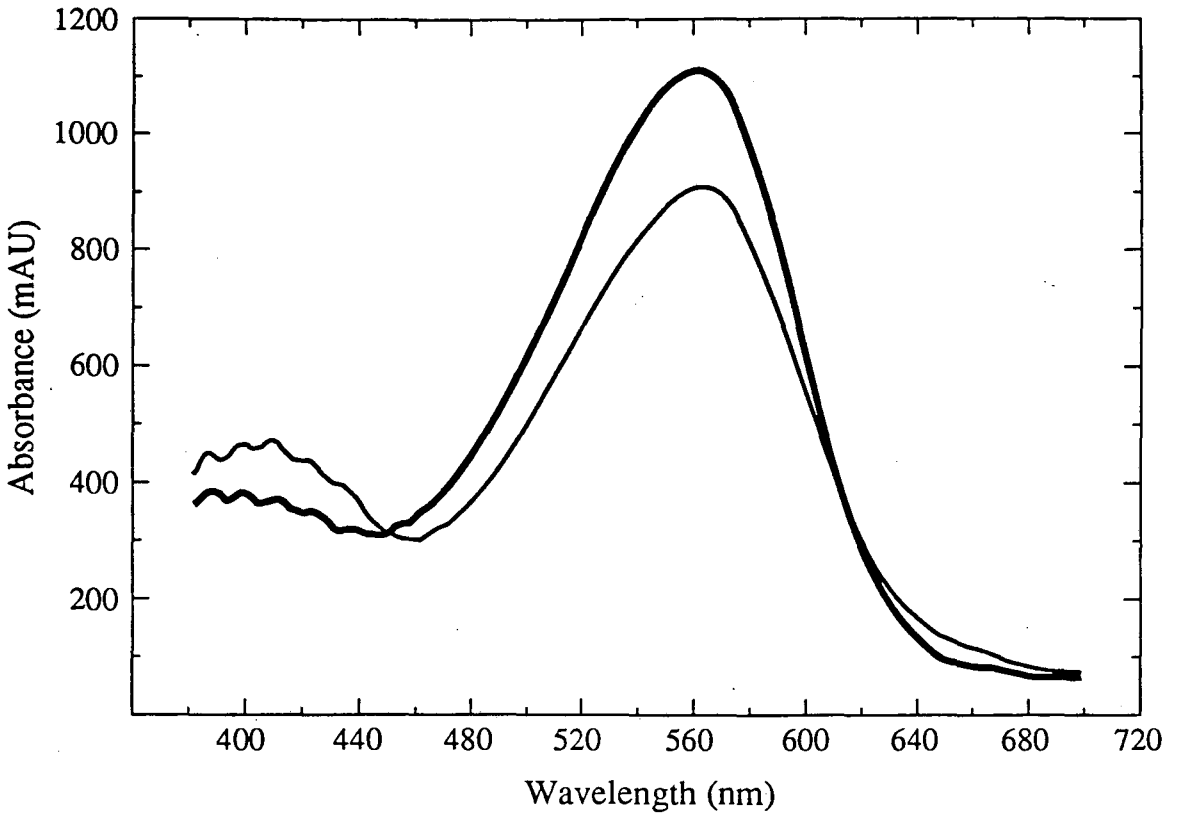

XBL 9112-5045

prepared at ambient humidity; even after the photoexciting light had been turned off for 32 seconds, there still existed a substantial M412 peak. The increase in the M-state lifetime, characteristic of dehydrated specimens, could be further exaggerated by subjecting the sample to 3-4 hours of vacuum. Not only is M decay greatly slowed at room temperature, but M formation is also lowered when the sample is equilibrated at low relative humidities (Korenstein & Hess, 1977a).

However, when this sample was hydrated at 81% relative humidity for 12 hours, no decrease in the absorbance at 568 nm and no rise in the absorbance at 412 nm could be measured after illumination of the sample, which shows that the decay of M occured more rapidly at room temperature than the few seconds required to replace the photomultiplier tube and start the scan. Kinetic measurements of hydrated samples of purple membrane show that the rise and decay of M occur in a few milliseconds at room temperature (Ames & Mathies, 1990). The restoration of a more normal photocycle behavior after glucose-embedded samples are equilibrated at 81% relative humidity suggests that a more fully hydrated state is produced by this procedure. In earlier studies it has been demonstrated that the charge pump fully recovers when dried films of bR are equilibrated, without glucose, at relative humidities above 75% (Varo & Keszthelyi, 1983).

When glucose-embedded films of purple membrane have been prepared at ambient temperature and humidity, I find that M is

sometimes not formed at all after the sample is cooled to lower temperatures, even though Becher et al. (1978) and others have found that nearly 100% M is formed in hydrated purple membrane films at the same temperature. As is demonstrated in Figure 3.3, even with glucose embedment, only a small amount of the bR underwent M conversion at 240 K in a sample that had been equilibrated at ambient humidity. I conclude that specimens exhibiting this behavior were dehydrated, even though a protocol similar to that which is used for preparing supposedly hydrated electron microscope specimens was followed. The observation that M is long-lived at room temperature while only a small amount of M is formed at lower temperatures demonstrates that glucose embedment alone does not provide a fully native hydration state for bR. When the sample is dried at an ambient humidity well below the deliquescence point, there is a possibility that the glucose which surrounds and embeds the specimen may extract water from the purple membrane to satisfy its own hydrogen bonding needs.

Gravimetric Studies

Gravimetric studies similar in principle to those conducted in other groups (Varo & Keszthelyi, 1983) were performed with thin films of glucose and glucose-embedded PM to determine the water content after equilibration at various relative humidities. The thin films of glucose (no PM) were used as control specimens. The results in Table 3.1 provide information concerning the capability that the glucose-embedded purple membrane film has for trapping

Figure 3.3 240 K visible spectra of glucose-embedded PM prepared at ambient humidity. Dashed trace is light-adapted PM at room temperature. Solid trace is light-adapted PM that had been cooled in the dark. Alternate dot and dashed trace is the spectrum recorded after 20 seconds of actinic light. At lower temperatures, the bR 568 peak shifts to 572 nm, is slightly narrower and absorbs more strongly. Very little M is formed by this sample at 240 K.

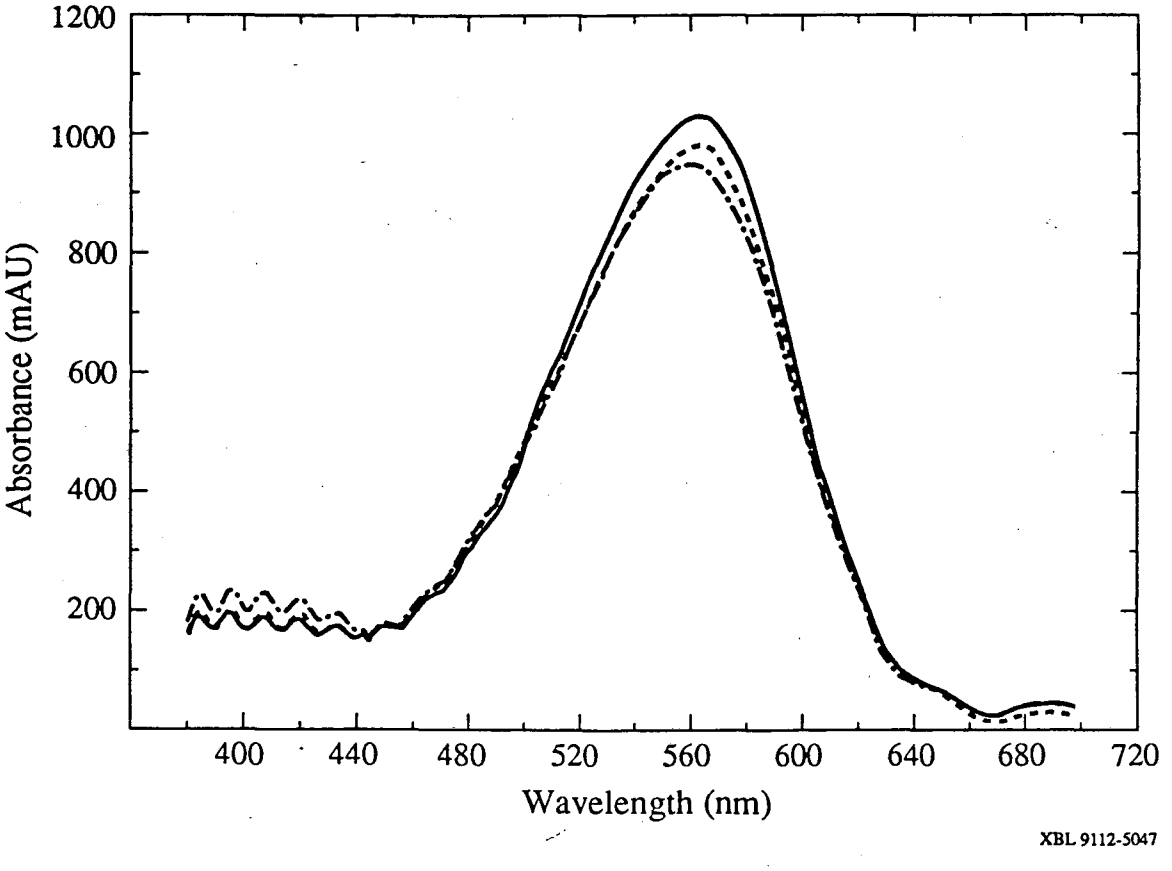
1200
1000
800
600
400
200
Absorbance (mAU)
400
440
480
520
560
600
640
680
720
Wavelength (nm)
XBL 9112-5047

Table 3.1 Gravimetric measurements of the water content in thin films of a) purple membrane embedded in glucose and b) glucose. The first column indicates the time that the specimen spent under each condition listed in the second column. The third column gives the mean value±standard deviation of the water mass in the specimen for the number of measurements listed in the fourth column, dependent on the condition and time. The masses of purple membrane, glucose, MOPS buffer and sodium-azide, added to a 2 ml aqueous solution, were 10.8, 43.4, 4.2 and .6 mg, respectively. The total solute mass in specimens of PM embedded in glucose is 59 mg. Specimens without PM had a total solute mass of 48.2 mg. The % water was calculated from the ratio (water mass/total solute mass). When hydrating the specimens at 100 % relative humidity, water uptake was complete after 48 hours. The data, in this case, are in the "solvated" row. The precision of the measurements was ±1 mg.

Table 3.1

A) GLUCOSE-EMBEDDED PURPLE MEMBRANE

Time	Condition	Water Mass		% Water
		Mean	# Measurements	
4 hrs.	40 °C - Oven	1±2 mg	8	2 %
4 hrs.	High vacuum	3±1 mg	4	5 %
	Ambient humidity	7±2 mg	6	12 %
24 hrs.	81 % humidity	20±1.8 mg	12	34 %
24 hrs.	100 % humidity	138±5.21 mg	6	234 %
36 hrs.	100 % humidity	171±5.63 mg	4	290 %
solvated	100 % humidity	215±3.04 mg	4	364 %

B) GLUCOSE

Time	Condition	Water Mass		% Water
		Mean	# Measurements	
4 hrs.	40 °C - Oven	1±2 mg	4	2 %
4 hrs.	High vacuum	3±1 mg	4	6 %
	Ambient humidity	7±2 mg	4	14 %
24 hrs.	81 % humidity	15±1.9 mg	8	31 %
24 hrs.	100 % humidity	140±4.34 mg	4	290 %
36 hrs.	100 % humidity	166±5.41 mg	4	344 %
solvated	100 % humidity	207±3.71 mg	4	429 %

water under various conditions of hydration. When the glucose-embedded PM specimens are equilibrated at 81 % relative humidity for twelve hours or longer, the water content stabilizes reproducibly at 34 % by weight. The same final water content is achieved whether the specimen was first oven-dried, exposed to a vacuum or spent 36 hours at 100 % relative humidity. The glucose specimens equilibrated at 81 % relative humidity contained a similar water content, 31 %. By way of comparison, a representative water content in thin films of purple membrane embedded in glucose that had been allowed to equilibrate at ambient humidity (unmeasured relative humidity) and temperature was 10 %. The control films of glucose equilibrated at ambient humidity and temperature had a mean water content of 12 %. Even though the relative humidity of the samples prepared at ambient humidity was not measured, the low standard deviation of the weight measurements indicates that the ambient relative humidity did not vary much between the days that these measurements were carried out. A relative humidity of 100 % causes glucose to deliquesce, i.e. water is taken from the atmosphere until the glucose is completely dissolved. I find that liquification occurs after the thin films of PM and glucose have taken up 3.64 g of water per 1.00 g of sample (purple membrane plus glucose).

These gravimetric experiments show that virtually all of the water can be extracted from thin films of glucose-embedded purple membrane when samples are oven-dried or exposed to a vacuum. Furthermore, the control measurements give virtually the same

results. It was found that no further amount of water could be extracted if the specimen is exposed to more than four hours of high vacuum. Conditions that exist in the sample compartment of an electron microscope, i.e. high vacuum, will cause slightly less water loss (See Table 3.1.) than drying in an oven at 40 °C. Even so, a specimen of glucose-embedded purple membrane that has been exposed to the vacuum of an electron microscope at room temperature will become too dehydrated to progress through a photocycle normally.

Summary

Adequate control of the hydration level will be crucial for electron microscopy studies of bR that couple structure to function. For example, Korenstein & Hess (1977b) report that the quantum yield of M is normal only when thin-film, purple membrane samples are equilibrated at high relative humidity. In the 240 to 260 K temperature range, however, glucose alone does not maintain purple membrane in the correct type of hydrated state where appreciable M can be formed. Other data provide evidence that a functionally important bR intermediate, N, can be trapped only if the purple membrane specimen is well-hydrated. Events ocurring in the N intermediate of bR's photocycle are thought to play an important role in the "reprotonation switch" (Fodor et al., 1988). Pfefferle et al. (1991) report that in order to trap the N intermediate in the bR photocycle at low temperatures, the thin film of purple membrane must be highly hydrated (i.e. 70 % water by weight). If the percent

water content drops to 50 %, still a relatively high percentage of water, then under the same conditions used to trap N, close to 100 % M state is trapped instead, at 230 K.

Glucose cannot be an ideal substitution as far as maintaining the protein surface in a native, hydrated environment is concerned. PM *in vivo* is bathed in an aqueous medium, and even though glucose preserves surface hydration of proteins, it is possible that it does not "fool" PM completely. Jaffe & Glaeser (1987) proposed that new features observed in difference Fourier maps of bR could be due to surface segments of the polypeptide being well-ordered in frozen-hydrated specimens, but not in glucose-embedded specimens. It is possible that their frozen-hydrated specimens are more hydrated than their glucose-embedded specimens because a thin layer of water was left on the PM surface in the former technique.

In summary, the evidence presented in this dissertation indicates that glucose alone does not provide a "fully hydrated" environment for bR, as judged by a slow decay of the M intermediate at room temperature and the difficulty of even forming an M intermediate at low temperatures. Glucose does afford some protection against high vacuum, since purple membrane specimens prepared for electron microscopy give high-resolution electron diffraction patterns that are characteristic of well-ordered crystals. Specimens prepared with little or no glucose, on the other hand, do not diffract. Thus, glucose embedment represents only a partial solution to the problem of specimen dehydration. I show that

an additional step in specimen preparation may be needed. This step involves tightly controlling specimen hydration. Equilibration of glucose-embedded samples at high humidity can result in a physical state that is demonstrably closer to the native, fully hydrated state. One should generally be cautious in assuming that glucose embedment results in the preservation of a completely native, hydrated state for biological macromolecules.

Chapter 4

TRAPPING NEARLY 100 % M

Trapping M at 240 K and 260 K

The purpose of the visible spectroscopy experiments is to "trap" the highest possible percentage of M using glucose-embedded PM samples with the equipment on hand. As such, these experiments are an important precursor to the FTIR and electron diffraction experiments. In order to have a good signal-to-noise ratio in the difference Fourier map, trapping a high % of M is necessary. Ideally, greater than 95 % is desired but greater than 90 % is tolerated. As the percent M formed falls below 90 %, it would become increasingly difficult to obtain interpretable results from the electron diffraction work. For example, in Figure 4.1, I show that with thin films of glucose-embedded PM, equilibrated at 81 % relative humidity, 99 % M can be reproducibly "trapped" at 240 K using the procedure described in the Methods and Materials section of Chapter 2. This is presumably all M_1 (Ormos, 1991, or see the results in Chapter 6). Glucose embedment is not a technique normally used in spectroscopy, but in our case it was required as a preliminary to electron diffraction work.

At 240 K, the protein may be "frozen" in the T conformation even though the chromophore is in the isomeric and protonation state characteristic of the C conformation. Because the protein cannot

Figure 4.1 Visible absorption spectra of bR recorded at 240 K. The sample was equilibrated at 81 % relative humidity. Solid trace records the light-adapted bR spectrum after the sample has been cooled in the dark. The dashed trace records the formation of M by showing the depletion of light-adapted bR. Scans were initiated at 570 nm and terminated at 750 nm.

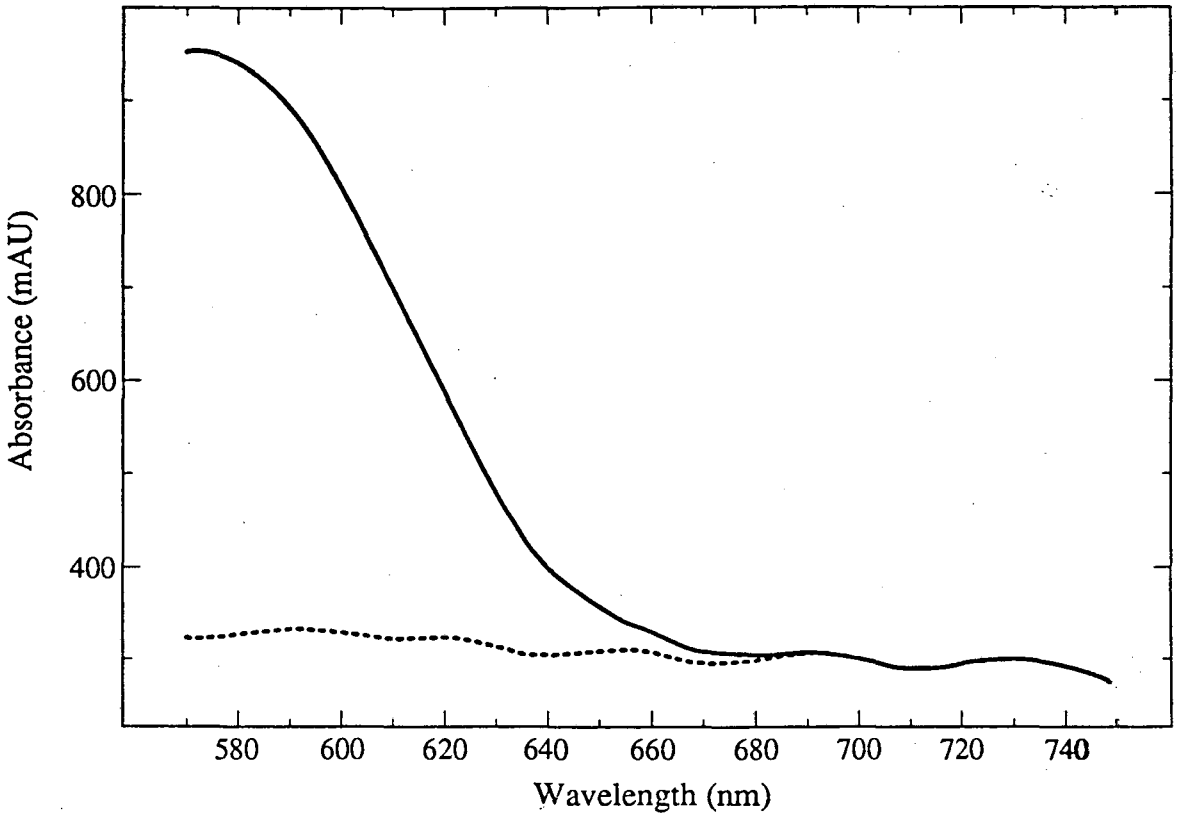
Absorbance (mAU)
800
600
400
580
600
620
640
660
680
700
720
740
Wavelength (nm)

XBL 921-4642

gain the C conformation, it is proposed that the proton originally on the Schiff base, but now donated to Asp-85 (L - M_1 transition), is returned to the Schiff base (M_1 - bR_{568}) and no pumping occurs (Ormos, 1991). The upshot of this, as far as our approach is concerned, is that by regulating the temperature, M_1 can be "frozen" for electron diffraction studies. (At 260 K, the protein is not too "frozen" to make the conformational switch, and the normal direction of the photocycle is taken.)

When films of PM and glucose are hydrated at 81% relative humidity, light-adapted, and cooled to 240-260 K in the dark, M is readily trapped upon photoexcitation. At 240 K, almost 100% of the bR can be momentarily trapped in the M intermediate. Figure 4.2 shows that when a high percentage of M is formed, light-adapted bR is depleted to a very small amount. As M decays, the 412 nm absorbance peak diminishes and the 572 nm peak absorbance grows. The half-life for the slow-decaying component at 240 K is ~ 35 minutes, as derived from the data shown in Figure 4.2. The possibility of trapping such a high percentage of M is consistent with the report that close to 100% M is trapped at 230 K for humidified PM samples (Pfefferle et al., 1991). Because the cold nitrogen gas can dry the specimen over the course of hours, I found it necessary to rehydrate the specimen after each session of measurements. The isosbestic point for the light-adapted bR and the M spectra of glucose-embedded PM occurs at the same wavelength as reported elsewhere for hydrated, PM-only samples (Lazarev & Terpugov, 1980).

Figure 4.2 (a) M decay at 260 K for a sample which has been equilibrated at 81 % relative humidity at room temperature. The dotted trace is light-adapted PM cooled in the dark. The heavy solid, light solid, dashed and alternate dot & dashed traces were started 260, 1060, 1360 and 1760 seconds, respectively, after cessation of the actinic light. (b) M decay at 240 K. Heavy solid trace is light-adapted PM cooled in the dark. The dotted, alternate dot & dashed, dashed and light solid traces were started 8, 260, 820 and 1260 seconds, respectively, after cessation of the actinic light. The isosbestic point for bR and M is at 455 nm, and is more clearly defined than the isosbestic point occuring at the same wavelength in the spectra taken at 260 K.

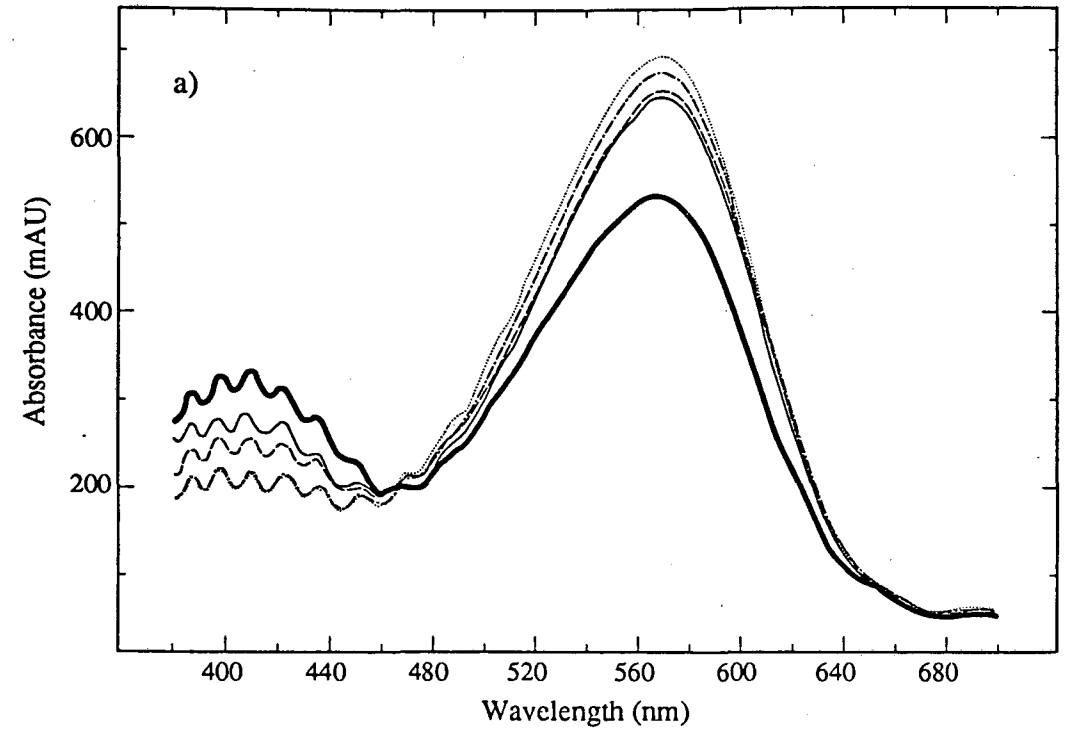
a)
Absorbance (mAU)
600
400
200
400
440
480
520
560
600
640
680
Wavelength (nm)

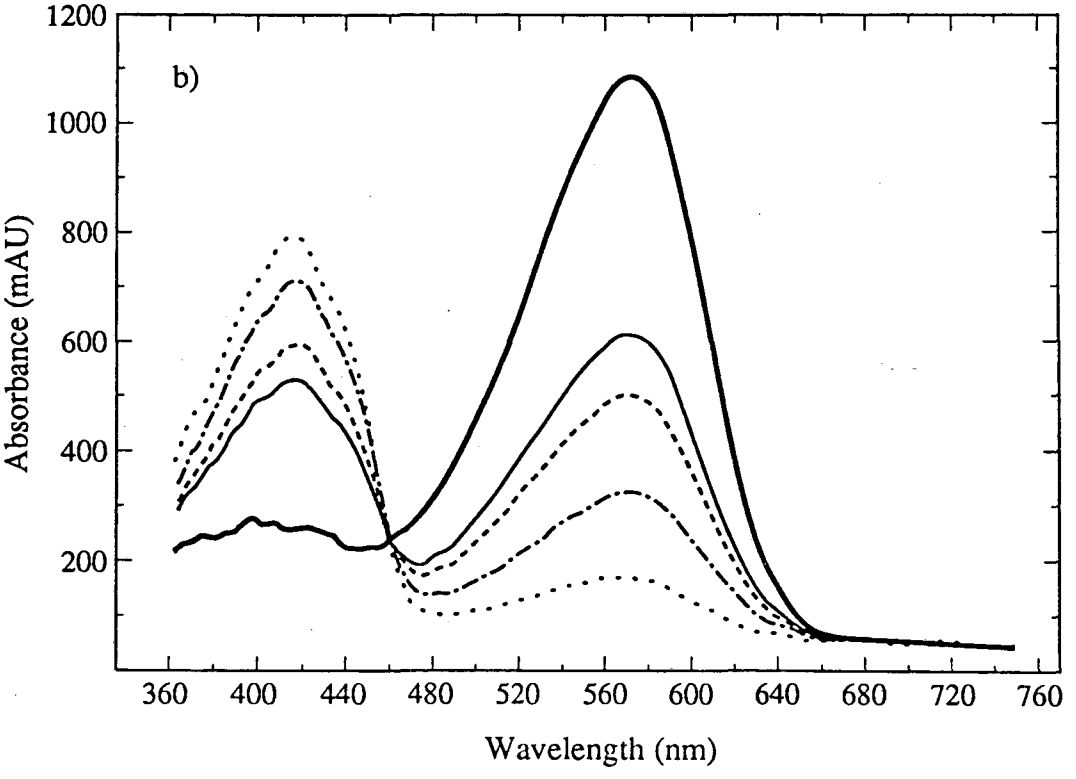
b)
Absorbance (mAU)
1200
1000
800
600
400
200
360
400
440
480
520
560
600
640
680
720
760
Wavelength (nm)

XBL 921-4645

I estimate that by following my protocol ~ 97 % M will be consistently "trapped" at 260 K. The ability to trap greater than 90 % M in glucose-embedded PM samples had also been demonstrated by Glaeser et al. (1986). However, they utilized a different protocol from mine for both preparing the specimen and trapping M. A high level of specimen hydration is apparently not necessary in order to trap a high percentage of M using their technique. (See the related discussion of the effects of hydration on M formation in Chapter 3.) When I followed their protocol of slowly cooling the specimen under continuous illumination using a dry sample, I still obtained greater than 80 % M (even on the first attempt). However, it is not clear in the work of Glaeser et al. (1986) if M_1, M_2 or a mixture of the two states was trapped.

By focusing more light on the sample, I went from consistently obtaining ~ 80 % M to greater than 90 % M at 260 K. It is possible that a greater % of M could be "trapped" at 260 K with a stronger actinic light source. However, Ormos (1991) reports that there is a significant N-intermediate component in his M - bR difference spectra taken at 260 K. As judged by the characterization of the N intermediate (Pfefferle et al., 1991), it may be that there is a greater concentration of N than M in the Ormos 260 K difference spectra (See the discussion in Chapter 6.). This can be explained by the models that best fit the bR photocycle kinetics, which allow for the thermal decay of M_2 to N and the back-reaction of N to M_2 (Mathies et al., 1991; Varo & Lanyi, 1990). Thus, it is unclear if

using a brighter source will indeed give more M at the expense of N. Note that there is no O intermediate expected to be present in the spectrum since O is not observed in the spectra of samples hydrated at relative humidities below 90 % (Varo & Lanyi, 1991).

The time that it takes for bR to decay to 90 % of its initial value at 260 K has ramifications for determining the percent M formed at time = 0. As discussed previously, ~ 8 seconds are required to replace the photomultiplier tube and initiate the scan after terminating the actinic light. It is possible that initially, almost 100 % M is formed at 260 K and by the time that the scan is started, ~ 10 % of the sample has reverted back to bR_{568}. However, the relative concentrations of M_1 and M_2 as a function of time cannot be determined by my visible absorption experiments. Since the photocycle passes through M_1 before reaching M_2 (Varo & Lanyi, 1991), it is possible that M_1 is dominant at earlier times and that, as M_1 goes to M_2, the concentration of M_2 does not approach 100 %.

A precaution needs to be heeded when trying to "trap" M_2 at 260 K. In Ormos' first FTIR difference spectrum (1991), representing the first 15 seconds after light cessation, the tail-end of the conformational change postulated to occur in the M_1 to M_2 transition is still observed, as characterized by the protein relaxation parameter, as defined by Ormos (1991). It is conceivable that plunge-freezing the electron microscope specimen in liquid nitrogen the second that the light is terminated will produce more M_1 than desired because the switch to M_2 has not been completed. However,

wait too long, and more N than desired will be "trapped". Thus, timing the instant of specimen freezing may be critical to obtaining 90 % M_2.

Decay Kinetics of M

The purpose of measuring the decay kinetics of M to bR_{568} in glucose-embedded PM at low temperature is two-fold. First, I would like to estimate the time-progression of non-M-intermediates over a period of ~ 30 seconds, the time it takes to complete four scans with the Perkin Elmer spectrometer I use for my FTIR measurements. To create difference FTIR spectra with an acceptable signal-to-noise ratio, I average a thousand or more scans together in increments of four; four scans are recorded immediately following exciting the light-adapted bR photocycle with actinic light (See Chapter 5.). By first measuring the decay kinetics, I can estimate the percentage of "contaminants" in the difference FTIR spectra of M - bR at 240 K and 260 K. Second, in order to design the EM protocol for trapping a high percentage (say 90 % or higher) of the M intermediate in specimens amenable to collecting electron diffraction patterns, it is necessary to know how much time can be alotted to trapping M at liquid nitrogen temperature once M decay has started.

Ancillary to the stated goals, I need to determine how many exponentials accurately fit the decay curves at 240 K and 260 K. Is the number of decay exponentials for glucose-embedded specimens

at low temperature the same as for PM-only specimens at 20 °C? It is accepted that two or three exponentials fit the M decay curve at 20 °C (Korenstein & Hess, 1977b).

The photocycle intermediates and the pathway that bR follows as it progresses through its photocycle have been well-characterized through the use of both time-resolved resonance Raman and multichannel visible spectroscopies at room temperature (Mathies et al., 1991; Varo & Lanyi, 1990). A consensus is building that the bR photocycle contains no branches. Also, thermodynamic studies indicate that the M_1 to M_2 step is irreversible (Varo & Lanyi, 1991). These two pieces of information place constraints on M decay kinetics.

Whether or not more than one exponential is used to fit the curve is judged by the amplitudes. If the amplitude of an exponential term is negligibly small, using some subjective cut-off, then it is not included in the sum of exponentials. I did not include any term with an amplitude less than 1 % of the sum of amplitudes. For the decay of M to light-adapted bR in glucose-embedded PM at 240 K, two exponentials accurately fit the decay curve. Table 4.1 shows that at low temperature, M decay is prolonged, thus allowing straight-forward kinetic studies. At 260 K, three exponentials fit the decay curve. As expected, the decay of M to bR at 260 K is significantly faster than at 240 K (Ormos, 1991).

Table 4.1 M decay kinetics for PM embedded in glucose and hydrated at 81 % relative humidity. The component amplitudes and time constants were determined by the multiple-exponential fitting routine, EXPFIT (Berry, unpublished work). The amplitudes were normalized so that the sum added to 1.00 AU. At 260 K, both 2-exponential and 3-exponential data are shown even though the curve fit to the data with 3 exponentials agrees more closely with the experimental data than does that with 2 exponentials.

TABLE 4.1

Temperature		Amplitude (mAU)	Time Constant (s)
	2 Exponentials		
240 K	fast decay	120	115
	slow decay	880	2157
	2 Exponentials		
260 K	fast decay	436	52
	slow decay	564	608
	3 Exponentials		
260 K	fast decay	153	16
	slower decay	379	86
	slowest decay	468	716

Is it feasible to use rapid cooling, after turning off the actinic light, to trap the initially high percentage of M reported in this work, in the time allowed before an appreciable amount (say 10 %) of M has decayed? Our M decay kinetics with glucose-embedded purple membrane at 240 K display bi-exponential decay, while at 260 K, three exponentials provide a closer fit to the decay curve. Table 4.1 shows that at these temperatures, M decay is prolonged, allowing straight-forward kinetic studies. By comparing the two exponential fits, it is seen that the fast decay rate for samples that have been hydrated at 81 % relative humidity increases by a factor of two and its contribution to the amplitude is a factor of four higher when M is trapped at 260 K compared with M at 240 K. The effect of adding another exponential to the curve fitting for the 260 K kinetic data is to add an even faster decay component, with a time constant of 16 seconds. Its amplitude is only 15 % of the total amplitude, however. On the basis of the measured decay kinetics, the percent concentration of M at 240 K decreases to 90 % of its starting value after 89 seconds, a relatively large amount of time. At 260 K, however, the percent concentration of M falls to 90 % of its initial value after only 8 seconds. As expected, the decay of M to bR at 260 K is significantly faster than at 240 K (Ormos, 1991).

Using the second method described in the Materials and Method section of Chapter 2 for estimating the percent M formed, data were obtained for the percent M as a function of time since switching off the light. Figure 4.3a presents the decay curves that fit the data points recorded at 240 K. It is seen that after 50 minutes there

Figure 4.3 M decay as a function of time, as measured by the regeneration of the 572 nm peak. M absorbance was scaled to 1000 mAU when extrapolated to zero time. The data points are absorbance measurements at "quasi-logarithmic" time intervals (Ormos, 1991) and are indicated by triangles. (a) 240 K decay curves. The data points are shown to be accurately fit by a sum of two exponential terms. After the decay data were fit with two exponentials, component curves, corresponding to each exponential term in the fit, were calculated and plotted. These are labeled, "slow", and "fast". Component absorbances add to the value of the curve fitting the data points for all time. (b) 260 K decay curves. The decay data were fit best with three exponentials. The three exponential terms are labeled as "slow", "faster" and "fastest".

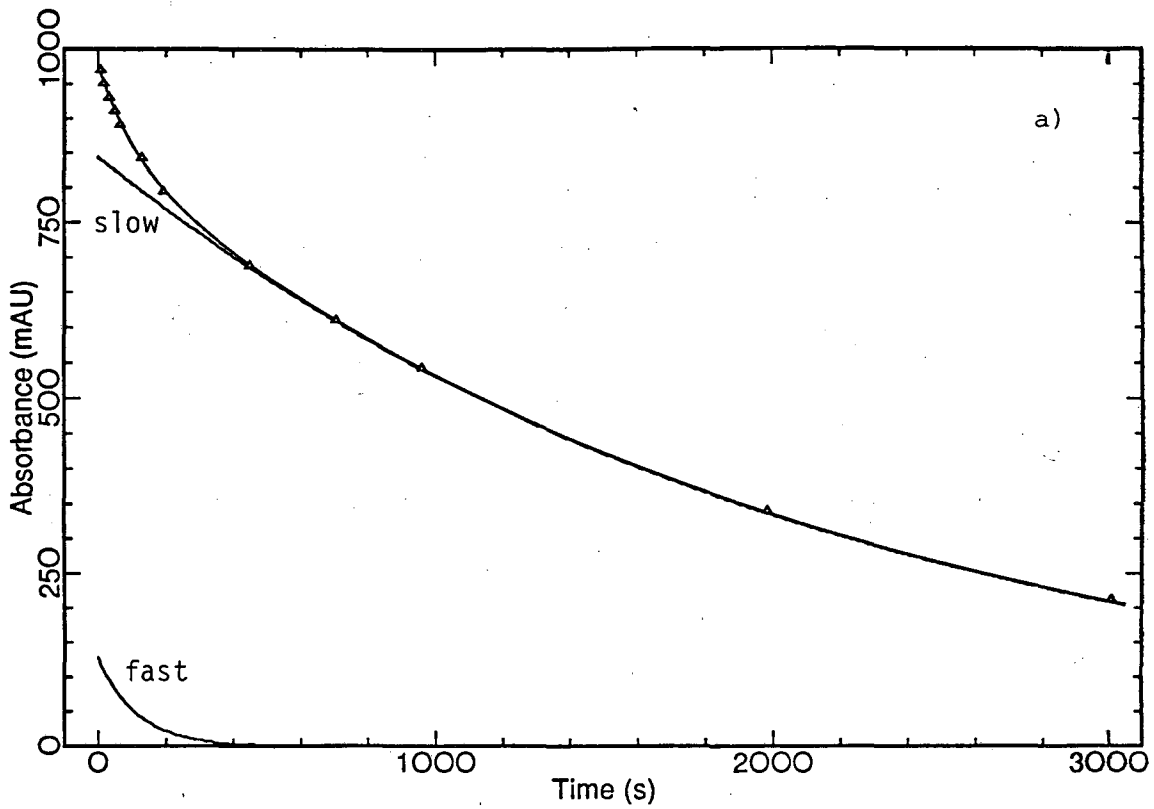
a)
slow
fast
Absorbance (mAU)
0
250
500
750
1000
0
1000
2000
3000
Time (s)

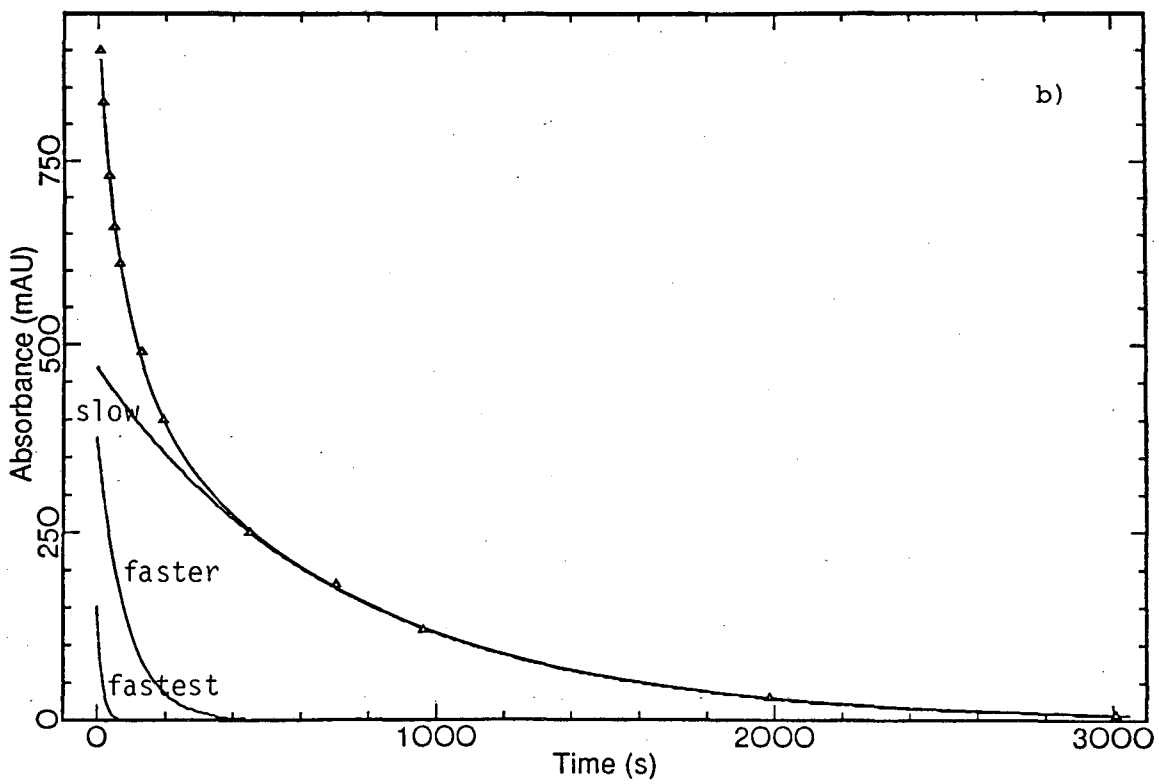
b)
slow
faster
fastest
Absorbance (mAU)
0
250
500
750
0
1000
2000
3000
Time (s)

still is more than 20 % M remaining. Figure 4.3a shows 12 data points ranging in time from 8 seconds to 3000 seconds. The "fast" decay component contributes amplitude to the curve fitting the data points only for the first 400 seconds of the measurements, and even then the amplitude is a small fraction of the total. Figure 4.3b presents the 260 K decay curves. At 260 K, light-adapted bR is regenerated after ~ one hour. Unlike the 240 K data, three exponentials are required to fit the 260 K, M decay data. At early times, the M decay fit has significant contributions from all three component exponentials. As with the 240 K data, only the "slow" decay component is present after ~ 400 seconds. Figure 4.3 provides a visual image portraying how fast the various exponential terms contributing to M decay occur. At 260 K, the fastest-decaying component disappears after ~ 50 seconds, while, at 240 K, the fastest-decaying exponential doesn't disappear until after ~ 500 seconds.

Figure 4.2 shows spectra obtained during the time-course of M decay at 240 K and 260 K, respectively. It is interesting that at both temperatures there appears to be an isosbestic point at ~ 455 nm in the time course recovery spectra (e.g. see Figure 4.2). Isosbestic points occur only in two-state systems. There is no contradiction between the appearance of an isosbestic point and multi-exponential decay, however. I suspect that the isosbestic point seen in Figure 4.2 is actually a "pseudo-isosbestic point". There are two reasons why one may be unable to detect deviations from the isosbestic point. First, the lifetimes of the third, fourth,

etc. species may be short and so undetected. Second, the absorbance values of other species may be close to the crossover absorbance at ~455 nm. In summary, a "good" isosbestic point in the spectra of Figure 4.2 does not rule out the presence of low amounts of L, N, etc. intermediates. It does, however, set limits on the concentration of other intermediates present, and thereby, it limits the rate constants of their decay relative to the forward and backward rates of M decay. For example, the pseudo-isosbestic point of Figure 4.2 indicates that intermediates other than the M and light-adapted bR states must be at low concentrations at temperatures between 240 K and 260 K. This conclusion is consistent with my results determining the percent concentration of M at 240 K and 260 K, which show that 90 % M or greater can be consistently trapped.

The visible absorption studies of M reported here are relevant to the question of how to trap the M states for electron diffraction studies. If initially M is formed through actinic excitation at temperatures in the range 240 K to 260 K, then by cooling the sample to liquid nitrogen temperature within a period of 8 seconds, M can truly be trapped indefinitely (Glaeser et al., 1986; Dencher et al., 1989). I believe that rapid cooling of "hydrated", glucose-embedded samples to low temperatures, to eliminate water loss, will be effective when the electron microscope is used to study glucose-embedded bR intermediates and any other biological molecule where the presence of water is crucial for proper functioning.

At "low" light intensities, the time required to form a saturating level of the M intermediate is determined by the light intensity rather than by the L - M rate constant. In order to estimate the time it takes to form M in glucose-embedded PM at low temperature, with the light source available to me, the specimen was exposed to varying time intervals of light. A plot of % M versus exposure time could be used to estimate the time constant for M formation. For short exposure times, the % M formed should rise linearly, and for longer times, the curve tracing the % M will flatten until a saturation exposure time is reached. The exposure time that would give 100 % M (if not for the competing decay process) is estimated by continuing the imaginary line running through the linear regime of the above-mentioned plot until it intersects the 100 % M horizontal line and then reading vertically down to the exposure time. From this exposure time, an upper bound on the time constant for M formation can be estimated. For example, at 260 K, the % M formed after as little as one second of exposure time was 75 %. Certainly, this percent of M is not in the regime of linear rise; I expect that this regime lies in a range where less than 50 % M is formed. Thus, one second is an upper bound for the M formation time constant. I measured the % M at exposure times of 1, 5, 10, 15, 20, 25 seconds. The table below gives values for the percent M formed as a function of the exposure time at 260 K and 240 K. The measurement time was ~ 8 seconds after termination of the actinic light.

Exposure Time (s)	%M 260 K	240 K
1	75	79
5	78	97
10	80	96
15	88	95
20	89	97
25	90	97

At 240 K, a one second exposure time netted 79 % M, and the curve was already saturated after five seconds, indicating that at this temperature, the M decay is not competing as strongly as at 260 K. Clearly, even a one second exposure time is not in the linear regime. Thus, at both temperatures, the time constant for M formation is less than one second.

Model of M Decay

A simple kinetic model of M decay in glucose-embedded PM at low temperature was derived in order to account for the measured kinetic data. I was guided by the fact that the exponential time-constant for the formation of M cannot be measured with my protocol because M formation is too fast. At both 240 K and 260 K, the time constant appears to be less than one second with the light intensity used. Also, the fast time component for the decay of M at 240 K is greater than 100 seconds, while at 260 K, it is ~ 15 seconds. From these pieces of information, I considered the highly simplified case that the decay rate is 0.01 x formation rate. With this model, I ask the questions: "What is the steady-state (t =

infinity) level, ie. fraction, of M that is formed?" and "How long does it take to reach 95 % of the steady state?" The answers are derived as follows.

Only the two-state model

$$bR \underset{k_2}{\overset{k_1}{\rightleftharpoons}} M$$

is considered. This is a reversible first-order reaction (Bray & White, 1966). The rate equations are,

$$\frac{d[bR]}{dt} = -k_1[bR] + k_2[M] \qquad (1)$$

$$\frac{d[M]}{dt} = k_1[bR] - k_2[M]$$

where [bR] and [M] are fractional concentrations. At equilibrium,

$$\frac{d[bR]}{dt} = \frac{d[M]}{dt} \equiv 0$$

and the ratio of equilibrium concentrations is

$$\frac{[M]_{eq}}{[bR]_{eq}} = \frac{[bR]_0 - [bR]_{eq}}{[bR]_{eq}} = \frac{k_1}{k_2} \equiv K$$

because $[bR]_0 = [M] + [BR]$ for all time. K is the equilibrium constant and $[bR]_0$ is the concentration of bR at t = 0.

$$[bR]_{eq} = \frac{k_2}{k_1 + k_2}[bR]_0 = \frac{[bR]_0}{1 + K}$$

Initially, there is no M, hence

240 K: $[bR]_0 = 1$ and $k_1 = 100\ k_2$

$$\therefore [bR]_{eq} = \frac{1}{100} \text{ and } [M]_{eq} = \frac{100}{101} \approx 99\ \%$$

260 K: $[bR]_0 = 1$ and $k_1 = 15\ k_2$

$$\therefore [bR]_{eq} = \frac{1}{16} \text{ and } [M]_{eq} = \frac{15}{16} \approx 94\ \%$$

This is the answer to the first question. Now, on to the second question.

Use $[M] = 1 - [bR]$ in (1):

$$\frac{d[bR]}{dt} = -k_1[bR] + k_2\{1 - [bR]\} \qquad (2)$$

Eliminate k_1 from (2):

$$k_1[bR]_{eq} = k_2\{1 - [bR]_{eq}\}$$

$$\frac{d[bR]}{dt} = \frac{k_2}{[bR]_{eq}}\{[bR]_{eq} - [bR]\}$$

Integrate:

$$\int_{1}^{[bR]} \frac{d[bR]}{[bR]_{eq} - [bR]} = \frac{k_2}{[bR]_{eq}} \int_{0}^{t} dt$$

$$\Rightarrow \quad \ln\left(\frac{[bR]_{eq} - 1}{[bR]_{eq} - [bR]}\right) = \frac{k_2}{[bR]_{eq}} t = (k_1 + k_2)t$$

$$\Rightarrow \quad \frac{[bR]_{eq} - [bR]}{[bR]_{eq} - 1} = e^{-(k_1 + k_2)t}$$

$$\text{Also,} \quad \frac{[M]_{eq} - [M]}{[M]_{eq}} = e^{-(k_1 + k_2)t} \qquad (3)$$

How long does it take to reach 95 % of the steady state?

Use (3):

240 K:

$$-(k_1 + k_2)t = \ln\left[\frac{\frac{100}{101} - \frac{95}{101}}{\frac{100}{101}}\right]$$

Let $k_1 = 1 \text{ sec}^{-1}$, $k_2 = 1/100 \text{ sec}^{-1}$

$$\Rightarrow \quad t = \frac{100}{101} \ln\left(\frac{100}{5}\right)$$

$$= 3 \text{ seconds}$$

260 K:

$$-(k_1 + k_2)t = \ln\left[\frac{\frac{15}{16} - \frac{14.25}{16}}{\frac{15}{16}}\right]$$

Let $k_1 = 1 \text{ sec}^{-1}$, $k_2 = 1/15 \text{ sec}^{-1}$

$$\Rightarrow \quad t = \frac{15}{16} \ln\left(\frac{.94}{.05}\right)$$

= 2.75 seconds (~ 3 seconds)

The 240 K results are consistent with my kinetic data. At 240 K, I am able to "trap" 99 % M. Since my empirical data show that a saturation level is already reached by five seconds, and 80 % of this level is reached after one second, it is reasonable that 95 % of saturation is reached after three seconds. However, the model does not fit my 260 K data. It has been shown that saturation is not reached until after 25 seconds of light exposure, not the 3 seconds predicted from the model. Furthermore, by extrapolating back to zero time, I show that 97 % M is formed as opposed to the 94 % predicted from the model. Thus, the two-state model is not an accurate description of the events at 260 K. The results derived from this simple analysis provide a useful reality check for my kinetic experiments.

Chapter 5

FTIR SPECTROSCOPY: SETTING UP THE EXPERIMENTS

Introduction

The purpose of the FTIR experiments described in this chapter is to determine if the M_1 and M_2 substates of the bR photocycle can be trapped separately with thin-film specimens of PM embedded in glucose. In conjunction with this, M - bR difference spectra are examined for the presence of other intermediates, L and N, that have well-defined difference bands (Engelhard et al., 1985; Roepe et al., 1987; Gerwert et al., 1989; Gerwert et al., 1990; Bousche et al., 1991; Braiman et al., 1991; Pfefferle et al., 1991). A short review of the basic principles and advantages of FTIR spectroscopy in addition to an abbreviated overview of how FTIR spectroscopy has been used to study bR will first be presented. As with the chapter describing the methods used with the visible absorption experiments, the end of this chapter has a section entitled, "Things That Can Go Wrong", as discovered when performing my difference FTIR experiments.

Basic Principles of FTIR Spectroscopy

A brief discussion of the basic principles of FTIR spectroscopy is included by way of background for the results and discussion of the M - bR spectra presented in the remainder of this chapter. Molecular vibration spectroscopy is differentiated into two types, infrared and Raman. Raman spectroscopy records the vibrations that

modulate a molecule's electronic polarizability, whereas, infrared spectroscopy records the vibrations that modulate a molecule's electric dipole moment (Bell, 1972). A molecule's atoms, consisting of the nucleus and surrounding shells of bound electrons, are constantly vibrating with respect to each other. Being much more massive than electrons, yet subject to essentially the same forces, atoms vibrate at much lower frequencies than do electrons. As a result, molecular vibration spectra appear in the middle infrared region between 3 - 15 micrometers (3500 - 600 cm^{-1}). The frequency of atomic motion not only depends on the atomic mass, but it also depends on the restoring forces binding an atom to its neighbors. The surrounding atoms are not infinitely massive, so they recoil in reaction to the thermal vibrations of the "central" atom, and pass the recoil on to their own neighbors. Of course, the coupled movement of atoms reflects the local molecular structure. Hence, IR bands characterize not individual atoms, but groups of atoms (e.g. -CH3).

The FTIR instrument has several advantages over the older dispersive infrared instruments. Early infrared spectrometers borrowed technology from visible absorption spectrophotometers. Either a prism or grating was employed to disperse the radiation into its component frequencies (Bell, 1972). Beams of specified frequency were directed through a narrow slit, passed through the sample and then recorded by a detector. In contrast, the FTIR spectrometer utilizes a Michelson interferometer. The Michelson interferometer divides a collimated IR beam into two beams (with a

beamsplitter) that subsequently follow different paths. One of these paths is constant, while the other path is varied by a movable mirror. The movable mirror is usually translated in one direction. However, the Perkin Elmer 1600 spectrometer I used employs a pair of parallel plane mirrors that rotate in a simple bearing in order to generate a variable path difference. Afterwards, the two beams are recombined at the same beamsplitter, passed through the sample and are recorded by a detector (Griffiths, 1975). The signal measured at the detector is called the interferogram. It is the IR intensity as a function of the optical path difference. The interferogram is related to the spectrum by the Fourier transform.

The advantages of the spectrometer based on the Michelson interferometer over the dispersive spectrometer are summarized.

1. *The Fellgett advantage.* Radiation of all wavelengths reaches the detector of the FTIR spectrometer simultaneously and continuously throughout the measurement. The dispersive spectrometer can only record each frequency sequentially. As a result, an FTIR spectrum can be recorded in a short time (on the order of a second). This facilitates repetitive scanning and signal averaging which increases the signal-to-noise ratio in the averaged spectrum.

2. *The Throughput (or Jacquinot) advantage.* The optical throughput of an interferometer, the product of the solid angle and the area of the beam at a given focus, is greater than the throughput

of a dispersive spectrometer because there is no need to filter the frequency with a monochromator.

3. *The Connes advantage.* The wavelength of radiation from a helium-neon laser is used as a standard since it is known very accurately. The beam from a helium-neon laser is passed through a different region of the beamsplitter than used by the infrared beam and is used to very precisely measure the movable mirror position. This gives an extremely high wavenumber precision. This advantage is crucial for creating difference spectra, since background absorbance bands cannot be completely subtracted if the wavenumber scale is shifted.

FTIR spectroscopy has been used to study structural changes in biological membranes and proteins (Parker, 1983). Difference FTIR spectra have aided the identification of specific chemical groups which change structurally during the bR photocycle (Bagley et al., 1982; Rothschild & Marrero, 1982). Difference FTIR spectroscopy has exhibited great sensitivity to small structural alterations, even those involving a single amino acid residue (Braiman et al., 1987; Roepe et al., 1987; Gerwert et al., 1990; Bousche et al., 1991). All groups in a biological molecule possess IR-active vibrational modes which results in a great deal of band overlap. A solution to this problem, that has worked admirably for bR, is to create difference spectra by subtracting the spectrum of the molecule in one state from the spectrum of the molecule in a different state. In this way, the difference bands that characterize changes in bR's chromophore,

Schiff base and aspartic acid residues as well as protein backbone alterations as bR progresses through its photocycle are separately observed (Braiman et al., 1988; Siebert et al., 1982; Bagley et al., 1982; Dollinger et al., 1986). The peak assignments have been made possible by site-directed mutagenesis of individual protein residues (Khorana, 1988) chemical and isotope modifications (Ebrey & Nakanishi, 1987; Rothschild et al., 1986; Bagley et al., 1985; Roepe et al., 1987) and by comparison with resonance Raman spectra (Rothschild et al., 1984).

Some of the bR structural changes give very small peak amplitudes in difference FTIR spectra (e.g. the aspartic acid bands between 1762 cm^{-1} and 1730 cm^{-1}). In practice, the ability to detect such small conformational changes depends on the signal-to-noise ratio obtainable. This ratio can depend on various factors, such as sample concentration, spectral resolution, detector sensitivity and signal averaging (Braiman & Rothschild, 1988). Usually, many thousand scans are averaged to create one difference spectrum (Braiman et al., 1987). The signal-to-noise ratio can also depend on the time available for recording biological states. For example, since the bR photocycle is complete after only 10 - 20 milliseconds from the start of an actinic flash at room temperature (Ames & Mathies, 1990; Varo & Lanyi, 1990; Braiman et al., 1991), there is little time to record spectra of bR intermediates. With fewer scans contributing to each spectrum, the signal-to-noise ratio is commensurately lower. Alternatives to time resolution are to slow the decay process by dehydration (Rothschild & Clark,

1979a; Rothschild et al., 1981), high pH (Siebert et al., 1982) and cooling (Engelhard et al., 1985; Gerwert & Siebert, 1986).

Many of the peaks between 500 cm^{-1} and 3600 cm^{-1} in FTIR spectra of bR have been assigned to structural groups (Rothschild and Clark, 1979a; Earnest et al., 1986). It has been noted that bR's Amide A and Amide I peak frequencies are unusually high (Rothschild & Clark, 1979b; Krimm & Dwivedi, 1982; Glaeser et al., 1991). Considering the high alpha-helical content of the 3-D model of bR (Henderson et al., 1990), it is expected that the Amide I peak frequency would be close to 1652 cm^{-1}. Instead, the peak frequency is blue shifted to > 1660 cm^{-1}, which appears to be unique among natural proteins. Krimm and Dwivedi (1982) have attributed the anomalously high Amide I and Amide A peak frequencies to the presence of $alpha_{II}$ helices. It has been suggested that future FTIR work on bR may aid the determination of alpha-helix conformation in the 3-D model (Glaeser et al., 1991).

Materials and Methods

Specimen Preparation

Stock solutions of PM were further purified through the use of sucrose density gradient centrifugation. It was discovered that a reddish brown sediment was deposited on the bottom of vials containing PM if the solution was left undisturbed for ~ one week. The sediment could not be red membrane, as red membrane is less

dense than PM and has an orange-red color (Oesterhelt & Stoeckenius, 1974). It must be an undefined aggregation of proteins. By utilizing sucrose density gradient centrifugation, the PM could be separated from the sediment. The sucrose concentration ranged from 30 % to 60 %. After two hours of centrifugation at 18,000 rpm, the sediment formed a pellet and the PM formed a band between the 40 - 50 % sucrose level. The ratio of absorbances at 280 nm (protein aromatic residues) over 568 nm (light-adapted bR) decreases as the PM is separated from the reddish brown sediment. Before separating the PM from the protein aggregates, this ratio was between 2.1 and 2.4; the high ratio must be due to light scattering. After separation, the ratio dropped to between 1.8 and 2.0. By way of reference, once a ratio of 1.8 is obtained, PM is considered pure enough to begin the 3-D crystallization process (Jap, unpublished results).

Infrared specimens were prepared as described for optical spectroscopy but deposited onto a CaF_2 window. After equilibration, a second CaF_2 window was placed on the sample and sealed with high vacuum grease to prevent water loss. Even so, a week after being sealed, the specimen was noticeably drier, as judged by the ratio of Amide A to Amide I bands (Roepe, 1987). These specimens, stored under ambient humidity, were used for dehydration studies. (See Figure 6.1.) FTIR measurements were performed with a Perkin Elmer 1600 using a lab-constructed cryostat.

Equipment and Calibration

Two photographs of the instruments used for the FTIR experiments are shown in Figure 5.1. The liquid nitrogen Dewar is shown in the top picture on the left of the spectrometer (unit with the screen) with a hose (insulated with black tubing) leading to the top of the glass cryostat. A hose from the red vacuum pump also leads to the top of the cryostat. The vacuum is monitored with a gauge, to the right of the spectrometer, that fits into a break in this hose. A Variac, in light-blue casing, sitting directly to the left of the spectrometer, is connected to a heating element inside the liquid nitrogen Dewar. A digicator, used to monitor the specimen temperature is sitting on top of the spectrometer. The IBM keyboard and interface are shown at the bottom of the picture. The Mercury Arc lamp (not shown) is just to the right of the edge of the top photograph. Light emitted from this lamp passes through a Fresnel lens seen in the bottom right hand corner of the photograph. The photograph at bottom is a view looking downwards on the sample compartment. Light enters from the bottom and passes through the second Fresnel lens (pieces of black tape identify it) and high-pass filter before reaching the front-surfaced mirror, positioned immediately to the right of the cryostat. The mirror is positioned such that the incoming light is reflected 90° so as to strike the sample perpendicular to the specimen plane. In this photograph, the IR beam would pass roughly horizontally from left to right. The mirror, as placed in this photograph, would obstruct the IR beam. Hence, it needs to be moved before starting a scan. Thermocouple

Figure 5.1 Photographs of instruments used for FTIR experiments. The top photograph shows the way each instrument was positioned and connected. All of the instruments are shown except for the Mercury Arc lamp which is just outside of the picture to the right. The bottom photograph shows the placement of the cryostat, mirror, Fresnel lens and high-pass filter in the Perkin Elmer 1600 sample compartment. Part of the cryostat support is out of focus in the foreground.

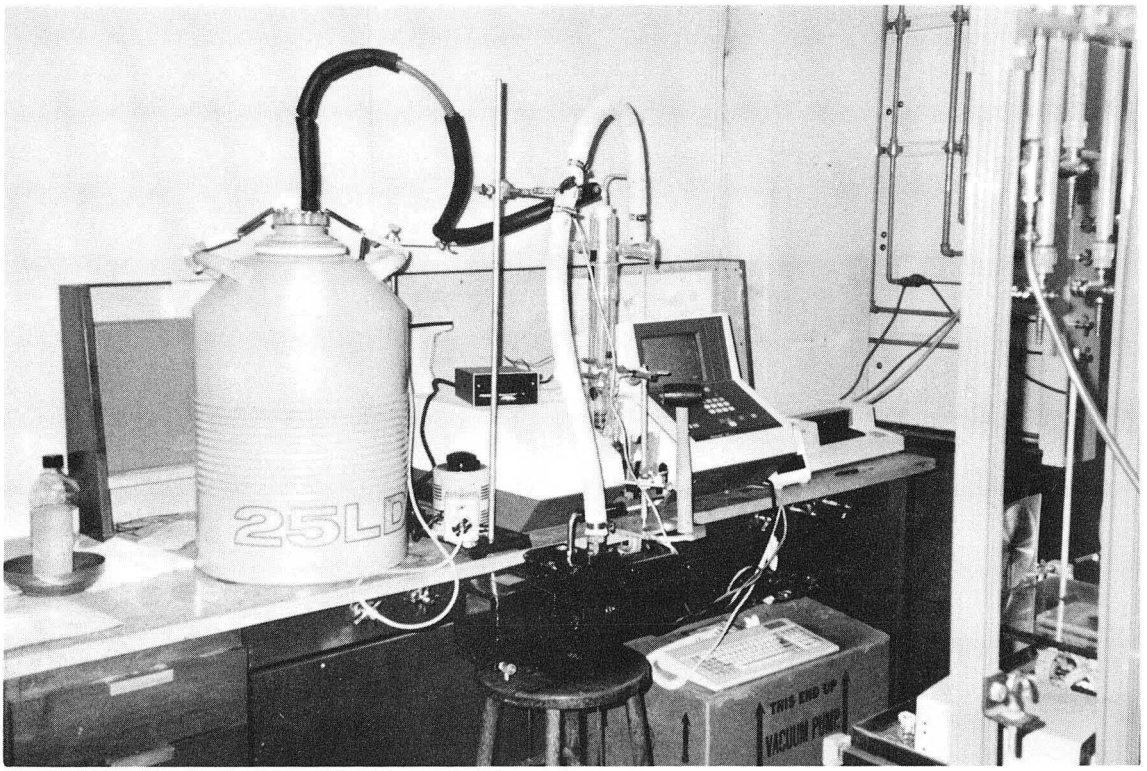
25LD
THIS END UP
VACUUM PUMP

wires are seen exiting from the top of the picture. Two wires are led through an orifice in the cryostat and make contact with the brass specimen holder.

Absorption flattening in my FTIR spectra can be caused by non-uniform sample optical density. In order to avoid absorption flattening, I endeavored to make samples with a uniform optical density across the area exposed to the IR beam. Although another group has used an "iso-spin" technique to make uniform specimens (Rothschild et al., 1981), I used elevated temperature (Glaeser et al., 1986) to enhance uniform drying.

Exposure to a plasma glow discharge was used to make the window surface more hydrophilic. It was found initially that CaF_2 windows are hydrophobic since the aqueous specimen would not spread on the surface. The resultant specimens would either be too thick or have cracks. The bell jar of a Denton evaporator, set in the glow discharge mode, is evacuated to better than 100 mTorr and the window is placed directly beneath the glow discharge ring. The current is raised until a blue aura is observed around the discharging element and held steady for 30 seconds. An aqueous sample placed on a glow-discharge treated window spreads to cover most of the surface area with a low contact angle. Glow discharge treatment aids specimen preparation by preventing cracks in the dried sample and by bringing the specimen optical density down to a range where spectra can be recorded with a good signal-to-noise ratio.

The area of uniform optical density of the thin PM and glucose film should be large enough to fill the aperture in the IR cryostat. The aperture has a diameter of 0.5 inches. After drying the specimen onto a CaF_2 window, it was noticed that there was a greater concentration of PM around the rim. An explanation for this behavior is provided by the observation that the fastest evaporation occurs at the area of greatest curvature. For a hydrophilic substrate, this occurs around the perimeter of the liquid drop. As the specimen perimeter dries, more solute mass is drawn by convection to the perimeter. After the sample has dried completely, there is an annulus of high optical density PM around the edge and a central area, approximately a fourth of the total specimen area that appears to have uniform optical density. It was found empirically that this central area of uniform optical density covers the aperture area when the volume of sample in the aqueous phase is at least 300 lambda.

Soft Apiezon wax (Q grade) and high-vacuum grease were used to hold the end windows onto the glass cryostat. Since the glass on the edge of the cavity is warped, it was thought that a soft wax rather than a hard wax could more evenly distribute the pressure caused by the vacuum on the end windows and avoid any stress on the KBr end windows and/or the glass that might crack them. However, at times, a vacuum leak is spotted where the end windows make contact with the cryostat. To eliminate leaks in this area, first a thin layer of silicone-based high-vacuum grease was applied to the glass joint and then a layer of Apiezon wax was applied

before a second coat of high-vacuum grease was applied. In this way, leaks were eliminated and the vacuum inside the cryostat was consistently 70 mTorr or better.

The Variac used to control the heating element placed in the liquid nitrogen Dewar required calibration in order to maintain a constant specimen temperature in the IR cryostat. As with the visible spectroscopy studies, gaseous nitrogen is used to cool the sample and maintain the low temperature. In order to calibrate the Variac, two sets of thermocouple wires were used. One set made contact with a side of the brass specimen holder. In order to have good thermal contact in the vacuum, thermally conducting grease was smeared on the side of the specimen holder and the ends of the wires. Without the grease, a loss of vacuum will cause the temperature reading to jump from -34 °C to -30 °C even though the thermocouple touches the brass. The other set made contact with a CaF_2 window without the specimen. In this way, the temperature at the window face could be calibrated to the temperature of the brass holder. When scanning, the temperature of the specimen can be known without wires and grease obstructing the IR beam.

Thermocouple on CaF_2 window:

Variac	Temperature (°C)
52	-14
59	-31
59.5	-32
60	-35

Thermocouple on brass plate:

Variac	Temperature (°C)
52	-14
59.5	-33

The temperature of the window and brass plate are within 1 °C at a Variac setting of 52, but they differ by 1 to 2 °C with a setting of 59.5. Because of greater thermal inertia in the IR cryostat compared with the visible cryostat, it takes as long as 90 minutes to stabilize the temperature. Once stabilized, the temperature remains constant as long as the level of liquid nitrogen in the Dewar doesn't change by much.

The atmospheric levels of carbon dioxide and water vapor in the IR beam path may vary between recording the light-adapted bR and M spectra. The carbon dioxide peaks, which lie between 2365 cm^{-1} and 2340 cm^{-1} (Sigma Library of FTIR Spectra), did not affect the IR region of interest. However, the water vapor spikes consistently appeared in the bR - M difference spectra, sometimes obscuring the aspartic acid, Amide I, Schiff base and ethylenic bands. (See Figure 5.2.) Two methods were developed to either avoid or subtract out the water vapor bands. One method involves purging the sample compartment with nitrogen gas. (The cryostat has no water vapor because the vacuum pump continuously evacuates the chamber.) Because of the elongated shape of the cryostat and the need to adjust by hand the mirror that is used for the external optics, a cover needed to be made for the sample compartment. For the sake of time, I decided to make a cover out of a polyethylene wrap with

Figure 5.2 M - bR difference spectrum between 1800 cm^{-1} and 1500 cm^{-1}, recorded at 240 K. The spectrum was an average of 64 scans. Water vapor spikes obscure features. The bands in the aspartic acid region, 1780 cm^{-1} to 1720 cm^{-1}, and the conformational marker region, 1675 cm^{-1} to 1645 cm^{-1} (Ormos, 1991), are particularly difficult to resolve.

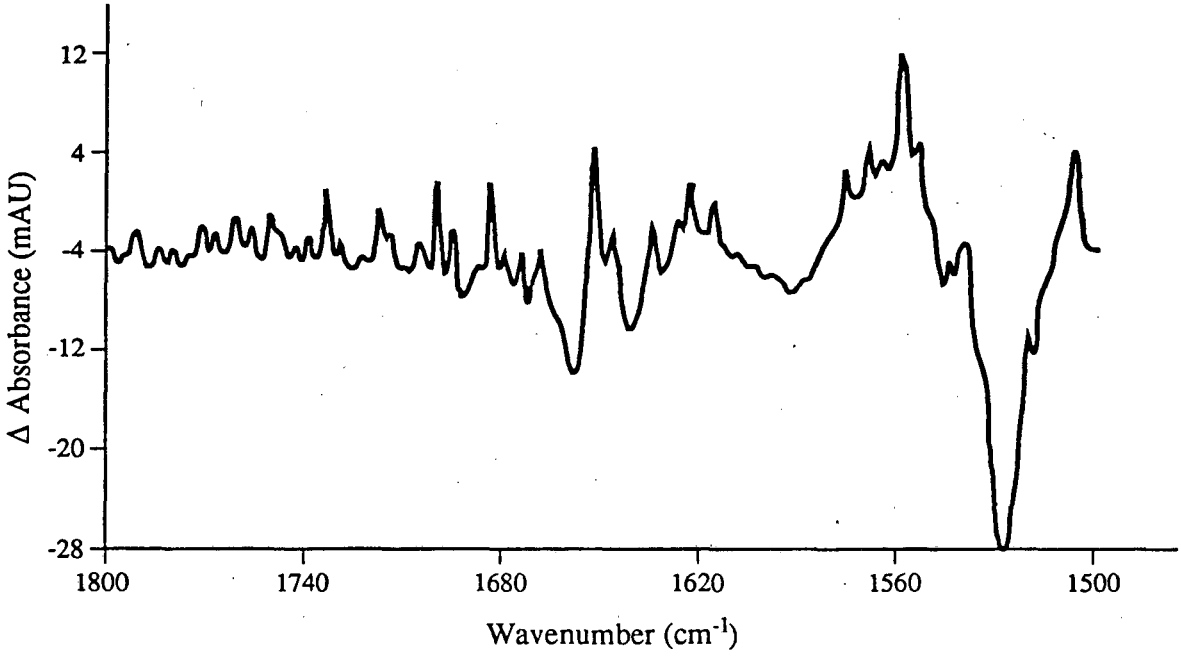
12
4
-4
-12
-20
-28
Δ Absorbance (mAU)
1800
1740
1680
1620
1560
1500
Wavenumber (cm-1)

XBL 921-4638

holes cut out for the cryostat and mirror to fit through. The perimeter was taped around the sample compartment. A hose was attached to an inhouse nitrogen gas line and connected to the inlet gas port on the Perkin Elmer 1600. With this arrangement, the amount of water vapor in the sample compartment was greatly reduced (See Figure 5.3.) But, due to the air movement caused by manual placement of the external mirror with each scan, there still remained a difference in the amount of water vapor present between the reference scans and the "M" scans--as judged by residual water vapor "spikes" in the difference spectrum.

The second method involves computationally subtracting the water vapor component from the difference spectrum. A 64-scan spectrum was made at low temperature under the same conditions as described in the protocol with one exception; there was no sample on the CaF_2 window. The importance of recording the spectrum at low temperature is that the baseline is temperature-sensitive. Figure 5.4 shows two examples of water vapor "templates" made at 260 K. Each of the many peaks always appears at the same wavenumber. Hence, the water vapor component cannot be averaged out by adding more scans as is accomplished with the random noise. The amplitudes relative to each other, however, will differ somewhat from scan to scan. (See Figure 5.4.) Using our VAX computers, the template is scaled (user-defined scale factor) and then subtracted from the difference spectrum. Scaling and subtraction is repeated until it is judged, by the smoothness of the resulting spectrum, that the best water vapor subtraction is

Figure 5.3 (a) 64-scan, FTIR spectrum of glucose-embedded PM between 1800 cm^{-1} and 1500 cm^{-1}. No purging of the sample compartment of the Perkin Elmer 1600 was attempted, although the cryostat was evacuated. Water vapor spikes clearly distort the Amide I and Amide II peak absorbances occuring at 1657 cm^{-1} and 1545 cm^{-1}, respectively. (b) 64-scan, FTIR spectrum of the same specimen recorded 60 seconds later, after the purging nitrogen gas was allowed to flow through the sample compartment. The water vapor spikes are greatly reduced.

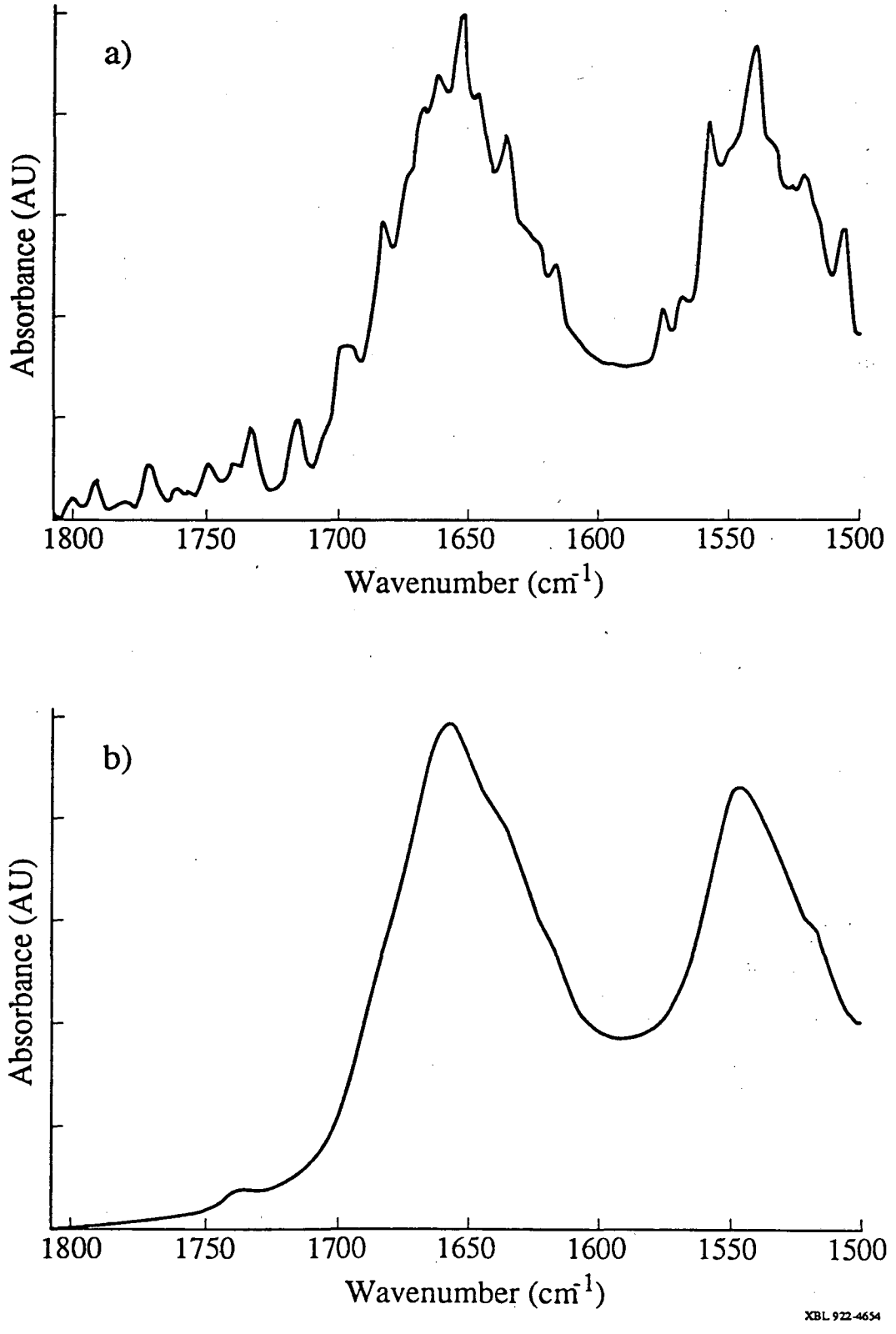
a)
Absorbance (AU)
1800
1750
1700
1650
1600
1550
1500
Wavenumber (cm-1)
b)
Absorbance (AU)
1800
1750
1700
1650
1600
1550
1500
Wavenumber (cm-1)
XBL 922-4654

Figure 5.4 (a) 64-scan, FTIR spectrum of water vapor spikes in the region, 1800 cm^{-1} to 1500 cm^{-1}, recorded at 260 K. The baseline is relatively flat. (b) A second example of a 64-scan spectrum of water vapor at the same temperature. The baseline is not as flat as that shown in (a). The relative amplitudes of prominent spikes differ slightly from (a) to (b).

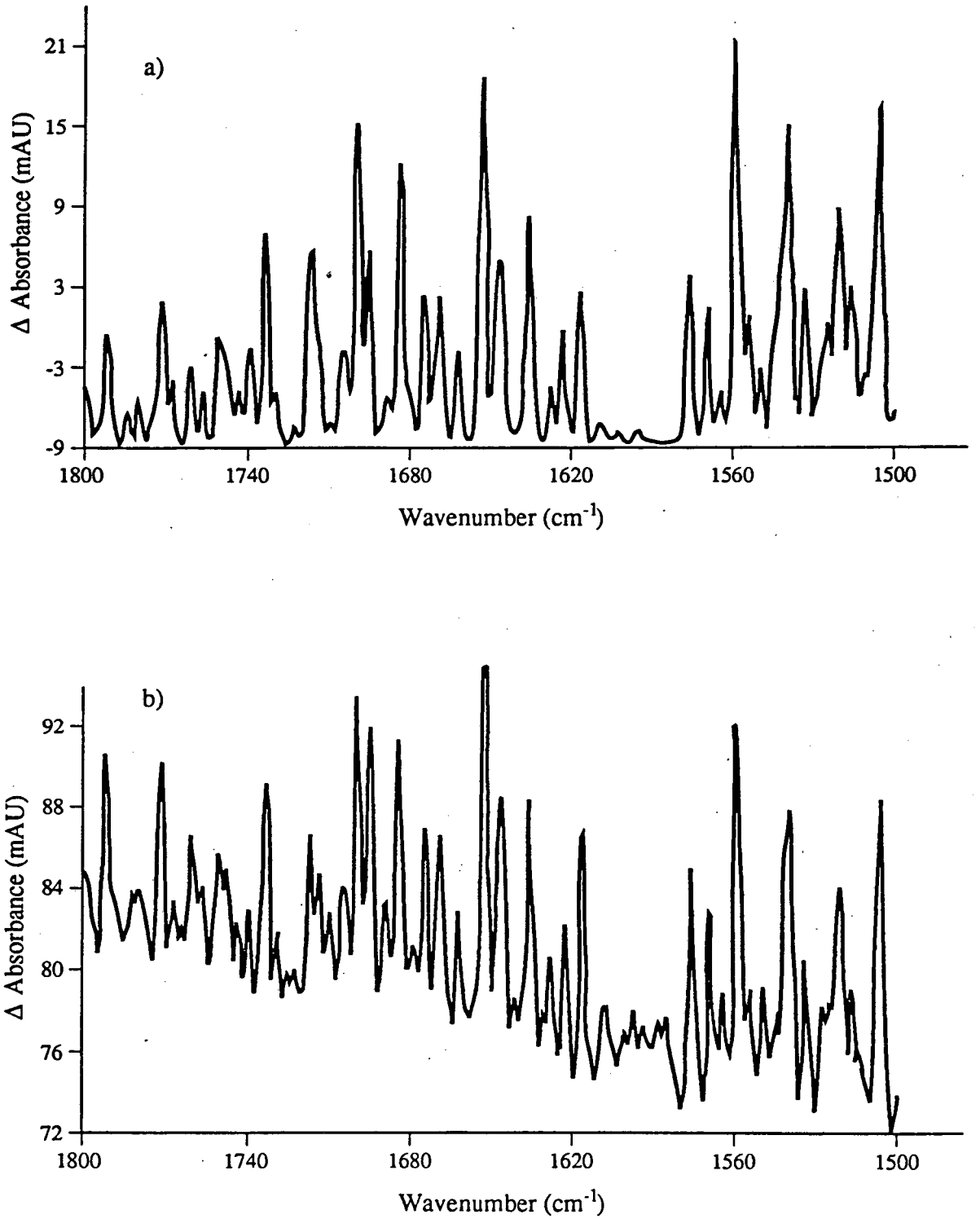
a)
Δ Absorbance (mAU)
21
15
9
3
-3
-9
1800
1740
1680
1620
1560
1500
Wavenumber (cm-1)
b)
Δ Absorbance (mAU)
92
88
84
80
76
72
1800
1740
1680
1620
1560
1500
Wavenumber (cm-1)

XBL 921-4636

accomplished. The computationally assisted subtraction of water vapor is imperfect because of the variation in water vapor peak absorbances between the template and the difference spectrum. Even so, nearly all of the water vapor component can be subtracted from the difference spectrum using this technique. (See Figure 5.5.) Of the two methods described for eliminating water vapor bands, the computational method was used ~ 75 % of the time since the rate of success was higher with the posterior elimination of water vapor rather than with the prior elimination of water vapor.

For glucose-embedded PM specimens prepared on CaF_2, it was found that an Amide I peak absorbance between 0.4 and 0.8 AU gave the best signal-to-noise ratio in the difference spectra. Absorbances above 0.8 AU exhibited shot noise that was due to a relatively small amount of IR light transmitted to the detector. (See Figure 5.6.) The signal-to-noise ratio is good in every region of interest in the difference spectrum except in the Amide I and Amide II peak regions, which have the highest absorbance (see Braiman et al., 1987; Figure 2). In this case, the solution to the problem is to average many thousands of scans together. The optimum optical density range will depend on the intensity of the IR source and the quality of the detector as well as the specimen thickness--i.e. the shot noise is instrument dependent. When the Amide I absorbance is below 0.4 AU, the signal in the difference spectrum is weak and many thousands of scans need to be averaged in order to distinguish small peaks (e.g., the aspartate region) from noise. When the Amide I peak absorbance lies between 0.4 and 0.8 AU, an adequate signal-

Figure 5.5 (a) 176-scan, difference FTIR spectrum of glucose-embedded PM in the light-adapted bR and M states, recorded at 260 K. Water vapor bands are present and obscure difference bands of interest. (b) Same spectrum after the water vapor component had been computationally subtracted. The subtraction was imperfect since a few water vapor spikes remain, though at a much lower amplitude. Structurally important difference bands are resolved.

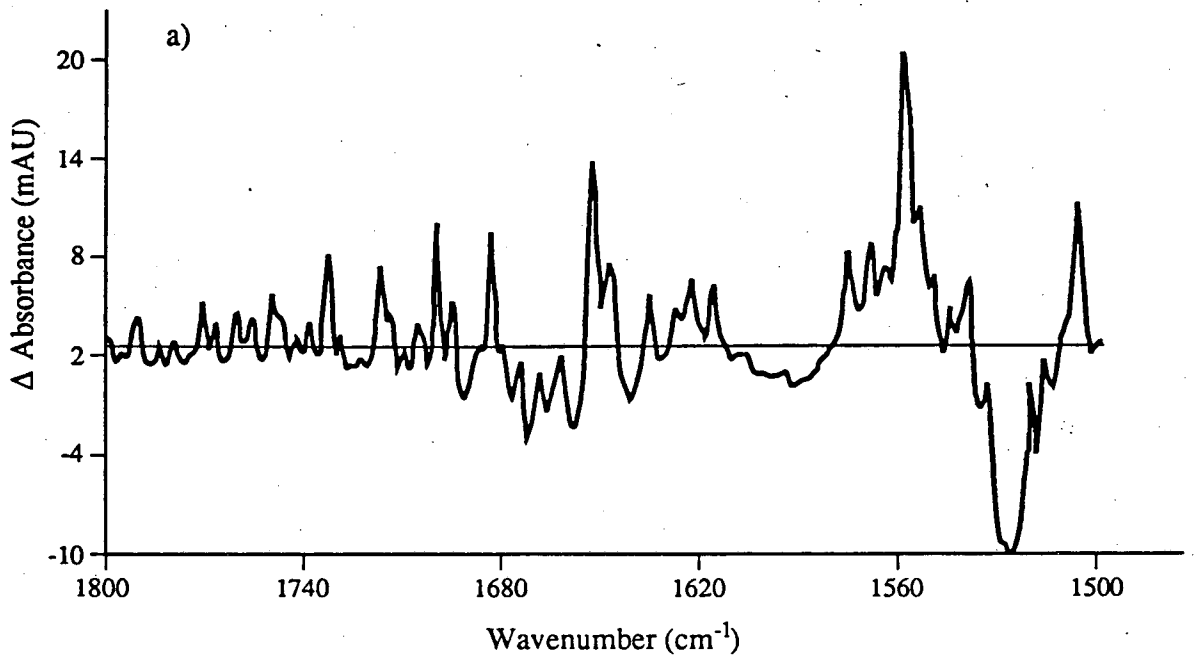
a)
20
14
8
2
-4
-10
Δ Absorbance (mAU)
1800
1740
1680
1620
1560
1500
Wavenumber (cm-1)

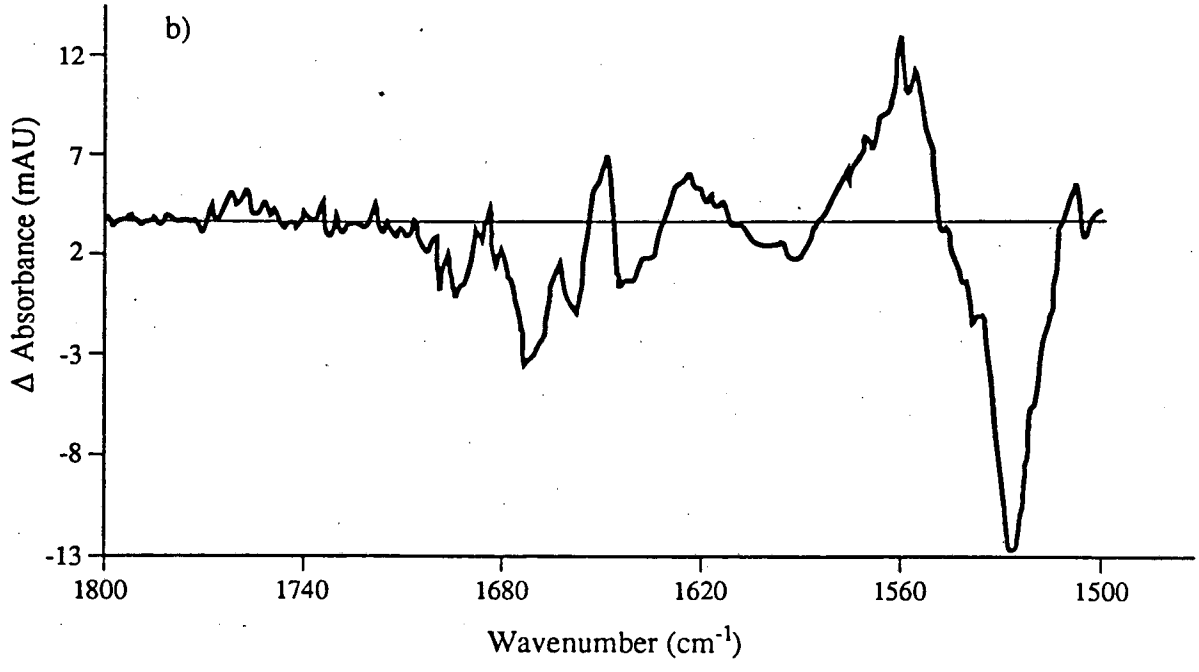
b)
12
7
2
-3
-8
-13
Δ Absorbance (mAU)
1800
1740
1680
1620
1560
1500
Wavenumber (cm-1)

XBL 921-4634

Figure 5.6 (a) 16-scan, IR absorption spectrum of glucose-embedded PM recorded at room temperature showing the Amide I and II absorbance peaks. The thin film optical density was more than twice that normally used to collect difference spectra. Scans were recorded after the Perkin Elmer 1600 sample compartment had been purged with nitrogen gas. Two such spectra were recorded in succession. (b) Difference spectrum calculated from the two spectra recorded in succession. In the wavenumber region, 1830 cm^{-1} to 1700 cm^{-1}, the noise level is low. The noise level is high where the absorbance is high, particularly close to the Amide I and II peak absorbances. The high shot noise level is unacceptable for M - bR difference spectra where the expected peak absorbances are as low as a few mAU. Cutting the spectrum optical density by half greatly improves the signal-to-noise ratio.

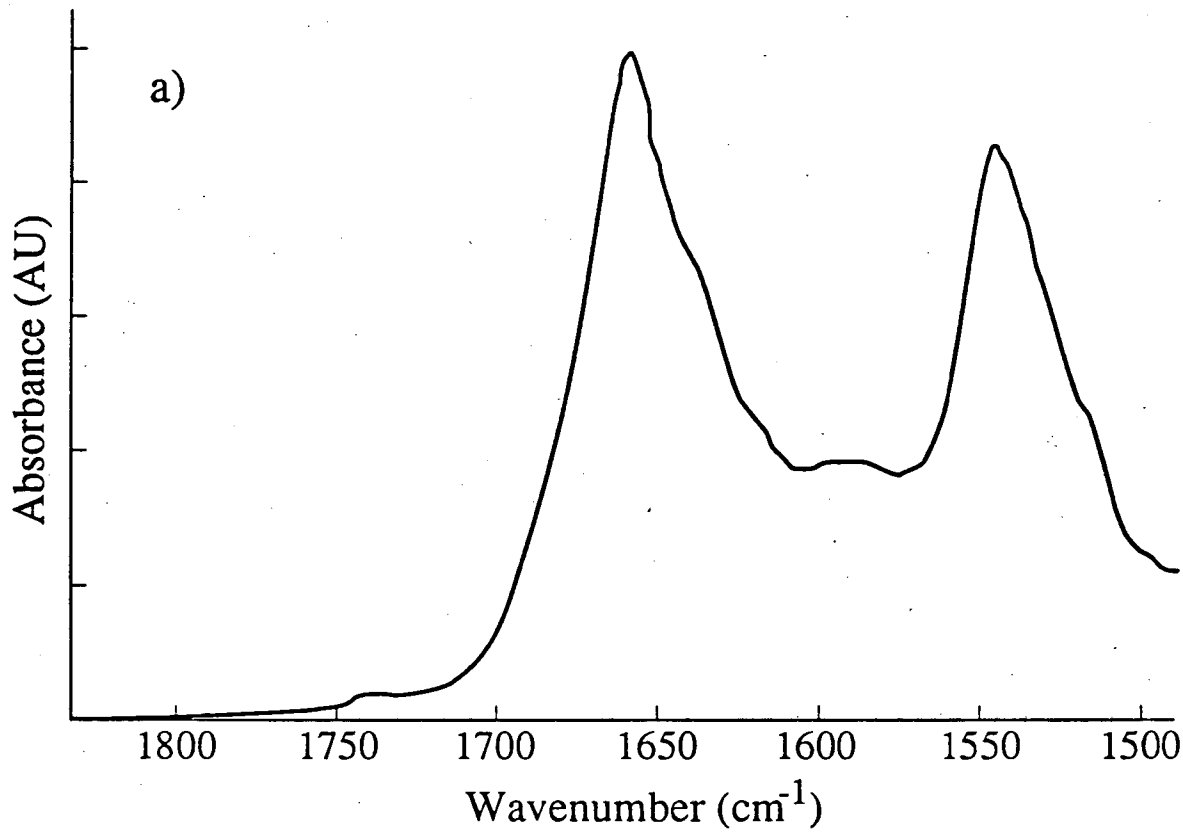
a)
Absorbance (AU)
1800
1750
1700
1650
1600
1550
1500
Wavenumber (cm-1)

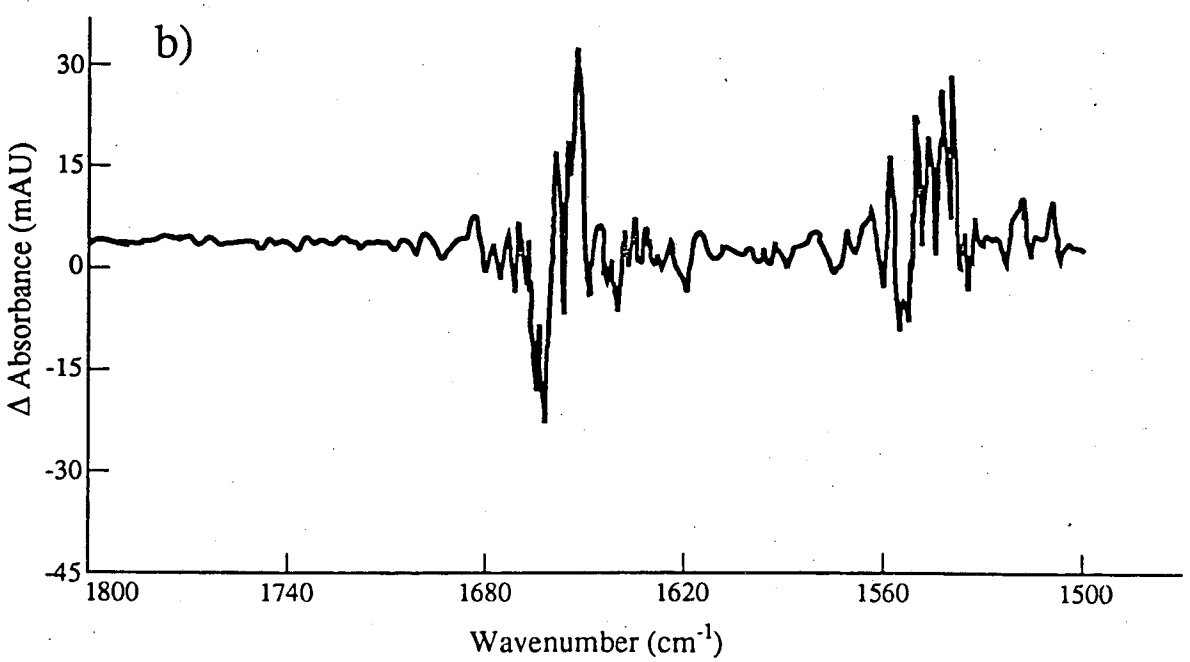
b)
30
15
0
-15
-30
-45
Δ Absorbance (mAU)
1800
1740
1680
1620
1560
1500
Wavenumber (cm-1)

XBL 922-4656

to-noise ratio in the difference spectrum is observed with an average of 1000 to 2000 scans. (See Figures 6.2 and 6.3).

Assuring that the specimen is not moved during and in-between IR measurements is critical in order to ensure that the bands seen in the difference spectrum are not artifacts of the IR beam passing through a different area of the specimen. New specimen areas could have different thicknesses. The IR beam could pass through the specimen at a different angle than before giving a different projected thickness. My protocol allowed the reference and "M" spectra to be recorded without handling the sample.

It is important to maintain a constant atmosphere in the sample compartment, both inside and outside of the cryostat. The environment inside the cryostat is more reproducible. A constant vacuum can be maintained. The vacuum pump was in operation continuously in order to replicate the environment surrounding the specimen for the "M" scans as well as for the reference spectrum. Continuous operation of the pump was advised because a slow leak was always observed. For example, after the pumping had been stopped, it took ~ 5 minutes for the vacuum to change by 40 mTorr.

A heat shield was devised to protect the specimen from unwanted heat emanating from nearby equipment. It was noticed that the close proximity of the vacuum pump to the IR cryostat resulted in an exchange of heat from the pump to the specimen. After the pump had been running for several minutes, the sample

temperature was raised by a few degrees. A simple heat shield, made from aluminum foil was inserted between the pump and cryostat. This eliminated the problem of heat transfer between pump and specimen.

I tested the wavenumber calibration of the Perkin Elmer using the well-characterized sharp peaks of polystyrene. The Sigma Library of FTIR Spectra provided an accurate wavenumber determination of polystyrene peak # 5. Using a thin sheet of polystyrene, a 16-scan spectrum was recorded at 2.0 cm^{-1} resolution. The "peak-finding" option on the Perkin Elmer accurately determined peak # 5.

Polystyrene peak # 5	
Sigma Library	1601.4 cm^{-1}
Empirical	1601.1 cm^{-1}.

It is seen that the wavenumber calibration is excellent and certainly within the resolution limit.

The relationship between apodization and spectral noise was investigated. The Perkin Elmer 1600 has the option of strong Norton-Beer apodization, weak Norton-Beer apodization or no apodization. When one examines the Fourier transform pair that relates the interferogram to the spectrum, it is seen that in order to obtain a complete spectrum, the integration must be performed over retardation values ranging from minus infinity to plus infinity. But, the internal mirror can only travel a finite distance. If the retardation ranges from $-\Delta$ cm to $+\Delta$ cm, then the interferogram is

effectively set to zero for all retardations greater than Δ and less than $-\Delta$. This amounts to boxcar truncation. The price paid for finite retardation is the loss of high-resolution information from the extremes of the interferogram. For example, take the case of a single, infinitely narrow emitting line source, i.e. a delta function. The interferogram of this "ideal" spectrum is an infinitely long cosine wave. Because the Fourier transform of the boxcar function is the sinc function, the delta-spectrum becomes a sinc-spectrum. The infinitely narrow line takes on width and acquires positive and negative side lobes. This phenomenon is known as ringing. In order to minimize ringing, the interferogram is usually multiplied by an apodizing function. Apodization can affect the noise level caused by false lobes. Strong Norton-Beer apodization will dampen ringing more than weak Norton-Beer apodization. Because of this, I decided to always use the strong Norton-Beer apodization function.

There were two opposing needs that surfaced in my work. One was a need to follow spectroscopically the manner in which M decays to bR. The 1669 cm^{-1} Amide I band behaves differently as a function of time at the two temperatures, 240 K and 260 K, in M - bR spectra (Ormos, 1991); it grows at 240 K, yet diminishes at 260 K as M decays. The other need was to collect difference spectra with a low noise level in order to unequivocally observe small bands, e.g. the aspartate bands. Initially, I designed the temporal spacing of my FTIR experiments to closely follow those of Ormos (1991). By using a quasi-logarithmic time scale, he obtains good separation between each of ten superimposed spectra. (See his Figure 1.) However,

because the Perkin Elmer 1600 that I use is remarkably slower than the Mattson Sirius that Ormos uses, the number of scans I can include with the calculation of each spectrum is much reduced. For example, at ~ 1000 seconds after M excitation, Ormos' spectrum consists of 1280 scans, whereas mine can have at most 256 scans. The number of scans, N, per spectrum affects the signal-to-noise ratio as $\sqrt{N}$. Because of the low signal-to-noise ratio in the difference spectra consisting of 4 or 16 scans, I was forced to forego the plan to record difference spectra as a function of time. Instead, I focused on averaging a thousand or more scans all recorded within 30 seconds after turning off the actinic light, in order to reduce the noise. I collected spectra 4 scans at a time. The first scan was initiated immediately after cessation of the actinic light with successive scans following right after the previous scan. The final spectrum has an effective time resolution of ~ 15 seconds.

Small inorganic marker molecules were used in an investigation to determine if the glucose IR bands could be eliminated from the spectrum in the same manner that water vapor bands are. By knowing the concentration of marker and glucose, the contribution of glucose to the spectrum can be subtracted. This requires an IR template spectrum of glucose and marker in the same relative concentration as used with the PM plus glucose plus marker specimens. The template spectrum would be scaled and subtracted from the PM specimen until the marker peak disappeared from this spectrum. In this way, the glucose spectrum can also be eliminated from the PM spectrum. The criteria I established for useful IR

marker molecules are as follows. First, a molecule's IR spectrum had to have a sharp peak in a wavenumber region devoid of any PM, water and glucose bands. This meant that it had to lie in the 2300 - 1900 cm^{-1} region. Second, it could not interact with PM to change the spectrum. Certainly, hydrophobic molecules which can partition into the membrane would not work. Upon searching through a catalog of IR spectra, I found that several cyano-compounds satisfied the first criterion. I made trial specimens with three candidate compounds prepared at various concentrations. Potassium cyanate worked well with glucose. A useful peak for glucose subtraction was observed with as little as 0.03 % (by weight) potassium cyanate. By recording spectra of thin films of hydrated, glucose and potassium cyanate specimens, it was determined that the sharp peak at 2166 cm^{-1} was displaced from the 2163 cm^{-1} peak recorded with 97 % pure potassium cyanate (Sigma Library of FTIR Spectra). I anticipated no problems due to this small wavenumber shift and proceeded to prepare hydrated specimens consisting of PM, glucose and potassium cyanate. However, when PM was added to the mixture, the marker peak disappeared, even with a high concentration of cyanate, 1.75 %. Clearly, the cyanate was interacting with the PM. The same results were observed with potassium ferricyanide. Perhaps, ionic molecules interact with the membrane to the extent that their spectral signatures are greatly changed. On the other hand, cyanomethyl-1-thio-galactopyranoside satisfied both criteria and the marker peak appeared where expected, i.e. at 2253 cm^{-1}.

Figure 5.7 shows a 16-scan spectrum of a hydrated specimen comprised of PM and glucose and "cyano-galactose" marker. The concentration of marker was .3 % (by weight in solution). The 2253 cm^{-1} peak is noticeable in Figure 5.7a. Figure 5.7b shows a blow-up of the marker peak region. The amplitude of this peak is clearly measurable. Reducing the "cyano-galactose" concentration by roughly 50 % so that the marker concentration is a tenth that of the glucose concentration would also give a usable peak. In order to use this IR marker molecule, however, diffraction patterns of EM specimens prepared with the same concentrations of PM, glucose and marker as used in the FTIR studies would need to be recorded to document that this mixture diffracts as well as "pure" glucose-embedded PM samples. Even though it is unclear how a galactose compound would affect the hydration-preserving properties of glucose, the low relative concentration of "cyano-galactose" marker to glucose (10 %) would predict the likelihood of obtaining excellent diffraction patterns. This compound remains a candidate for glucose-subtraction and may be valuable for future work.

The CaF_2 windows were cleaned with detergent and/or heptane. Detergent was sufficient to clean off the glucose and PM. But, heptane was necessary in order to clean off the high-vacuum grease that had been spread around the perimeter of the windows. Distilled water was used in order to avoid the unknown solutes present in tap water.

Figure 5.7 (a) FTIR spectrum of PM embedded in glucose with an organic, IR marker molecule. The thin-film specimen consisted of 1.95 % glucose, .55 % PM and .3 % cyanomethyl-1-thio-galactopyranoside. The spectrum is comprised of 16 scans. The marker molecule has a sharp peak at 2253 cm^{-1}. Scanning was accomplished at room temperature. The sample compartment was not purged, hence sharp water vapor bands are observed between 1950 cm^{-1} and 1350 cm^{-1}. The tremendous noise fluctuations seen in the strong, broad Amide A band, 3600 cm^{-1} to 3100 cm^{-1}, are due in part to the high specimen absorbance in that band and due in part to water vapor bands; though the former far outweigh the latter. Water absorbs strongly in the Amide A region, hence, the height of this band relative to the Amide II band is an indicator of the extent of specimen hydration (Braiman et al., 1987). The ratio noted here is typical for specimens hydrated at 81 % relative humidity. The multitude of bands below 1500 cm^{-1} are glucose bands. Glucose absorbs strongly between 1150 cm^{-1} and 1000 cm^{-1}. (b) A close-up of the wavenumber region surrounding the 2253 cm^{-1} absorbance peak. The peak amplitude can be clearly determined above the noise level.

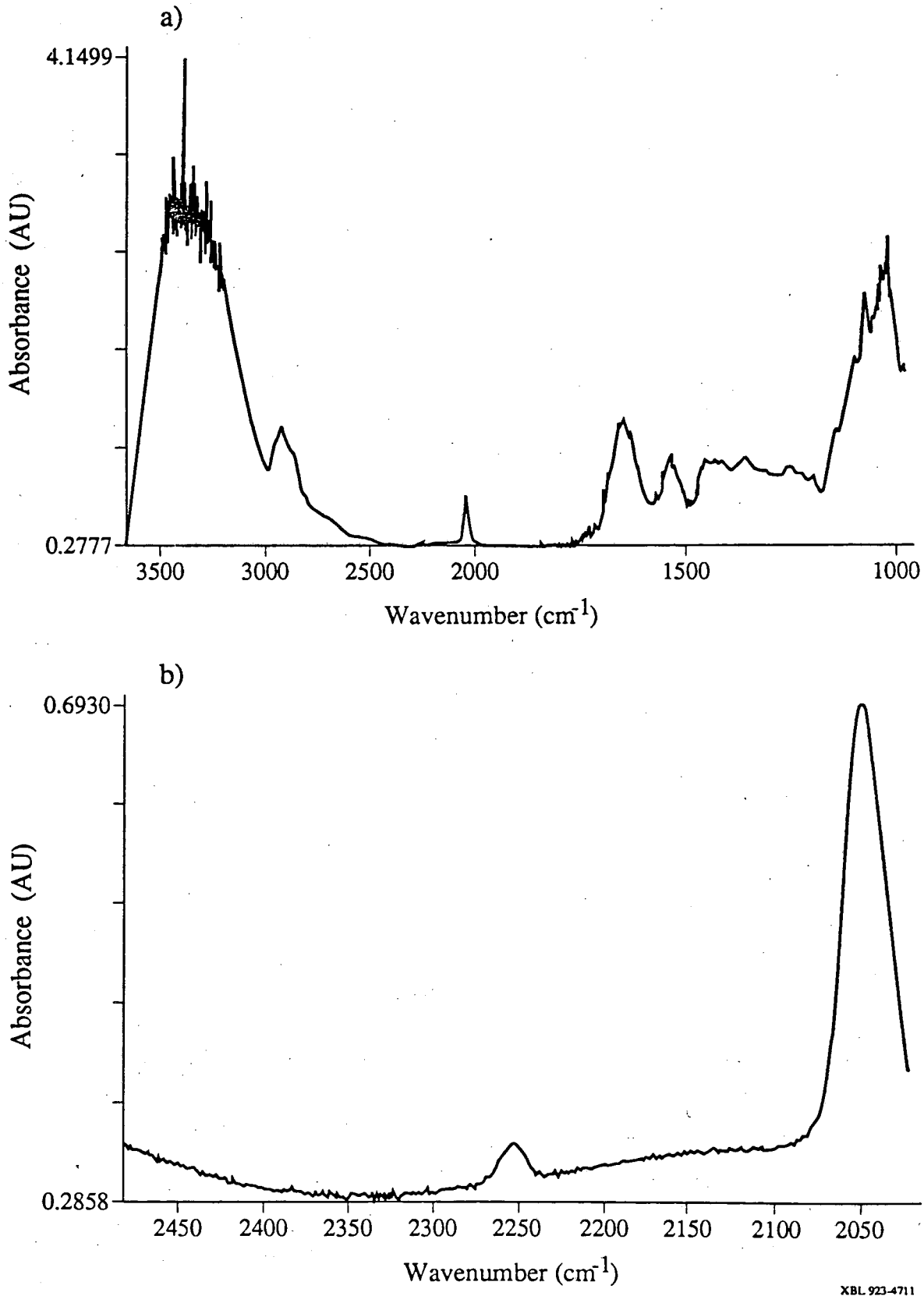
a)
4.1499
0.2777
Absorbance (AU)
3500
3000
2500
2000
1500
1000
Wavenumber (cm-1)
b)
0.6930
0.2858
Absorbance (AU)
2450
2400
2350
2300
2250
2200
2150
2100
2050
Wavenumber (cm-1)
XBL 923-4711

Programs

CURVY84 in conjunction with TX84 is a flexible plotting program when using a Tektronix emulator window on a VAX. I found it prudent to modify the software so that from left to right the horizontal axis goes from high to low wavenumbers. It is traditional in the IR community to present spectra left to right from high to low wavenumbers--far be it for me to buck tradition. My spectra, like Ormos' (1991) spectra, run from 1800 to 1500 cm^{-1}. I created a COMMAND file to run my version of CURVY and called it CURVY.COM.

Since the Perkin Elmer has no disk drive, and until the last few months of data collection had no internal board to transfer data to a computer, an innovative design was required to transfer digital data. Initially, a general utility program to transfer data between computer operating systems, BITCOM, was used to capture FTIR spectra. Rick Burkard established a protocol to transfer data from the Perkin Elmer to an IBM PC in the physical chemistry teaching lab. After the data were copied to a floppy disk, a PC (either a Zenith in the Glaeser lab or an IBM in the biophysics teaching lab) was used to transfer the data to our VAX computers. Another general utility program, KERMIT, was used to transfer data from the PC to the VAX. In order to avoid misplaced bits in data transfer, a slow baud rate of 1200 was critical when going from the Perkin Elmer to the PC. By contrast, a baud rate of 19200 was used between the PC and the VAX. Rick Burkard wrote a program, FTIREAD, specific for spectra transfer from the Perkin Elmer to a PC. Data are transferred in

binary format. It has the advantage of chopping off the long header while copying only the data. Hence, computer disk space is saved--a plus with the 100 and more spectra saved on disk.

After spectra are transferred to the VAX, the data are run through a number of Fortran programs (Organick & Meissner, 1974) to properly scale the information, computationally subtract water vapor bands, create difference spectra, and plot spectra. Initially, FTIREAD was designed to only capture the data as it was being sent from the Perkin Elmer 1600 to an IBM PC. I created a program, FTIRDEC, that detected where the variable header information ended and the binary data began. It converted the data from binary to decimal format and also scaled the data to its original real format. This is necessary because the Perkin Elmer1600 converts all real data to large integers before it transfers them to peripherals or other computers--it is easier to deal with integers when coding in binary and the large numbers assure that no significant figures are lost. Later, Rick Burkard created CAPREAD, that does what FTIRDEC did, but without the conversion to reals. Afterwards, it was incorporated into FTIREAD. Thus, by the time the data arrived at the VAX, the spectra were ready for storage and manipulation. After the upgrade board was installed, the possibility of creating and displaying a difference spectrum on the 1600 became available. FTIRABS was the corresponding program on the VAX that allows digital manipulation and display of such a difference spectrum. To investigate noise levels and to separate noise spikes from water vapor spikes, two programs were created. FTIRNON provides a look

at the raw spectrum in a non-water-spike region, 2300 cm^{-1} to 2000 cm^{-1}, and FTIRDIFFNON provides a look at the difference spectrum in the same wavenumber region. No water vapor bands appear in this flat, low-absorbance region. Hence the noise level can be compared with the noise level and water vapor spikes in the 1800 cm^{-1} to 1500 cm^{-1} region. With the improved version of FTIREAD, the first program a raw spectrum normally sees is FTIRRES, which simply partitions the integers into the right arrays and scales them. After the reference and "M" spectra are run through FTIRRES, the difference spectrum can be generated by FTIRDIFFRES. A header is tacked onto the data, that is now truncated to the wavenumber range of interest, i.e.1800 cm^{-1} to 1500 cm^{-1}, that instructs the plotting routines. My version of CURVY is next run and either TX84 or LW84 is run to plot the spectrum on the terminal window or paper, respectively. LPR is the DCL command used to obtain a plot from the laserprinter.

VAPORRES is the program designed to subtract water vapor bands. It works on either the reference spectrum or the "M" spectrum. The philosophy behind the program is straightforward. A water vapor "template" spectrum is scaled and subtracted from one of the raw spectra until the water vapor components in both spectra are roughly equal. This may require several iterations of the sequence: VAPORRES, FTIRDIFFRES, CURVY and TX84. Figure 5.5 shows how successful this approach can be. The water vapor subtraction in individual spectra can become tedious, however. VAPORAVE was created to subtract the water vapor component from

averaged difference spectra. It differs form VAPORRES in that the template is subtracted from a difference (not raw) spectrum. Essentially, this program saves time. Many hundreds of 4-scan spectra contaminated with water vapor spikes can first be averaged and then the resultant difference spectrum can be processed through VAPORAVE.

Adding spectra together in order to average and scale data is performed routinely. At times, it is expedient to scale spectra. For example, spectra that have been added together on the 1600 may need to be scaled once on the VAX in order to make the absorbance range consistent. Likewise, the background may need to be scaled. The program that does this is FTIRSCALE. The program that averages spectra together is called AVERAGERES.

All of the aforementioned Fortran programs work with 2.0 cm^{-1} resolution spectra only. Each such spectrum contains 3951 data points calculated at each wavenumber between 4400 cm^{-1} and 450 cm^{-1}. Sampling theory dictates that exact recovery of 2.0 cm^{-1} resolution spectral information requires sampling at wavenumbers separated by no more than 1.0 cm^{-1} (Goodman, 1968).

Since some of the data presented in this dissertation were made with 4.0 cm^{-1} resolution, I list the relevant Fortran programs and comment briefly on salient differences. Most of the program names are similar to their higher-resolution counterparts.

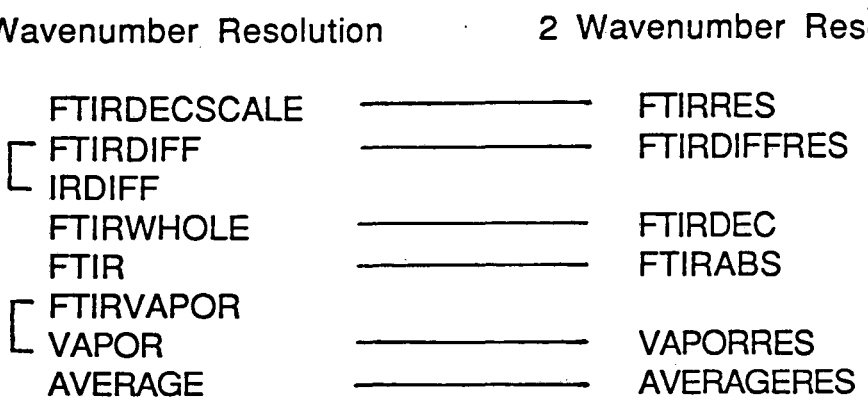

IRDIFF supplements FTIRDIFF by plotting the difference spectrum over the entire wavenumber range, i.e. 4400 - 450 cm^{-1}. The purpose of FTIRVAPOR is to provide a close-up view of a water-vapor corrected spectrum in the flat and gently sloping 1800 cm^{-1} to 1770 cm^{-1} region. This wavenumber region in the difference spectrum gives a good view of several water vapor spikes without any PM bands. It is easily seen when the peaks in this 30 cm^{-1} region flatten indicating successful water vapor subtraction. One drawback to this approach is that "perfect" subtraction in this small wavenumber region may not give "perfect" subtraction in all wavenumber regions, because water vapor peak absorbances will vary slightly from spectrum to spectrum. Hence, when computationally subtracting water vapor from my difference spectra, I found it more useful to examine the entire region and choose a scale factor that gave the "cleanest" spectrum. This meant that small water vapor peaks remained in some regions in order to eliminate the water vapor component in structurally more important regions, e.g. Amide I.

Perkin Elmer generously provided an upgrade board for the 1600 after I discussed my experiments with the sales rep and indicated my need for further instrument capability. In fact, the upgrade board was crucial to the success of my averaging scheme. Were it not for the ability to add scans together on the 1600, the task of adding several thousand scans four at a time would be prohibitive. Besides adding spectra, this board provides the following capabilities, among many, that I have used in my experiments. The DIFF software creates a difference spectrum in a new storage register. I found it handy to peek at difference spectra whenever I desired instead of going through the entire rigmarole of programs to arrive at a difference spectrum--no more surprises in the outcome! A number pad is available for inputing numbers and performing simple mathematical functions, e.g. multiplication, division. I found it useful when commanding the instrument to take a non-standard number of scans and for scaling and averaging spectra. The FLAT software will perform up to fourth-order flattening of the spectrum in a user-defined region. I found it to be unwieldy when flattening the baseline and liable to modify the spectrum in undesired ways, e.g. peaks higher or lower than they should be, if one is not very careful. Fortunately, only a few of my baselines required correction. (See Figure 5.8.) The SMOOTH software performs as its name implies; it will eliminate the high-frequency component from the interferogram which results in noise reduction and feature smoothing in the spectrum. Since the level of random noise is very low in my spectra averaged from hundreds of scans, I would only use SMOOTH on the residual water vapor spikes. SMOOTH requires the

Figure 5.8 (a) 64-scan, FTIR difference spectrum recorded at 260 K. The "sag" in the middle is due to the baseline (b), which was recorded after the 64 "M" scans. (c) Difference spectrum after the baseline was corrected. The correction entailed computationally subtracting the baseline from the original spectrum. I found that the baseline is not always stable, and sometimes becomes "warped" over time.

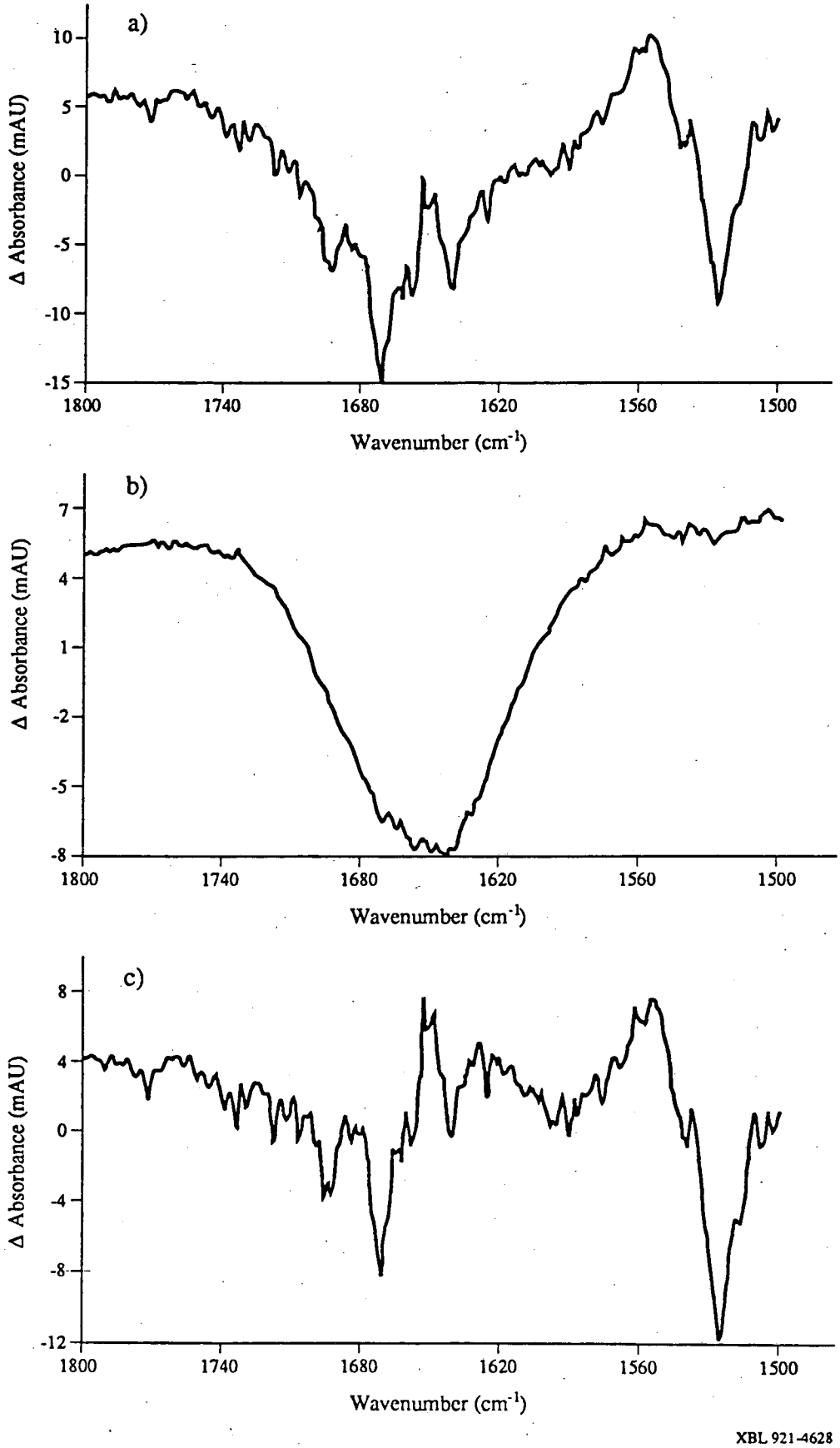
a)
10
5
0
-5
-10
-15
Δ Absorbance (mAU)
1800
1740
1680
1620
1560
1500
Wavenumber (cm-1)
b)
7
4
1
-2
-5
-8
Δ Absorbance (mAU)
1800
1740
1680
1620
1560
1500
Wavenumber (cm-1)
c)
8
4
0
-4
-8
-12
Δ Absorbance (mAU)
1800
1740
1680
1620
1560
1500
Wavenumber (cm-1)

XBL 921-4628

user to input the width of the feature to be distinguished. I found that the width of most of the water vapor spikes was comparable with certain features in the difference spectrum peaks that I wished retained, e.g. conformational marker bands in the Amide I region. Hence, my spectra were not SMOOTHed.

The upgrade board had the capability of running user-created programs. These programs are METHOD files which consist of a list of commands that the instrument executes at the touch of a button. Alphanumeric fields describe the sequence of commands and are stored even when the power is off (unlike spectra). A METHOD file that follows the time-course protocol for recording difference spectra was created to greatly simplify the spectrometer operating procedure.

"Things That Can Go Wrong"

Since the IR cryostat has an extra opening to the chamber that is normally evacuated when scanning, I investigated the possibility of humidifying specimens right in the cryostat holder. This idea was proposed during the months when the specimen was not sandwiched between two windows, leaving one face exposed. Even though the use of two windows predominates in FTIR studies, I chose initially to leave one specimen face exposed in order to more closely approximate the protocol used to prepare specimens on EM grids. The opening to the cryostat has a diameter of 20 mm where I attached a short hose leading to a reservoir of saturated ammonium

sulfate solution. This arrangement avoids the potential pitfall of changing specimen hydration during the ~ 10 minutes it takes to transfer the specimen from the hydrator to the cryostat and the additional time spent cooling the specimen to a temperature where water loss is negligible. Once the specimen is hydrated, the hose can be disconnected and the ground glass joint stopper can be replaced in a matter of a few seconds. The specimen can be cooled to less than 0 °C before the vacuum pump is started. Hence, one is more confident that the hydration level remains constant with this arrangement. The problem with this arrangement, though, is that the atmosphere over the reservoir is not transported effectively into the cryostat. In fact, when I replaced the saturated salt solution with distilled water and detached the tube from the cryostat so that the reservoir was exposed to the ambient atmosphere, no change in the water level was observed after three weeks. After the failure of the external reservoir, I thought that an internal reservoir might be fruitful. I placed a small reservoir of saturated ammonium sulfate solution inside the cryostat. But, of course, when I attempted to evacuate the chamber, the solution flew everywhere.

The unfruitful hydration results induced me to seek to maintain a constant specimen hydration level by sandwiching the specimen between two CaF_2 windows, the edges being coated with high-vacuum grease--even though this would differ from specimen preparation on EM grids. Care must be taken so that the grease does not come in contact with the specimen, as the grease solubilizes PM. This deviation from EM protocol is justified since it is thought that

there will be no water loss in the vacuum of the electron microscope anyway because the sample will be maintained at liquid nitrogen temperature. Furthermore, specimen preparation for the electron microscope can be accomplished in a glove box under a controlled high humidity until the grid is plunged in liquid nitrogen.

The Perkin Elmer 1600 available for my use had the irritating problem that the internal mirror would catch on a wire. The result is that the retardation is off so that when the Fourier transform of the interferogram is calculated, periodic spikes would dominate the spectrum. Figure 5.9 shows a 4-scan spectrum where in only one scan the mirror caught on the wire. Clearly this spectrum is unusable. Trouble with the mirror is unpredictable and is evident in only ~ half of the spectra taken. In order to free the mirror, the machine had to be tapped one or more times; then the next spectrum recorded would appear normal. Since the difference spectrum resembled that of Ormos (1991), I assumed that there was no residual error due to a possible mirror misalignment caused by rubbing against the wire or tapping the housing. I kept a rubber mallet at the side of the instrument and whenever I saw a spectrum like the one in Figure 5.9, I would lightly hit the cover housing the mirror assembly. Of course, such spectra were immediately deleted from the storage register. The solution derived for this problem was unsatisfactory but, in the absence of a service contract, deemed manageable--it simply took me twice as long to collect usable spectra--an unfortunately necessary approach.

Figure 5.9 4-scan, FTIR spectrum of glucose-embedded PM. In the first of 4 scans, the internal mirror assembly caught on an adjacent wire. The other three scans were normal. The wild noise fluctuations seen are thus due to a quarter of the scans. This problem occured with roughly half of the recorded spectra.

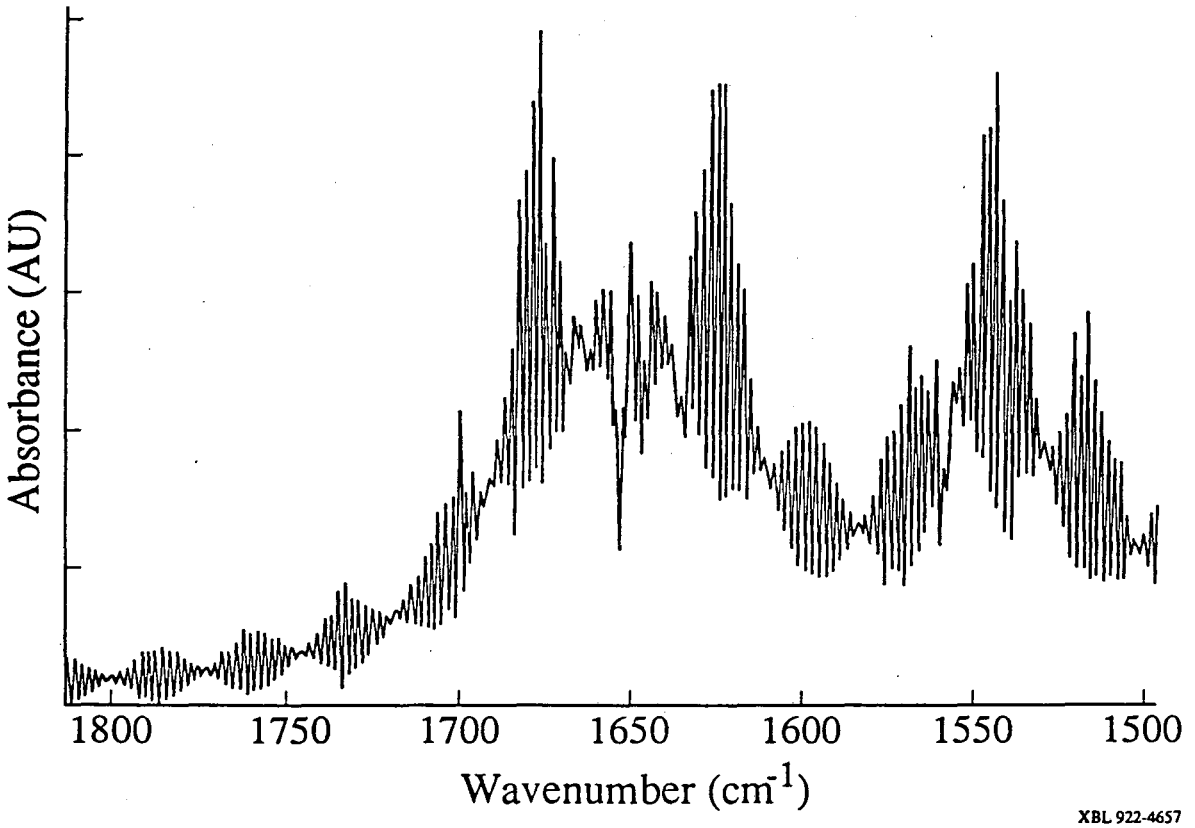
Absorbance (AU)
1800
1750
1700
1650
1600
1550
1500
Wavenumber (cm-1)
XBL 922-4657

I noticed that peaks in the important Amide I region of the difference spectra I collected appeared more "pointed" with different relative amplitude ratios than expected. (See Figure 5.10.) I was concerned that these phenomena could result from the spectral sampling using the resolution I chose. (Ormos used 2.0 cm^{-1} resolution.) Initially, I collected 4.0 cm^{-1} resolution data exclusively because of the faster available scan times. It takes ~ 7 seconds per scan at 2.0 cm^{-1} resolution, but only ~ 4 seconds per scan at 4.0 cm^{-1} resolution. 4.0 cm^{-1} resolution spectra have 1976 data points each. After examining Ormos' difference spectra, I determined that no bands of interest would become unresolved if I used 4.0 cm^{-1} resolution. In addition, the number of scans would be double what I could collect with 2.0 cm^{-1} resolution given the time constraints governed by Ormos' protocol (1991). Despite the justification for 4.0 cm^{-1} resolution, 2.0 cm^{-1} resolution spectra may be more useful. I investigated 2.0 cm^{-1} resolution spectra and found that the "pointiness" was diminished, but that the relative amplitude ratios did not change much. (I discovered later that the bands in question depend on the specimen hydration state.) Shortly thereafter, I abandoned the goal of collecting time-course spectra, and instead focused on averaging many scans together to improve the signal-to-noise ratio. Since the question of the effects of scanning speed and resolution was now moot, I collected the remaining data at 2.0 cm^{-1} resolution.

Initially, large KBr windows (50 mm in diameter) were used as end windows for the IR cryostat. These windows proved inadequate

Figure 5.10 8-scan, M - bR spectrum taken at 260 K. Resolution was 4.0 cm^{-1}. The 1669 cm^{-1} and 1658 cm^{-1} negative conformational marker bands exhibit amplitudes lower than expected. (See Figure 6.3.) These two peaks in particular appear more "pointed" than those recorded with 2.0 cm^{-1} resolution, and the ratio of 1669 cm^{-1} to 1658 cm^{-1} is low. There also appears an unusual "spike" on the 1560 cm^{-1} ethylenic band.

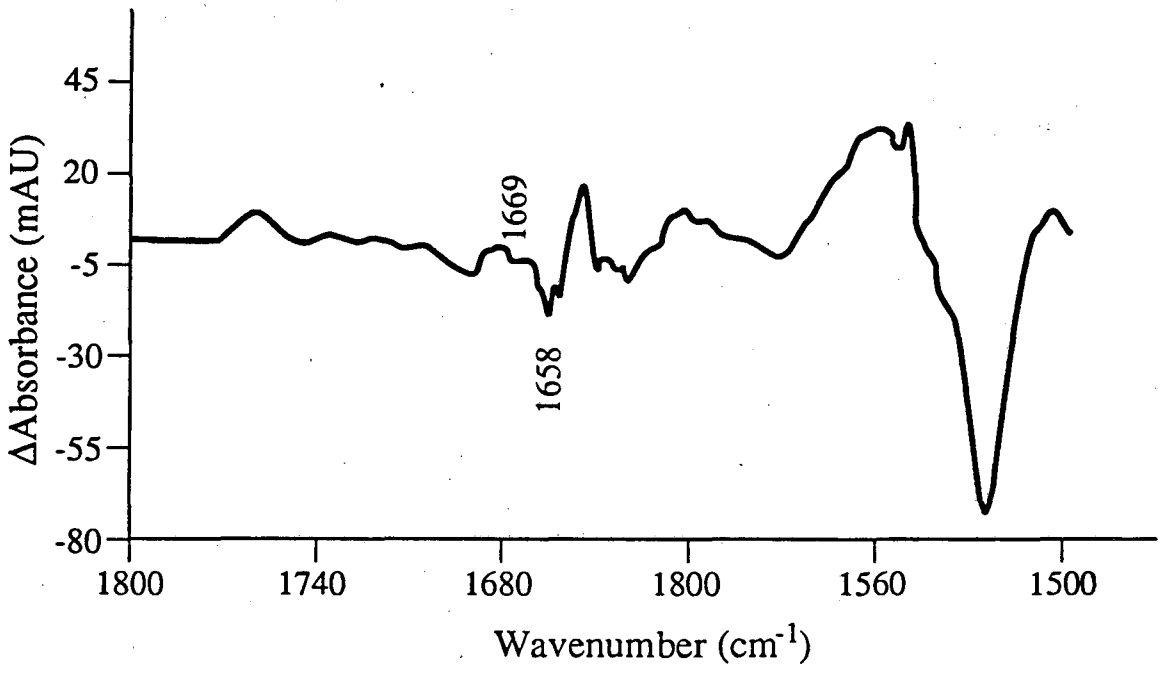
45
20
-5
-30
-55
-80
ΔAbsorbance (mAU)
1669
1658
1800
1740
1680
1800
1560
1500
Wavenumber (cm-1)

XBL 921-4631

for two reasons. The first is that clear KBr crystals slowly dissolve under ambient humidities--this "fogs" the window which affects the background absorbance. Storage with a dessicant in a closed chamber is necessary between sessions. Also, from time-to-time, surface polishing is needed to clear off the opaque KBr that had dissolved. Second, a crack (caused by vacuum pressure) developed in one of the windows. KBr crystals are subject to stress fractures. Because of these problems, smaller CaF_2 windows (25 mm in diameter) were substituted. The smaller windows were centered in an aluminum endplate and held in place with an O-ring coated with high-vacuum grease. With this arrangement, the problems associated with KBr windows were ended.

Initially, specimens prepared on CaF_2 were dried with air pumped through a dessicant (Earnest et al., 1986). But, this technique was abandoned in favor of the one used to dry glucose-embedded PM on mylar because the optical density was not uniform with air-pumped drying.

Chapter 6

DIFFERENCE FTIR SPECTROSCOPY SHOWS THAT M_1 CAN BE TRAPPED SEPARATELY FROM M_2

Difference FTIR Spectra at 240 K and 260 K

My difference infrared data provide evidence that the protein conformational change purported to occur between the M_1 and M_2 states is partially blocked when PM is dehydrated. I find that dehydrated infrared specimens "trap" predominantly M_1 instead of M_2 at 260 K. If the PM sample is well-hydrated, however, the M_2 intermediate in the bR photocycle (along with some N intermediate) can be "trapped" at 260 K (Ormos, 1991). This observation supports a recent kinetic analysis which shows that the irreversible decay of M_1 to M_2 is greatly slowed at low humidities (Varo and Lanyi, 1991).

Contrasting behavior of the conformational marker bands in the Amide I region in an M - bR difference spectrum are used to distinguish the two M intermediates. The two most notable bands occur at 1669 and 1658 cm^{-1}. M_1 is characterized by a strong 1658 cm^{-1} band and a relatively weak 1669 cm^{-1} band. M_2 is characterized by the converse. (See Ormos, 1991; Figure 1) At 260 K, our infrared specimens, those equilibrated at ambient relative humidity, showed a strong 1658 cm^{-1} band and a weak 1669 cm^{-1} band, indicative of M_1. Figure 6.1 shows an M - bR spectrum that appears to be M_1 - bR (Compare Ormos, 1991; Figure 1.) with hints of

Figure 6.1 Infrared absorbance difference spectrum of M - bR in the wavenumber range, 1800 - 1500 cm-1, recorded at 260 K. The specimen is equilibrated at ambient temperature and humidity, and it is therefore not fully hydrated. 556 scans of both light-adapted and "M" samples were averaged together to form the spectrum. The spectrum was not smoothed. A straight baseline is drawn through the spectrum where the true zero lies.

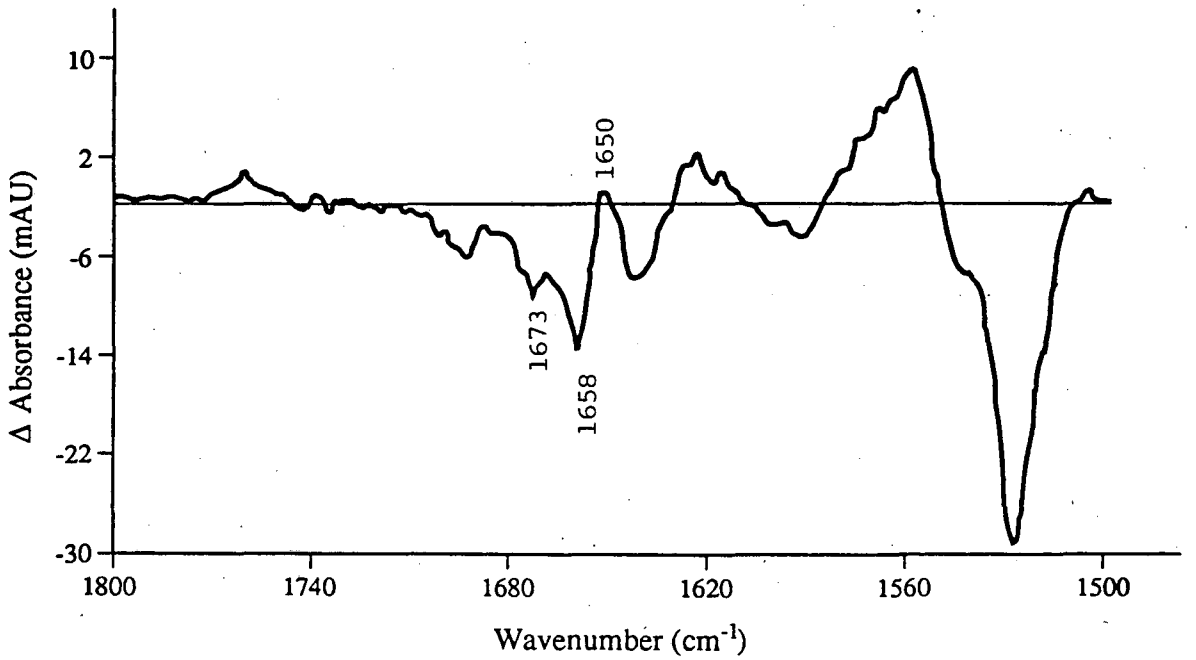
10
2
-6
-14
-22
-30
Δ Absorbance (mAU)
1650
1673
1658
1800
1740
1680
1620
1560
1500
Wavenumber (cm-1)

XBL 921-4627

M_2 - bR present, as judged by these characteristics: a slightly higher 1650 cm^{-1} "peak" than expected for M_1 - bR, and a 1560 cm^{-1} peak that is narrower than observed with M_2 - bR.

An M - bR spectrum employing thin films of glucose-embedded PM that were equilibrated at 81 % relative humidity and recorded at 240 K was obtained by averaging 1056 scans for both the reference and the "M" intermediate, respectively. Figure 6.2 displays this difference spectrum. A number of difference bands are worth discussing. The strong ethylenic pair with peak absorbances at 1560 cm^{-1} and 1527 cm^{-1} indicates that the retinal in M is 13-cis (Braiman & Mathies, 1980). The Schiff base pair at 1641 cm^{-1} and 1624 cm^{-1} indicates that the Schiff base nitrogen has been deprotonated (Lewis et al., 1974; Ames et al., 1989). The 1762 cm^{-1} band, assigned to Asp-85 is protonated in M (Braiman et al., 1988). The bands in the Amide I region, in particular, the 1673 cm^{-1} and 1659 cm^{-1} bands provide evidence that conformational changes in bR's peptide backbone have occured between resting-state bR and the M_1 substate.

Averaging many more scans in the 240 K difference spectrum would not affect the amplitudes of the bands or the peak positions, as discussed in latter paragraphs dealing with reproducibility. With 1056 scans, there still exists some noise in the difference spectrum, as judged by the lack of smoothness in the broad 1762 cm^{-1} and 1560 cm^{-1} bands, among others. [For an example of a smooth 240 K difference spectrum, see Ormos (1991).] Many more

Figure 6.2 M - bR, FTIR absorbance difference spectrum recorded at 240 K. The sample was equilibrated at 81 % relative humidity. Both the reference and the "M" spectra are averages of 1056 scans.

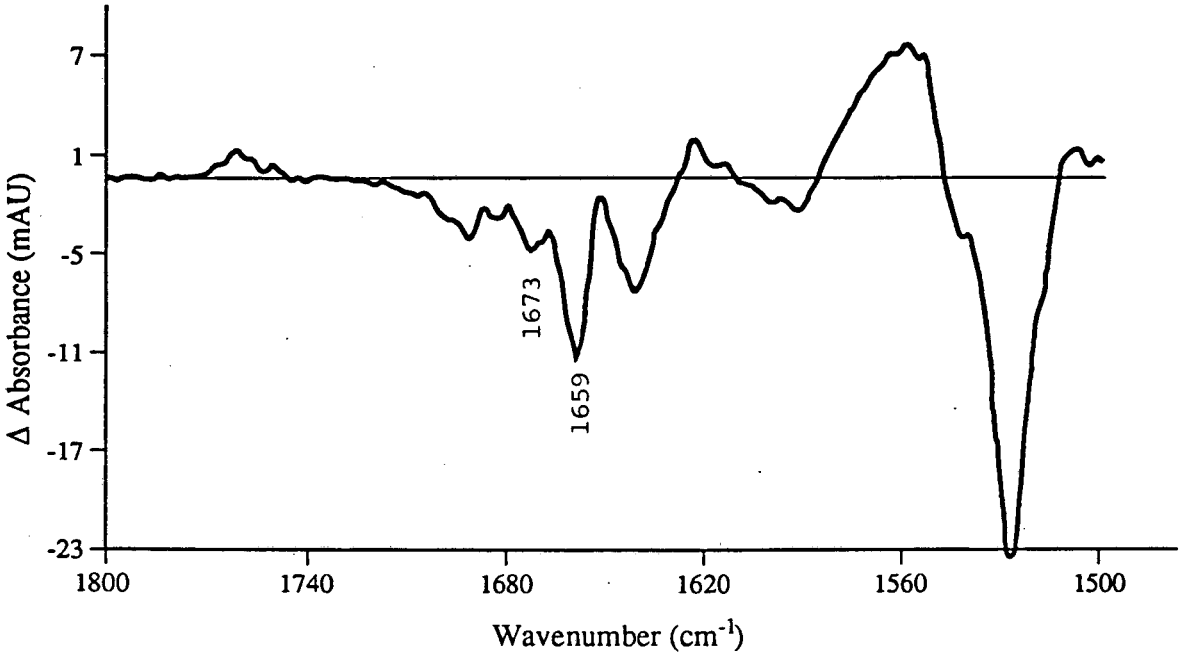
7
1
-5
-11
-17
-23
Δ Absorbance (mAU)
1673
1659
1800
1740
1680
1620
1560
1500
Wavenumber (cm-1)

XBL 921-4633

thousands of scans are normally averaged together to attain a high degree of smoothness. For example, Braiman et al. (1987) averaged 14,000 scans together to eliminate the tremendous noise fluctuations observed when fewer than 100 scans were used to create an M - bR spectrum. For random noise, the signal-to-noise ratio goes as $\sqrt{N}$, where N is the number of scans employed in the spectrum. The bottom line of this discussion as applied to my 1056-scan spectrum is that I would need to collect a few more thousand scans in order to significantly affect the noise level in the glucose-embedded PM spectrum. I conclude that the amount of effort needed to significantly improve the noise level in the difference spectrum would not be justified, as many key features are already relatively far above the noise.

The M - bR spectrum for glucose-embedded samples, equilibrated at 81 % and recorded at 260 K, averaged from 1600 scans, is presented in Figure 6.3. Many bands in this difference spectrum differ in appearance and amplitude from the equivalent bands in Figure 6.2. The positive ethylenic band is narrower, while the positive Schiff base band is wider. More importantly, the 1650 cm^{-1} "peak" is well above the zero line and the relative amplitudes of the 1671 cm^{-1} and 1658 cm^{-1} bands are opposite those recorded at 240 K. The significance of this last observation is discussed by Ormos (1991). One implication of Ormos' work is that M_1 can be trapped at 240 K and M_2 can be trapped at 260 K. The spectra displayed in Figures 6.2 and 6.3 for specimens of glucose-embedded

Figure 6.3 M - bR, FTIR absorbance difference spectrum recorded at 260 K. The sample was equilibrated at 81 % relative humidity. Both the reference and the "M" spectra are averages of 1600 scans.

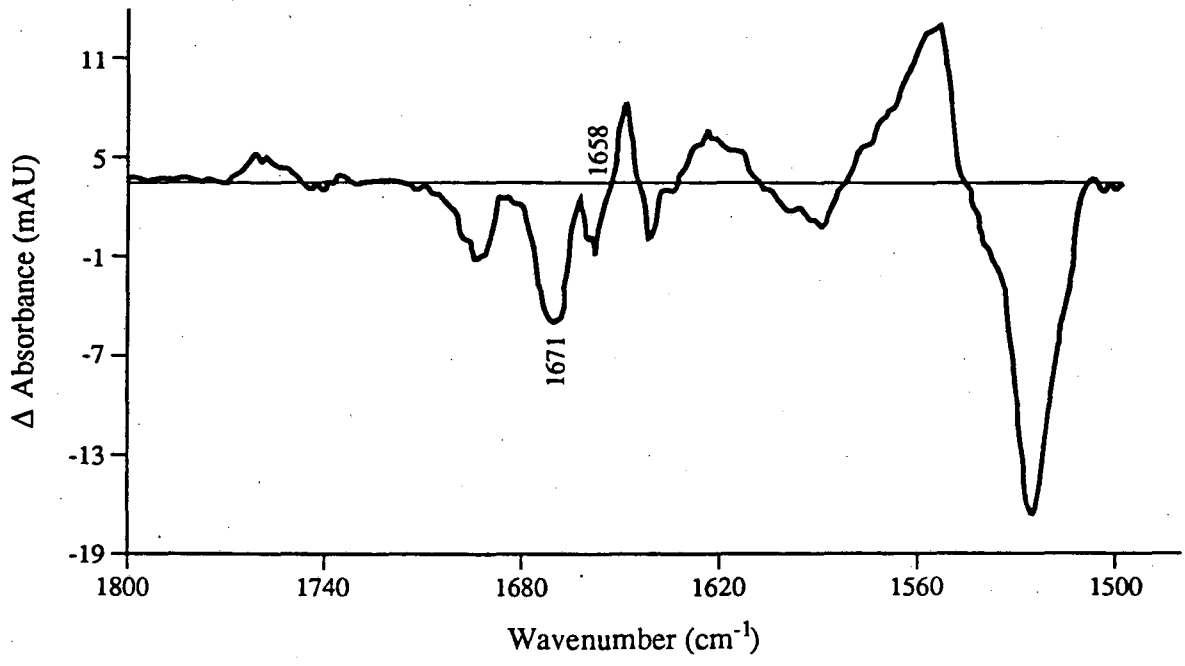
11
5
-1
-7
-13
-19
Δ Absorbance (mAU)
1658
1671
1800
1740
1680
1620
1560
1500
Wavenumber (cm-1)

XBL 921-4632

PM show that glucose embedment does not alter these results, to be discussed in greater detail later.

It is important to mention how the results derived from the visible spectroscopy experiments, reported in an earlier chapter, relate to the FTIR results. I have demonstrated that 99 % M can be formed at 240 K, and 97 % M can be formed at 260 K. Visible spectroscopy cannot differentiate M_1 from M_2, but FTIR spectroscopy can. Difference FTIR spectroscopy cannot provide the percent M formed. However, it can provide evidence that there is a structural difference between samples trapped at 240 K and 260 K. Difference FTIR spectroscopy can also provide information that both samples, though structurally different from one another, are M-state intermediates.

The results derived from visible spectroscopy and those from FTIR spectroscopy are complementary. FTIR spectroscopy can show that two structurally distinct M states are trapped at two different temperatures. Visible spectroscopy can show that there is a minimum of non-M "contaminants" (most likely, L and N intermediates) in the distinct M substates. In this chapter, I will demonstrate the importance of employing as many different spectroscopic measurements as possible that bear on the research at hand (Glaeser et al., 1991). These results will be crucial for interpreting the Fourier difference maps of M_1 - bR and M_2 - bR proposed to follow from the work of this thesis.

The computational subtraction of water vapor works remarkably well and its success is due in part to the instrument capability of resolving the "fine structure" of the water vapor bands at higher resolution. Even though all of the aspartic acid, conformational marker, Schiff base and ethylenic bands in the M - bR difference spectrum are resolved with 4.0 cm^{-1} resolution, many of the water vapor bands, especially those with smaller amplitudes, are not well-resolved. I document the loss of band resolution in a 4.0 cm^{-1} resolution water vapor spectrum. Figure 6.4 shows a water vapor "template" recorded at 260 K and used to computationally subtract water vapor spikes. By comparing Figure 6.4 with Figure 5.4, one notices that all of the strongly absorbing water vapor spikes appear in both spectra at identical wavenumbers. However, most of the small-amplitude spikes are "swallowed" by their large-amplitude neighbors (or are shoulders) in the 4.0 cm^{-1} resolution spectrum. Clearly, a 4.0 cm^{-1} resolution water vapor template should be used only with 4.0 cm^{-1} resolution difference spectra; and even then, the water vapor subtraction by computational means does not work as well as does the subtraction with 2.0 cm^{-1} resolution (both template and difference spectra).

In order to avoid temperature-induced artifacts in the difference spectrum, it is important to hold the specimen temperature constant. As a thin film of hydrated PM is cooled, there appears a wavenumber upshift of the Amide II band and a wavenumber downshift of the Amide I and Amide A bands (Earnest, 1987). Changes in peak amplitudes are not reported in the FTIR

Figure 6.4 64-scan spectrum of water vapor in the range, 1800 cm^{-1} - 1500 cm^{-1}, recorded at 260 K. 4.0 cm^{-1} resolution was employed with this spectrum.

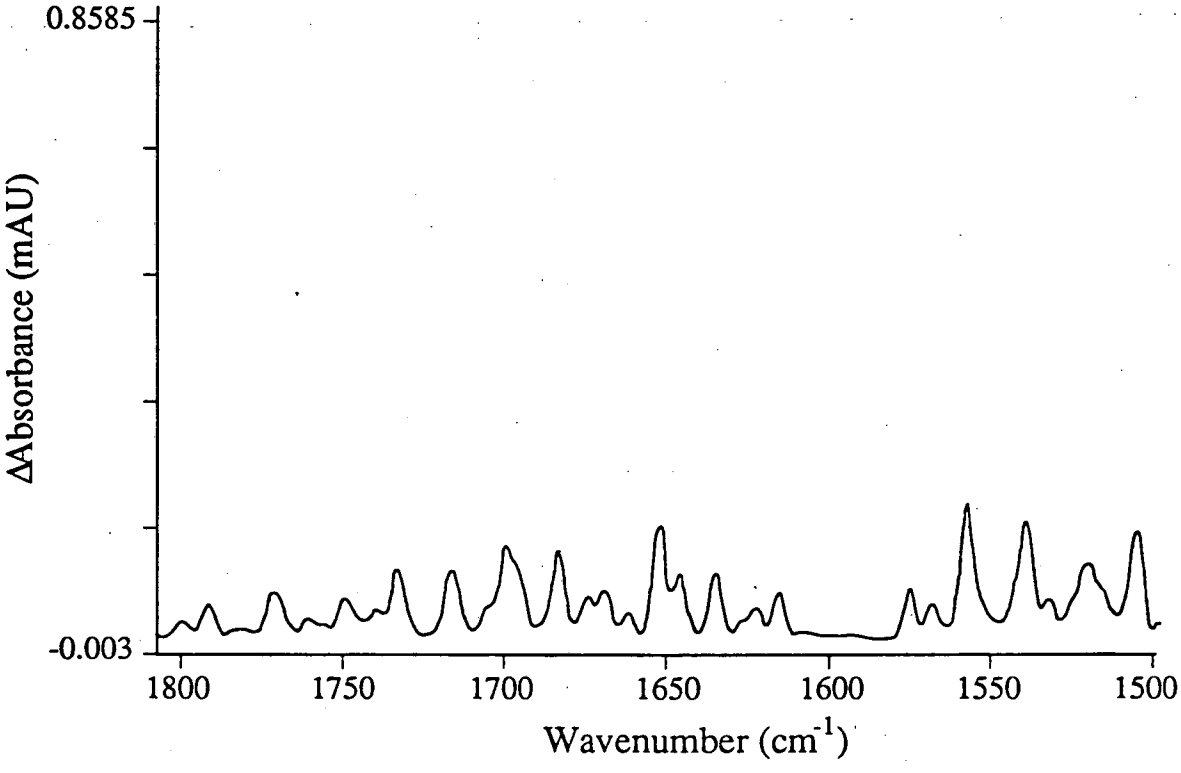
0.8585
-0.003
ΔAbsorbance (mAU)
1800
1750
1700
1650
1600
1550
1500
Wavenumber (cm-1)

XBL 922--4687

literature concerning bR. Figure 6.5 shows a difference spectrum created by subtracting a light-adapted bR spectrum recorded at 260 K from a 293 K, light-adapted bR spectrum. The broad negative peak centered at 1640 cm^{-1}, the sharp 1553 cm^{-1} peak and the negative 1530 cm^{-1} peak result from the wavenumber shifts of the Amide I and II peak absorbances. I noted with alarm that these absorbance peaks are larger than most of the bands observed in my M - bR difference spectra. Because of this observation, I found it expedient to hold the specimen temperature within 1 °C of the desired temperature, for both the reference and "M" spectra, to obtain difference spectra with flat baselines. I report that if the temperature at which scans are taken varied by more than four degrees then I would notice that my difference spectra took on characteristics like those shown in Figure 6.5.

Reproducibility of Spectra

Are the spectra recorded at 240 K and 260 K and averaged from many scans reproducible? If so, how far can the data be subdivided (more or less randomly) until the spectra no longer appear the same? To answer these questions, I first divided the 1056 scans contributing to the 240 K difference spectrum (See Figure 6.2.) into roughly equal halves. Each component difference spectrum, packaged in groups of roughly 60 scans for digital data transferal from the Perkin Elmer spectrometer to our VAX computers, that contributed to the "whole", averaged difference spectrum was arbitrarily placed in one of two piles. Figure 6.6 displays the 240 K data divided in

Figure 6.5 Difference spectrum created from two spectra of light-adapted bR recorded at different temperatures. The 260 K spectrum is subtracted from the 293 K spectrum. Both spectra were averaged from 64 scans using 2.0 cm^{-1} resolution. Scanning was done in the dark to prevent photocycle activation at the lower temperature. One specimen was used to record both spectra, which was not moved (except by thermal contraction/expansion) during or in-between scanning. The Amide I absorbance was ~ 0.7 AU. Conditions for specimen scanning were identical, by intention, except for the temperature difference.

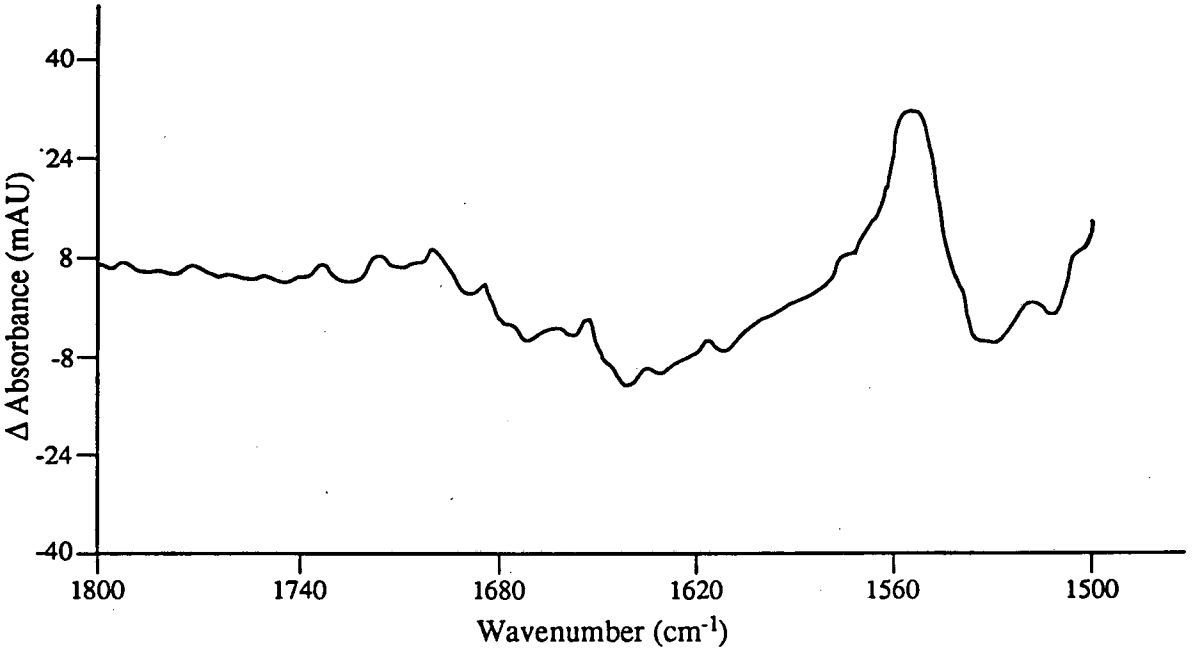
40
24
8
-8
-24
-40
Δ Absorbance (mAU)
1800
1740
1680
1620
1560
1500
Wavenumber (cm-1)

XBL 922-4688

Figure 6.6 Two M - bR spectra created by randomly dividing into roughly equal groups all of the (usually) 64-scan, 240 K spectra that contributed to the difference spectrum of Figure 6.2. a) The top difference spectrum, arbitrarily designated "first half", consists of 552 scans, and b) the "second half" difference spectrum consists of 504 scans. The true zero line is drawn through the spectra and differs from zero absorbance because the baseline shifts up or down with time when using a Perkin Elmer 1600 FTIR instrument. The delta absorbance scale is identical in both spectra to facilitate comparisons. Peak positions and peak absorbance ratios for this spectrum are shown in Tables 6.1 and 6.2.

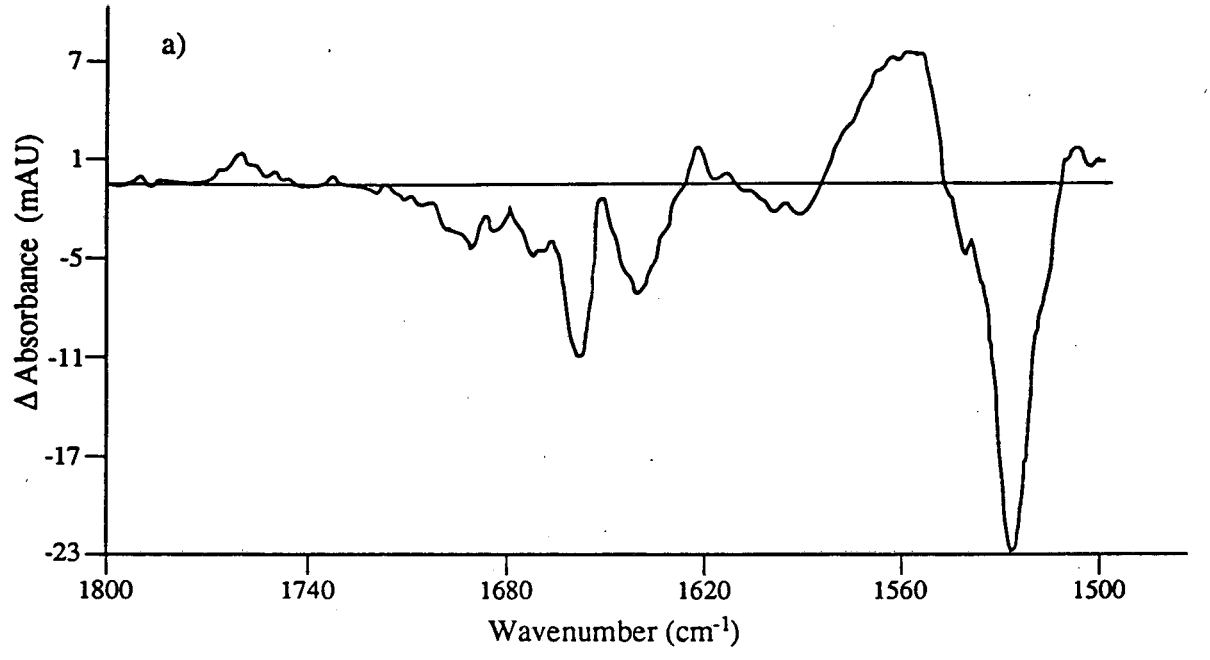
a)
7
1
-5
-11
-17
-23
Δ Absorbance (mAU)
1800
1740
1680
1620
1560
1500
Wavenumber (cm-1)

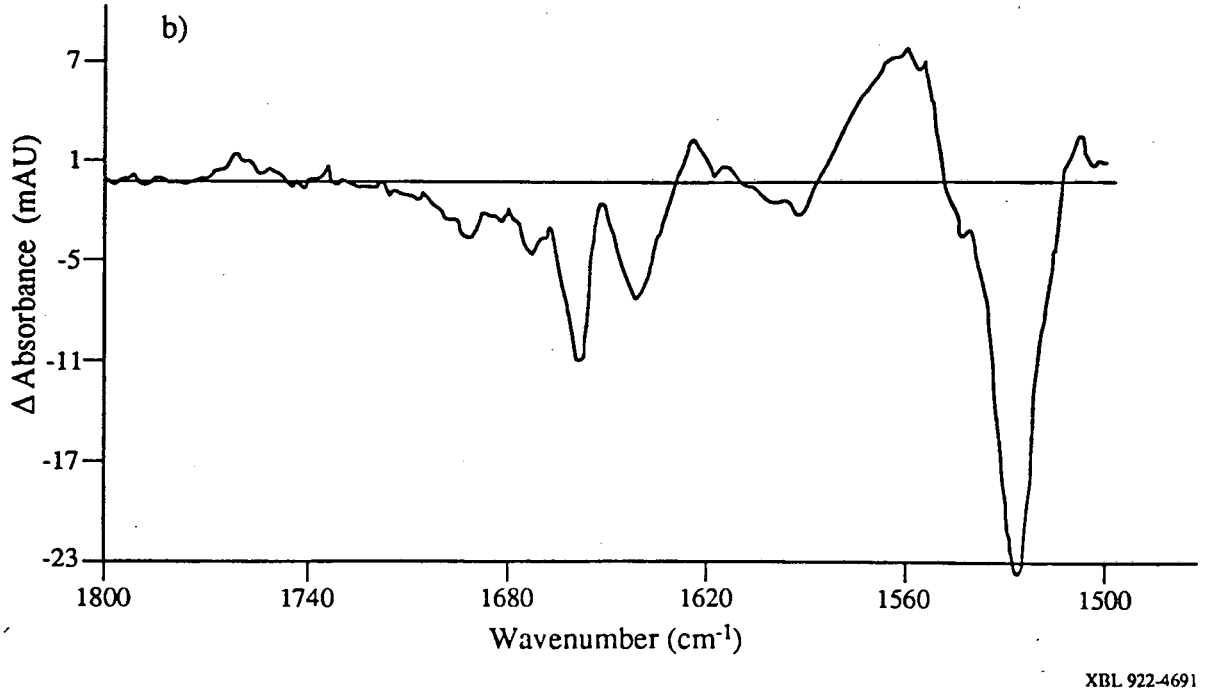
b)
7
1
-5
-11
-17
-23
Δ Absorbance (mAU)
1800
1740
1680
1620
1560
1500
Wavenumber (cm-1)

XBL 922-4691

this way and averaged. One difference spectrum consisted of 552 scans, while the other difference spectrum consisted of 504 scans. By comparing each "half" spectrum to the "whole", it is seen that the noise level is almost imperceptibly higher in the halves. The halves and the whole spectra appear almost identical. Tables 6.1 and 6.2 confirm the visual evidence of sameness by providing a quantitative comparison of the difference spectra. In Table 6.1, seven important difference bands found in the region, 1800 cm^{-1} to 1500 cm^{-1}, are listed and a comparison of the wavenumbers where the absorbance peaks are found is made. The wavenumber correlation between the "whole" data and the two halves is striking. The only differences appear in the "second half" data; and the differences are found to be small. The Asp-85 peak appears at 1762 cm^{-1} in the "whole" spectrum, but appears at 1761 cm^{-1} in the second half" spectrum, and the ethylenic band appearing at 1527 cm^{-1} in the "whole" spectrum is observed at 1528 cm^{-1} in the "second half" spectrum. An apparent shift of 1 cm^{-1} may not be significant since the spectra were recorded with 2.0 cm^{-1} resolution.

Table 6.2 provides a comparison of the peak absorbance ratios. Ratios were used instead of absolute absorbances because the optical density differed from sample to sample, which affects difference peak amplitudes. The ethylenic ratio, 1560:1527, is a useful diagnostic to differentiate the 240 K difference spectrum from the 260 K difference spectrum because in the former, this ratio is reported to be 35 %, while in the latter, it is 56 % (Ormos, 1991). Negative bands in the M - bR spectra, e.g. 1641, 1659 and

Table 6.1 The wavenumbers of peak positions for seven difference bands is tabulated. The output of the FTIR spectrometer consists of absorbance values spaced by 1.0 cm^{-1}, making it possible to read off the peak absorbance with an accuracy of 1.0 cm^{-1}. The absorbance at each integral wavenumber between 1800 cm^{-1} and 1500 cm^{-1} is available for perusal in digital format. The wavenumbers on each row correspond to the M - bR spectrum is indicated in the leftmost column. The band assignments are reported at the top of each table and constitute positive-negative band pairs for all bands in the spectrum, except the protonated asp-85 band at 1762 cm^{-1}. The table at top comprises 240 K spectra, and the table at bottom comprises 260 K spectra. The wavenumbers of peak positions for Ormos' two difference spectra were reported in Ormos (1991).

TABLE 6.1

240 K

	Wavenumber (cm-1)						
	Asp-85	Amide I		Schiff	Base	Ethylenic	
Whole	1762	1673	1659	1641	1624	1560	1527
First half	1762	1673	1659	1641	1624	1560	1527
Second half	1761	1673	1659	1641	1623	1560	1528
First quarter	1762	1674	1659	1642	1624	1560	1527
Second quarter	1762	1672	1659	1641	1624	1560	1527
Third quarter	1761	1672	1660	1641	1624	1555	1528
Fourth quarter	1761	1673	1659	1640	1623	1559	1528
Ormos	1762	1669	1658	1639	1624	1564	1526
No glucose	1762	1670	1658	1641	1622	1558	1528

260 K

	Wavenumber (cm-1)						
	Asp-85	Amide I		Schiff	Base	Ethylenic	
Whole	1762	1671	1658	1642	1624	1555	1526
First half	1762	1673	1658	1642	1624	1555	1527
Second half	1762	1669	1658	1642	1624	1556	1526
First quarter	1762	1671	1658	1642	1624	1555	1526
Second quarter	1762	1674	1659	1641	1624	1559	1526
Third quarter	1762	1671	1658	1642	1624	1555	1526
Fourth quarter	1762	1671	1658	1642	1624	1559	1526
Ormos	1758	1669	1658	1639	1624	1556	1526

Table 6.2 Six peak absorbance ratios are tabulated by column. The percent ratios on each row correspond to the M - bR spectrum indicated in the leftmost column. The table at top comprises 240 K spectra, and the table at bottom comprises 260 K spectra. Peak amplitudes were measured with a ruler from the zero line. Spectra taken from published sources, i.e. Ormos (1991), Gerwert (1989, 1990), were enlarged many times in order to more accurately measure the peak amplitudes.

Table 6.2

240 K Peak Absorbance Ratios (%)

	1560/1527	1624/1560	1641/1527	1659/1527	1673/1527	1762/1560
Whole	35	29	30	47	19	22
First half	33	30	30	46	20	21
Second half	35	30	30	47	19	24
First quarter	32	28	32	46	23	26
Second quarter	33	38	28	44	15	23
Third quarter	36	34	26	42	17	21
Fourth quarter	47	21	36	55	24	21
Ormos	35	30	25	32	17	20
No glucose	32	20	31	45	27	32

260 K Peak Absorbance Ratios (%)

	1560/1527	1624/1560	1641/1527	1659/1527	1673/1527	1762/1560
Whole	47	33	18	23	43	18
First half	50	38	14	21	44	19
Second half	45	30	21	24	43	17
First quarter	44	13	25	32	49	17
Second quarter	65	36	10	14	43	23
Third quarter	37	53	15	22	50	19
Fourth quarter	43	36	17	23	39	21
Ormos	56	17	15	18	39	10
Gerwert89	28	25	32	39	24	
Gerwert90	14	26	14	14	7	

1673 cm^{-1}, are compared to the negative ethylenic band. Similarly, the positive band, 1624 cm^{-1}, is compared to the positive ethylenic band. Table 6.2 shows that there is great consistency between the peak absorbance ratios derived from the "whole" spectrum and its two "half" spectra.

The procedure of data subdivision was repeated with each of the two 240 K "half" spectra to create four "quarter" spectra. Figure 6,7 shows the four averaged spectra. It is evident that the noise level is higher in these spectra, as judged by the "spikes" riding on top of the difference bands. Most noticeable is the cleft in the 1560 cm^{-1} band in the "third quarter" spectrum and the spike appearing at almost the same wavenumber in the "fourth quarter" spectrum. It is also worth noting the variation in the height of the 1650 cm^{-1} "peak" among the four spectra. In the first and third quarter spectra the 1650 cm^{-1} "peak" lies well below the zero baseline, while in the second and fourth quarter spectra this "peak" extends to the baseline.

Tables 6.1 and 6.2 provide quantitative information concerning the variations in the quarter spectra noticed at first glance. Table 6.1 shows that there is greater variation in the absorption peak wavenumbers between the "quarter" spectra as compared with the variation in the "half" spectra. Even so, a comparison of where each band lies in all of the spectra reveals that the peak band absorbances vary by no more than 2 cm^{-1} in all of the spectra, except for the single exception of the positive ethylenic band in the

Figure 6.7 Four 240 K, M - bR spectra created by randomly dividing into roughly equal groups spectra that contributed to the two spectra in Figure 6.6. The spectra were arbitrarily designated, "first quarter", "second quarter", "third quarter" and "fourth quarter". The delta absorbance scale is identical in all four spectra. The true zero is indicated by a horizontal line running through each spectrum. Peak positions and peak absorbance ratios for this spectrum are shown in Tables 6.1 and 6.2.

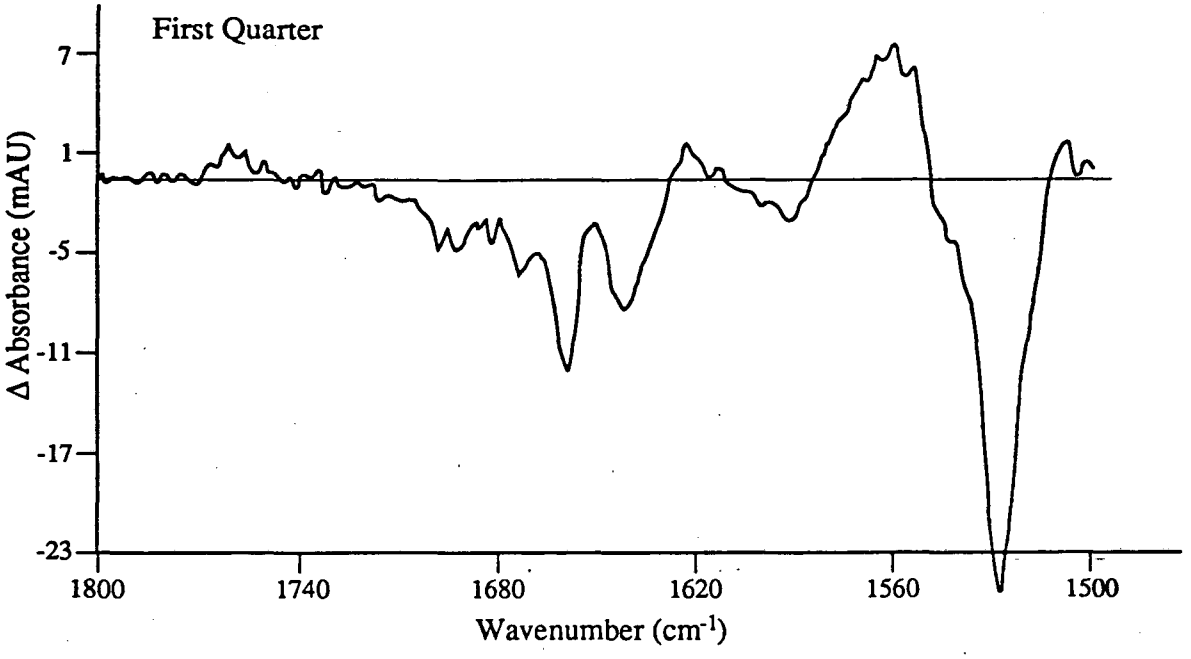
First Quarter
7
1
-5
-11
-17
-23
Δ Absorbance (mAU)
1800
1740
1680
1620
1560
1500
Wavenumber (cm-1)

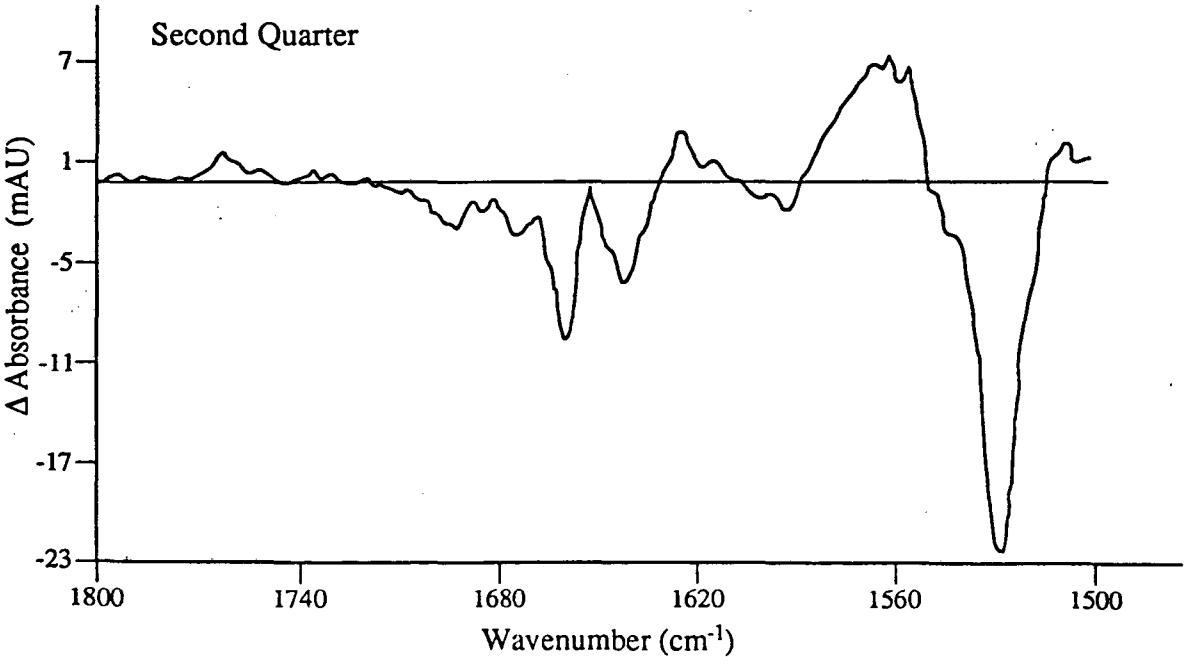
Second Quarter
7
1
-5
-11
-17
-23
Δ Absorbance (mAU)
1800
1740
1680
1620
1560
1500
Wavenumber (cm-1)

XBL 922-4686

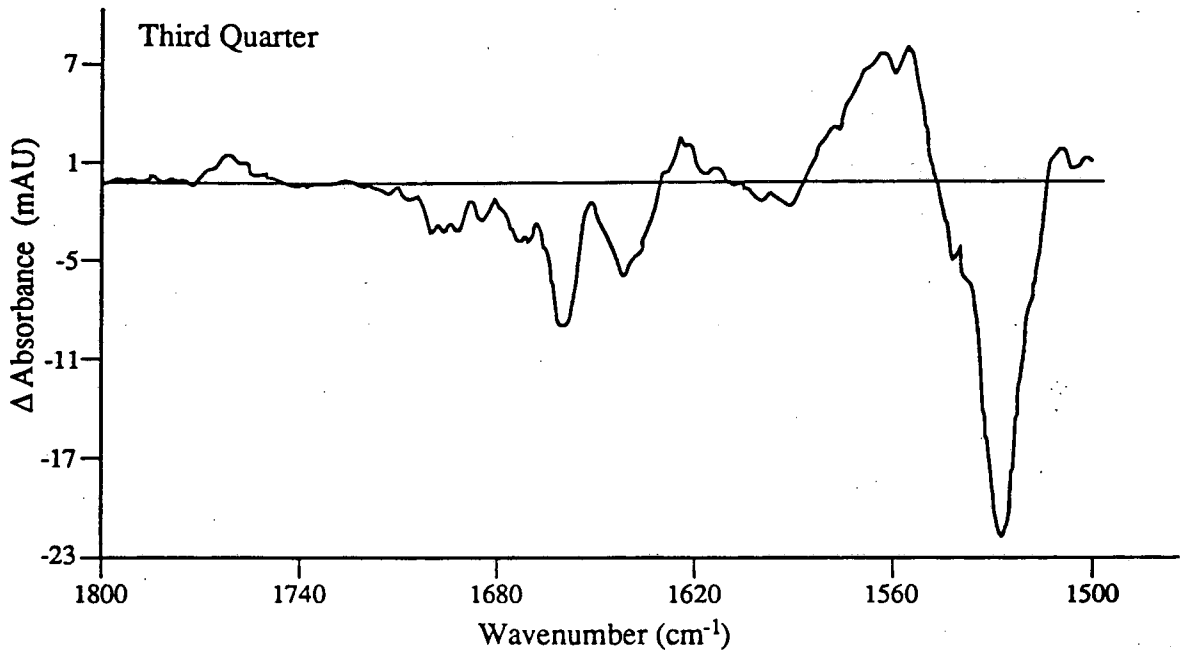
Third Quarter
7
1
-5
-11
-17
-23
Δ Absorbance (mAU)
1800
1740
1680
1620
1560
1500
Wavenumber (cm-1)

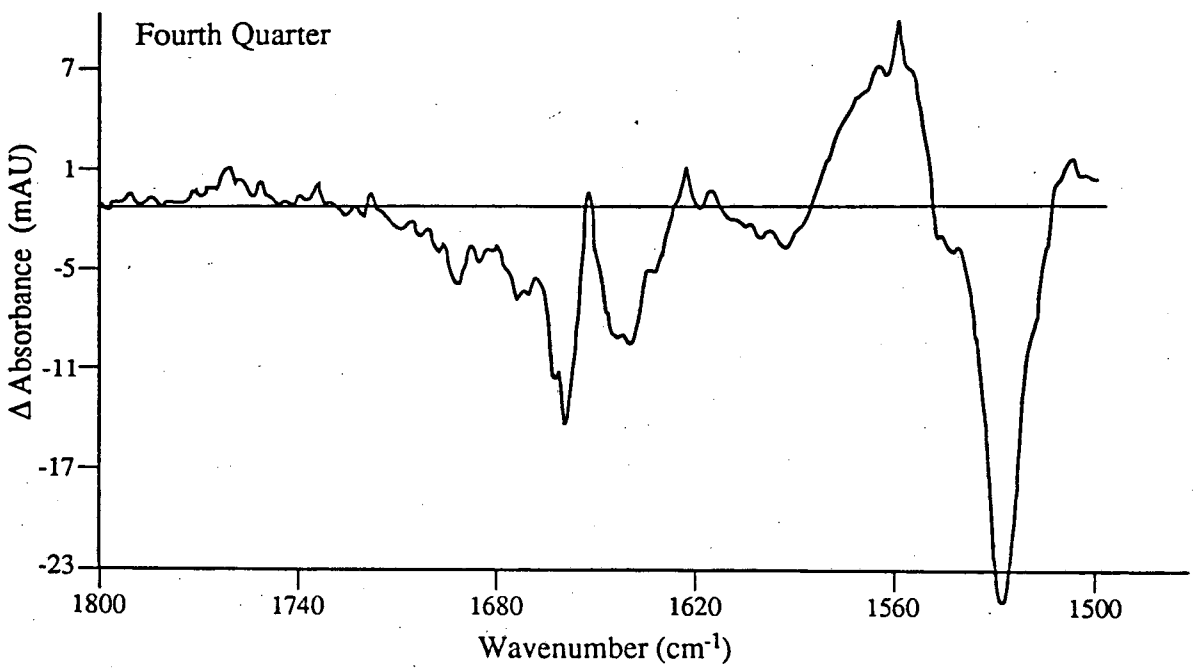
Fourth Quarter
7
1
-5
-11
-17
-23
Δ Absorbance (mAU)
1800
1740
1680
1620
1560
1500
Wavenumber (cm-1)

XBL 922-4694

"third quarter" difference spectrum. This peak appears at 1555 cm^{-1} instead of the expected 1560 cm^{-1} position. But, this wavenumber shift may not be significant, as the noise may have skewed this particular peak.

Table 6.2 gives evidence of significant variance in the ratios of peak absorbances among the four "quarter" spectra. The 1560:1527 ratio has a low of 32 % and a high of 47 %, taken from the "first quarter" and "fourth quarter" spectra, respectively. Similar variations are also found with other peak ratios. The variations in peak absorbance ratios are not due to "contaminating" the spectra with an M_2-N mixture, because a substantial M_2-N component would dramatically alter the 1659 cm^{-1} and 1673 cm^{-1} peaks (Ormos, 1991). Clearly, the conformational marker bands in the "quarter" spectra are characteristic of 240 K, FTIR difference spectra of bR. These results answer the questions of reproducibility and the extent to which the spectral data may be subdivided before reproducibility is lost. I conclude that the 240 K, M - bR difference spectrum displayed in Figure 6.2 is reproducible, as judged by the "half" spectra. However, the reproducibility starts to break down among the "quarter" spectra. The breakdown is far from complete as the major bands in the difference spectra are still well-resolved from each other and the noise, and occur at the same wavenumbers. (Review Table 6.1.)

The question of reproducibility of M - bR difference spectra of glucose-embedded PM samples is also applicable to the 260 K data

collected with a Perkin Elmer 1600 FTIR instrument. The 260 K difference spectrum of Figure 6.3 was generated from 1600 scans. Figure 6.8 shows the two "half" spectra averaged from difference spectra arbitrarily divided into two groups. The "first half" spectrum consists of 762 scans and the "second half" spectrum was comprised of 832 scans. A visual inspection reveals that, outside the regions of the strongly absorbing amide I and amide II bands, the noise level in these difference spectra appears to be roughly the same as that in the "whole" difference spectrum. Table 6.1 shows that the wavenumbers where the absorbance peaks are found in the "half" difference spectra differ by no more than 2 cm^{-1} from the corresponding wavenumbers in the "whole" difference spectrum. The greatest difference is recorded at the 1671 cm^{-1} band. In the "first half" spectrum, this band has a peak at 1673 cm^{-1}, while in the "second half" spectrum, the peak lies at 1669 cm^{-1}. These results still compare favorably with the position of the band in the "whole" spectrum. Table 6.2 shows that the peak absorbance ratios in the 260 K "half" spectra resemble those in the "whole" spectrum. The greatest difference between band absorbance ratios is found with the 1624:1560 ratio. This ratio in the "first half" spectrum is 38 %, while the "whole" spectrum ratio is 33 %. The "half" ratio that most closely matches the "whole" ratio is the Amide I:ethylenic ratio, 1671:1526.

The same procedure of subdivision as applied to the 240 K "half" data was followed for the 260 K "half" data. As judged by the small variations in peak positions and band absorption ratios

Figure 6.8 Two M - bR spectra created by randomly dividing into roughly equal groups all of the (usually) 64-scan, 260 K spectra that contributed to the difference spectrum of Figure 6.3. a) The top difference spectrum, arbitrarily designated "first half", consists of 768 scans, and b) the "second half" difference spectrum consists of 832 scans. The true zero line is drawn through the spectra and differs from zero absorbance because the baseline shifts up or down with time when using a Perkin Elmer 1600 FTIR instrument. The delta absorbance scale is identical in both spectra to facilitate comparisons. Peak positions and peak absorbance ratios for this spectrum are shown in Tables 6.1 and 6.2.

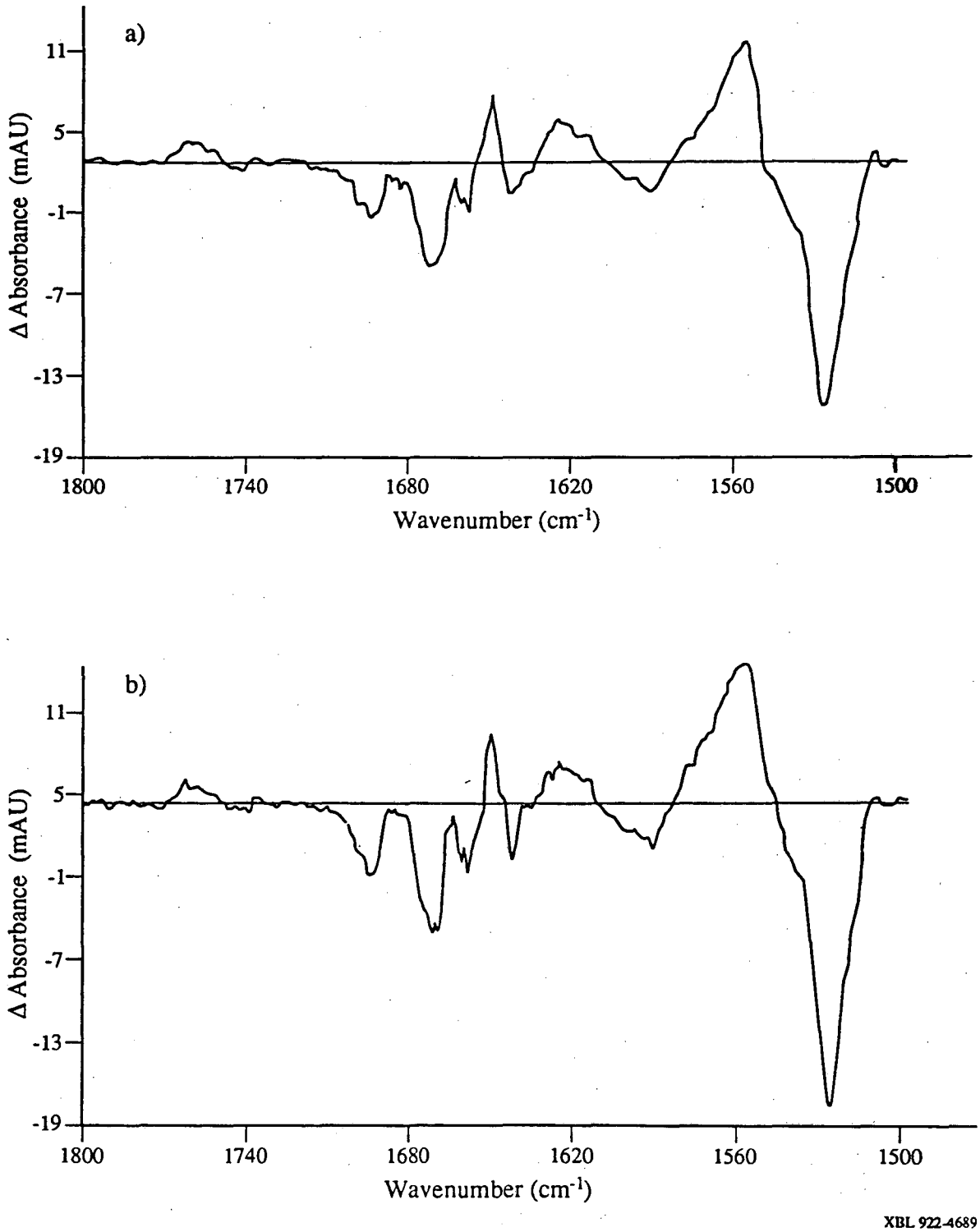
a)
11
5
-1
-7
-13
-19
Δ Absorbance (mAU)
1800
1740
1680
1620
1560
1500
Wavenumber (cm-1)
b)
11
5
-1
-7
-13
-19
Δ Absorbance (mAU)
1800
1740
1680
1620
1560
1500
Wavenumber (cm-1)
XBL 922-4689

(See Tables 6.1 and 6.2.) between the "whole" spectrum and the "half" spectra, it is evident that the 260 K difference spectrum is reproducible. However, it may be argued that these variations are an indication that reproducibility is starting to break down. Figure 6.9 displays four "quarter" difference spectra, each averaged from roughly 400 scans. Upon visual inspection, it is clear that the noise is greater in the "quarter" spectra than in the "half" spectra. Nowhere is this more vivid than with the "second quarter" spectrum. The noise is so great in this spectrum that the broad 1762 cm^{-1}, Asp-85 peak becomes concealed. Moreover, noise spikes form deep clefts in the 1650 cm^{-1} band and the 1555 cm^{-1} band.

As before, the wavenumbers of peak positions and peak absorption ratios were determined for the "quarter" spectra. Upon examining the wavenumber results in Table 6.1, a pleasant surprise surfaces. The peak wavenumbers are amazingly uniform considering the level of noise in the difference spectra. The Asp-85 peak position does not vary by as much as 1 cm^{-1} between the "whole", "half" and "quarter" spectra. The 1658 cm^{-1}, 1642 cm^{-1}, 1624 cm^{-1} and 1526 cm^{-1} peaks also exhibit small variations, if any, in wavenumber. The positive ethylenic peak varies the most. The "second quarter" and "fourth quarter" spectra have ethylenic peaks at 1559 cm^{-1}, differing by 4 cm^{-1} from the "whole" spectrum.

The gratifying uniformity displayed in Table 6.1 is not carried over to the results of Table 6.2. There are wild variations in peak absorbance ratios among the "quarter" spectra. In no ratio is this

Figure 6.9 Four 260 K, M - bR spectra created by randomly dividing into roughly equal groups spectra that contributed to the two spectra in Figure 6.8. The spectra were arbitrarily designated, "first quarter", "second quarter", "third quarter" and "fourth quarter". The delta absorbance scales were not chosen to be the same among spectra, because of the wide variations in ethylenic signals. Vertical scales were chosen in order to more clearly observe the features in the difference bands with smaller amplitudes. This is especially true of the "second quarter" spectrum. The true zero is indicated by a horizontal line running through each spectrum. Peak positions and peak absorbance ratios for this spectrum are shown in Tables 6.1 and 6.2.

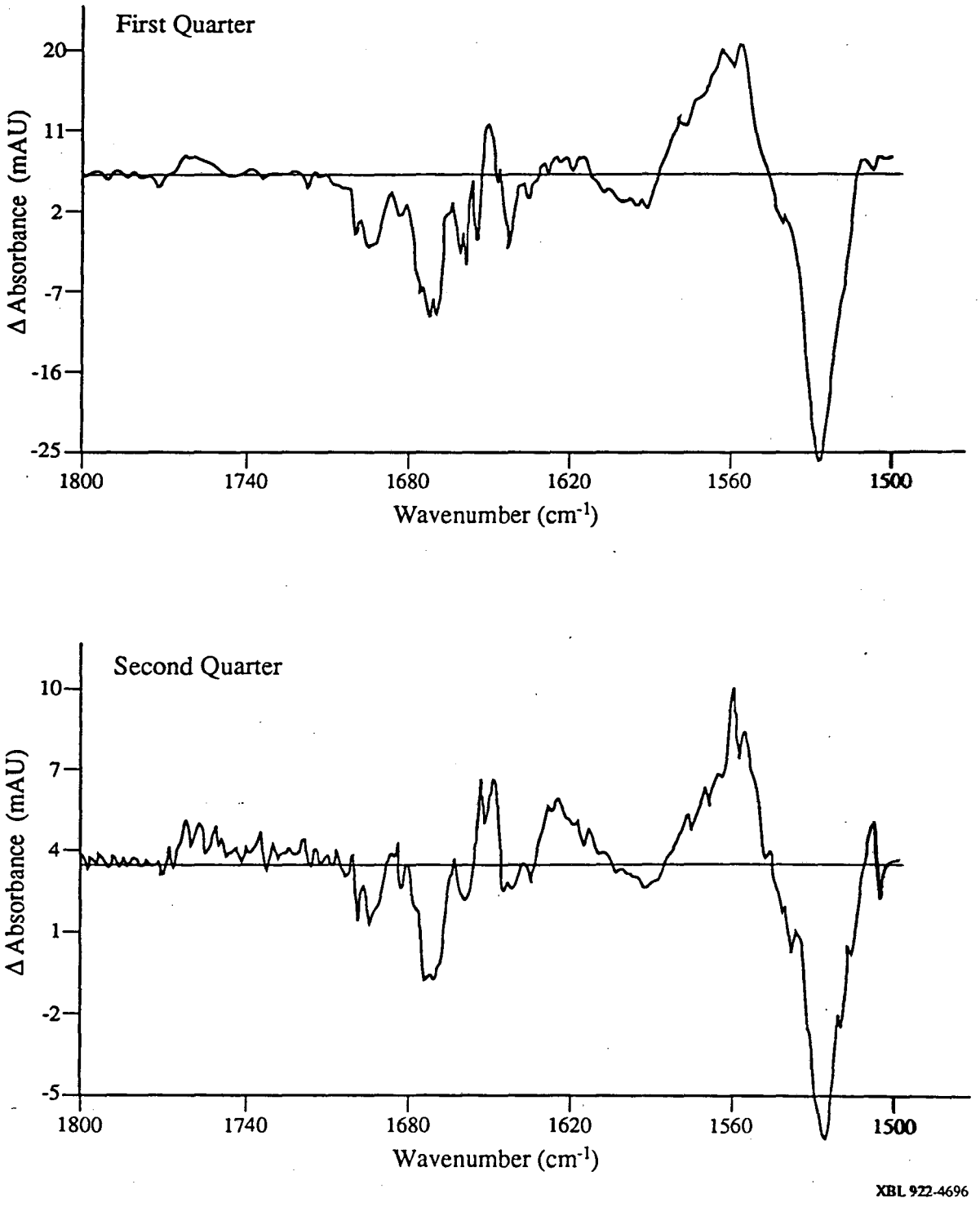
First Quarter
20
11
2
-7
-16
-25
Δ Absorbance (mAU)
1800
1740
1680
1620
1560
1500
Wavenumber (cm-1)
Second Quarter
10
7
4
1
-2
-5
Δ Absorbance (mAU)
1800
1740
1680
1620
1560
1500
Wavenumber (cm-1)
XBL 922-4696

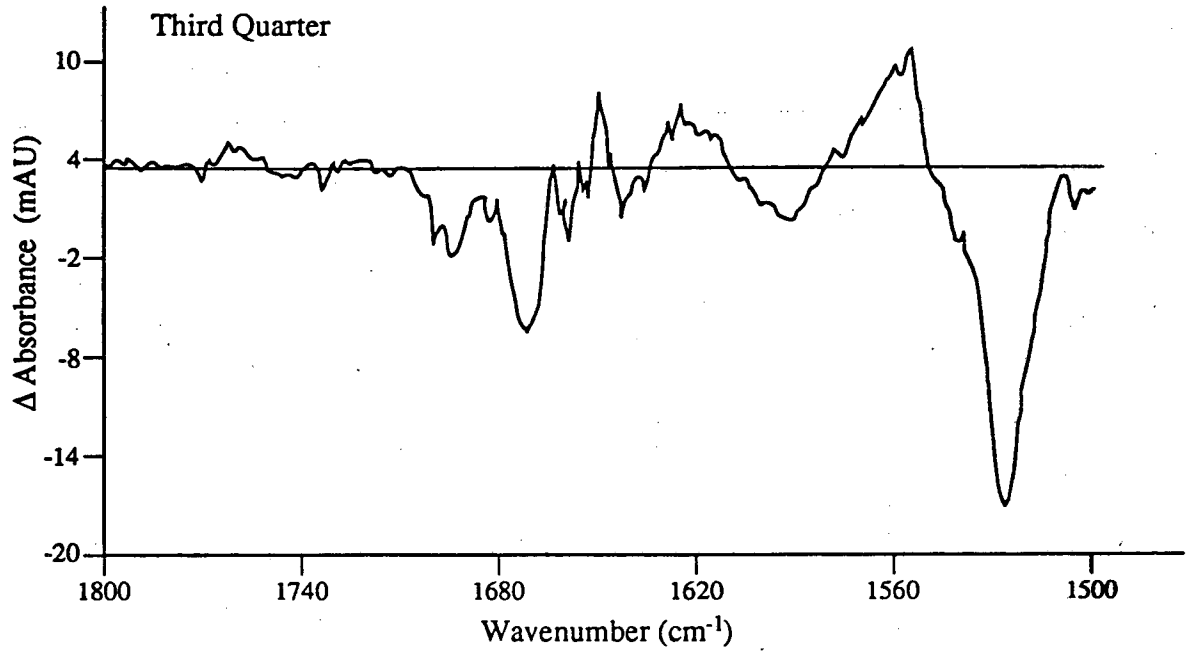
Third Quarter
10
4
-2
-8
-14
-20
Δ Absorbance (mAU)
1800
1740
1680
1620
1560
1500
Wavenumber (cm-1)

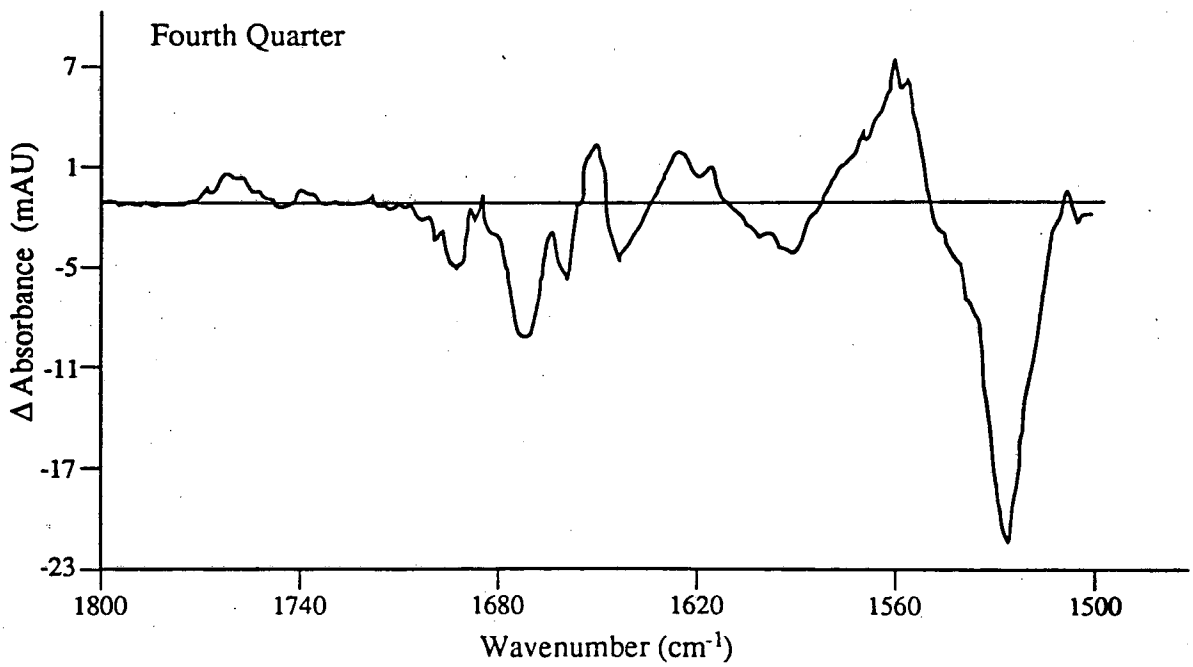
Fourth Quarter
7
1
-5
-11
-17
-23
Δ Absorbance (mAU)
1800
1740
1680
1620
1560
1500
Wavenumber (cm-1)

XBL 922-4698

more manifest than with the 1624:1555 ratio. The low is 13 %, while the high is four times greater. This large difference in ratios may not be completely due to noise. A slightly warped baseline may have contributed to the ratio discrepancies. It appears that the baseline is somewhat bowed in the 1580 cm^{-1} to 1630 cm^{-1} region in the "first quarter" difference spectrum. No correction was attempted to remedy this. I adopted a philosophy whereby baseline correction was applied sparingly to my difference spectra out of a concern that the resultant spectra would not accurately represent factual M - bR, FTIR spectra. Notwithstanding the slight variation in peak positions, the much greater variation in peak absorbance ratios leads me to conclude that reproducibility is well on its way to breaking down among the 260 K "quarter" spectra. Overall, the conclusion presented in this work is that the M - bR spectra obtained from glucose-embedded PM is reproducible, both for 240 K data and for 260 K data, as judged by how close the "half" spectra resemble their mother spectrum. An idea of how many scans are needed to obtain reproducible results with the samples and equipment used is also demonstrated.

Comparison with Previously Published Spectra

Can the differences in the ratios of peak absorbances and wavenumbers of peak positions between the spectra recorded with glucose-embedded PM samples and those reported by Ormos (1991) (Peruse Tables 6.1 and 6.2.) be attributed to glucose embedment? Or, can they be due to a "sample" difference? By "sample" difference, I

infer the possibility that my samples and those of Ormos might have somewhat different amounts of additional intermediates, such as N or L, as well as the M intermediate. The basis for this inference stems from the report that there is a significant concentration of the N intermediate along with M_2 in Ormos' 260 K difference spectrum (Ormos, 1991). Similarly, the L intermediate may have contributed to the 240 K difference spectrum, even though evidence for this happening is not reported by Ormos. A discussion of the energetics involved at different stages of the bR photocycle (Varo & Lanyi, 1991) indicates that M_1 can back-react to L. My FTIR protocol for trapping M helps to address this question because it is the same as my visible spectroscopy protocol, in which it was shown that 90 % or greater M can be trapped at both temperatures.

Answers to the questions posed in the previous paragraph may be provided by M - bR difference spectra taken with hydrated, no-glucose PM samples. Figure 6.10 displays a difference spectrum averaged from 556 scans, all recorded at 240 K, taken from specimens prepared via the protocol described previously, but without glucose. A few noticeable differences between the spectrum in Figure 6.10 and the 240 K spectrum in Figure 6.2 are observed. First, in the no-glucose spectrum, there are two bands in the protonated aspartic acid region, at 1762 cm^{-1} and 1738 cm^{-1}, which have absorbance peaks clearly above the noise, while in the glucose-embedded sample, Figure 6.2, the 1738 cm^{-1} peak is not above the noise level. In previous work, the 1762 cm^{-1} band is attributed to protonation of Asp-85 while the 1738 cm^{-1} band is

Figure 6.10 M - bR spectrum recorded at 240 K from hydrated specimens of thin-film PM that had not been glucose-embedded. 556 scans were averaged to create this difference spectrum. The true zero is indicated by a horizontal line extending through the spectrum. Peak positions and peak absorbance ratios for this spectrum are shown in Tables 6.1 and 6.2.

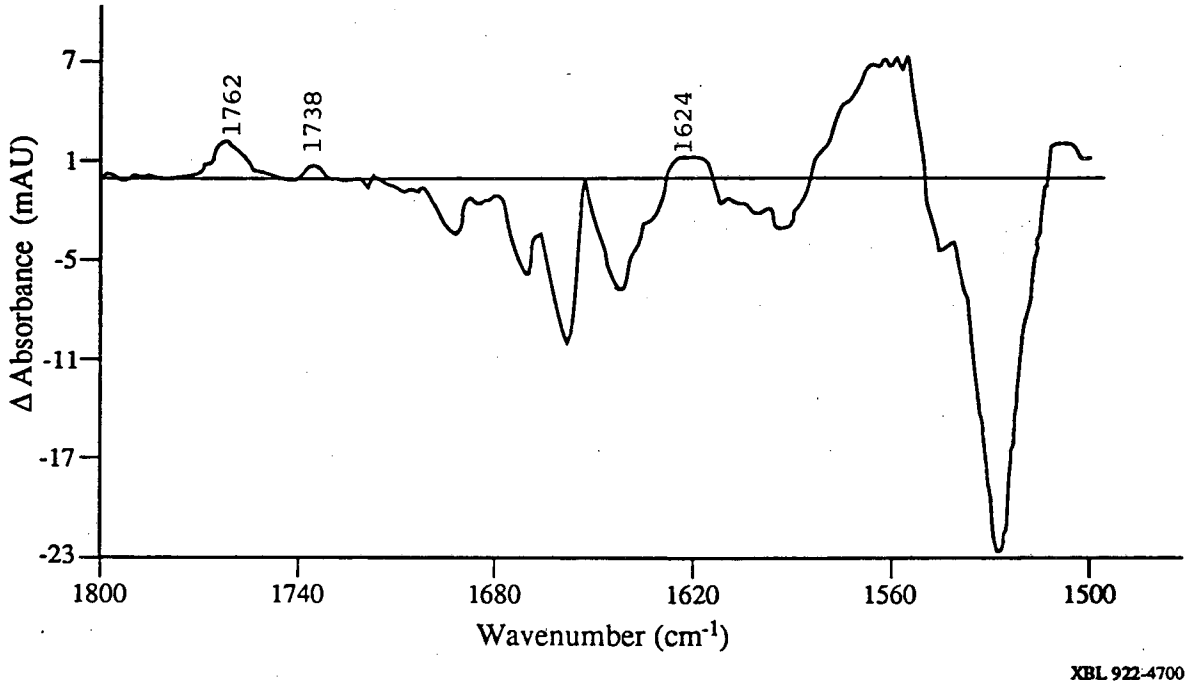
7
1
-5
-11
-17
-23
Δ Absorbance (mAU)
1762
1738
1624
1800
1740
1680
1620
1560
1500
Wavenumber (cm-1)
XBL 922-4700

attributed to Asp-212 (Braiman et al., 1988; Gerwert et al., 1989). Moreover, these two bands have stronger amplitudes relative to the major, 1560 cm^{-1} ethylenic band, in the no-glucose spectrum compared with the glucose-embedded PM spectrum. Second, the 1624 cm^{-1} absorbance peak is broader in Figure 6.10 than the same peak in Figure 6.2.

The absence of a 1738 cm^{-1} band in the difference spectra of glucose-embedded PM specimens is intriguing. During M formation, the nature of the Asp-212 side chain hydrogen bond changes (Gerwert et al., 1989). The 3-D model of bR shows that Asp-212 is one of the residues lining the chromophore binding pocket (Henderson et al., 1990). A point-mutation, Asp-212 to Glu, causes a large red shift of ~ 30-35 nm of the bR_{568} peak (Khorana, 1988). This spectral shift indicates that Asp-212 interacts with the retinal in some way. Furthermore, the Asp-212 to Glu and Asp-212 to Asn mutants exhibited a much reduced ability to pump ions across purple membrane (Khorana, 1988). How would glucose-embedment selectively alter the hydrogen-bonding nature of a single, buried aspartic acid residue? It is hard to imagine. Future work may need to address the issue of whether the 1738 cm^{-1} peak can be observed in the spectra of well-hydrated, thin-films of PM embedded in glucose.

A comparison of the wavenumbers of peak positions in Table 6.1 and peak absorbance ratios in Table 6.2 provides information on the possible spectral effects of glucose embedment. The 1670 cm^{-1}

Amide I difference band of the no-glucose spectrum is closer to the reported position of the band in Ormos' spectrum (1991) than to the corresponding band in the glucose-embedded PM spectrum. The same may be true of the 1658 cm^{-1} band. However, the opposite is true of the Schiff base 1641 cm^{-1} band and the ethylenic 1558 cm^{-1} band. It is interesting to note that the Asp-85 band has the identical peak position, 1762 cm^{-1}, in all three spectra used for comparison. The differences in peak position wavenumbers cannot be attributed to the variable number of scans contributing to each spectrum, for the no-glucose spectrum has the same number of scans as do the "half" spectra, which agree with their respective "whole" spectrum.

Table 6.2 shows that in every case, the no-glucose difference spectrum has peak absorbance ratios that closely approximate the ratios of the glucose-embedded PM spectrum. The agreement between the two spectra is excellent except for the 1560:1527 and the 1673:1527 ratios. I conclude that the differences observed between my glucose-embedded and no-glucose spectra are small. This result leaves the door open for a number of non-competing interpretations. Do the differences between my spectra and those of Ormos reflect protocol and instrumental perturbations between researchers? The results described in this work discourage the interpretation of differences seen in glucose-embedded PM difference spectra compared with the Ormos PM difference spectra based solely on the effects of glucose. I conclude that at least part of the differences are due to variations in the presence of other intermediates between my spectra and Ormos' spectra.

Latitude in the analysis of peak absorption ratios is necessary in view of the expected variance from sample to sample. Such variance is noted in the FTIR contributions to the M and light-adapted bR spectra which are published in the literature. For example, Gerwert et al. (1989) report an M - bR difference spectrum recorded at 272 K. Another M - bR difference spectrum is reported by Gerwert et al. (1990) that is recorded with the same protocol and with a specimen prepared by the method previously reported (Gerwert et al., 1989). The only difference was that the spectrum was taken at 270 K. The wavenumbers of peak positions appears to be identical in the two spectra. Yet, the ratios of peak absorbances are rather different. The last row of Table 6.2b documents the differences. All of the ratios, save the 1624:1555 ratio are much lower in the 1990 difference spectrum. The ratio discrepancies cannot be attributed to the small temperature difference, as the M - bR spectra recorded by Roepe et al. (1987) at 220 K and 250 K do not exhibit a similar extent of ratio differences. It is possible that part of the difference in relative amplitudes is due to sample orientation and the fact that the infrared beam is somewhat polarized (Nabedryk & Breton, 1986). This discussion of differences observed in spectra where little or no difference would be expected is applicable to the analysis of peak absorption ratios. In particular, if the spectra published by Gerwert and coworkers show large absorbance ratio differences, then the smaller differences among the "half" spectra shown in Table 6.2 can be attributed to natural variance. Thus, one must conclude that the 260 K "half" spectra accurately mirror the

"whole" spectrum. Also, the 240 K "no-glucose" spectrum is a reliable mirror of the glucose-embedded PM spectrum.

To further aid the judgement of how similar the glucose-embedded PM spectra are to Ormos' 240 K and 260 K spectra, plots of my spectra were superimposed on those of Ormos. My spectra were scaled and a constant offset was applied so that the fit to Ormos' spectra are as close as possible. To this end, I used a discrete least-squares approximation (Burden and Faires, 1985) as a fitting routine. An algorithm was implemented to find the constants *a* and *b* that minimize the least-squares error:

$$\text{Error} = \sum_{i=1}^{301} [O_i - (aP_i + b)]^2$$

Where O_i represents Ormos' spectra, digitized at each integral wavenumber between 1800 cm^{-1} and 1500 cm^{-1}, i.e. 301 absorbance data points, and P_i represents my glucose-embedded PM spectra. The results for the 240 K spectra are shown in Figure 6.11, and the results for the 260 K spectra are shown in Figure 6.12. A cursory glance at Figure 6.11 reveals that the fit is good in the protonated aspartic acid and the ethylenic regions. However, the difference bands in the Amide I region from one spectrum appear to be shifted with respect to the same bands in the other spectrum. One also notices that the amplitudes of the bands in this wavenumber region differ somewhat between spectra. Applying a critical eye to the traces of Figure 6.12, one sees that the least-squares fit for the

Figure 6.11 Discrete least-squares approximation of the 240 K, M - bR spectrum of glucose-embedded specimens to Ormos' first 240 K difference spectrum. The constants, *a* and *b*, were determined that minimized the least-squares error,

$$\text{Error} = \sum_{i=1}^{301} [O_i - (aP_i + b)]^2$$

where the O_i come from Ormos' spectra, digitized at each integral wavenumber between 1800 cm^{-1} - 1500 cm^{-1}, i.e. 301 absorbance data points, and P_i represents my glucose-embedded PM spectra. . The two spectra are superimposed with the glucose-embedded PM spectrum shown as the dashed trace, and Ormos' difference spectrum as the solid trace.

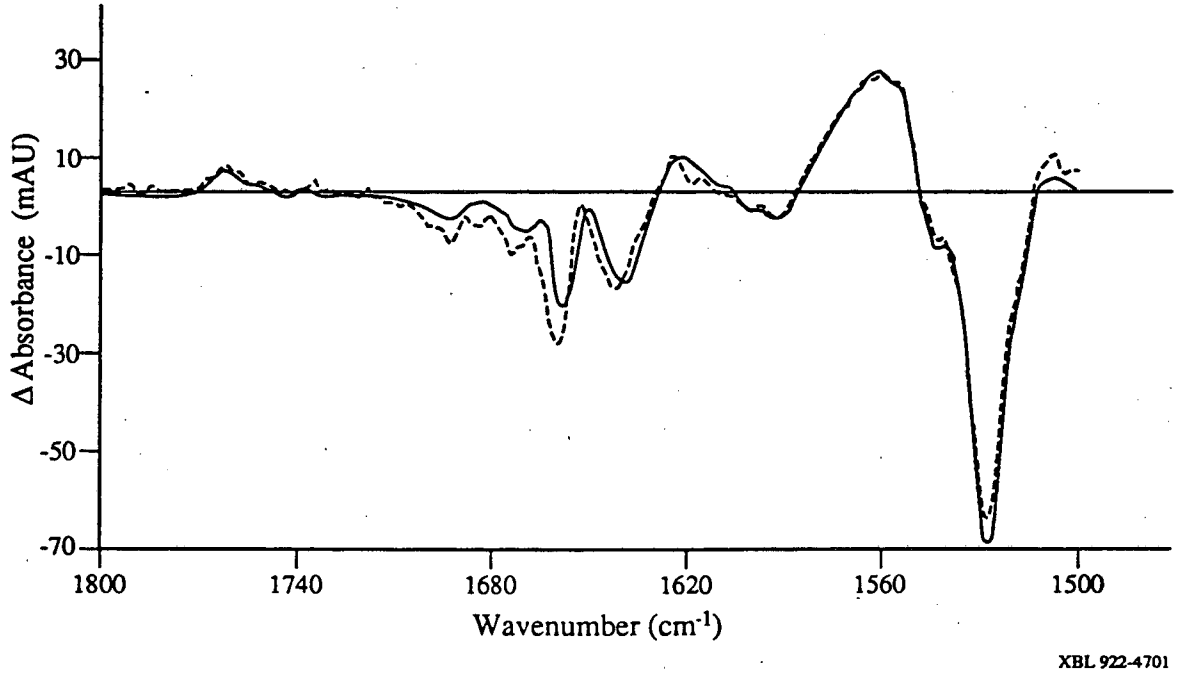
30
10
-10
-30
-50
-70
Δ Absorbance (mAU)
1800
1740
1680
1620
1560
1500
Wavenumber (cm-1)
XBL 922-4701

Figure 6.12 Discrete least-squares approximation of the 260 K, M - bR spectrum of glucose-embedded specimens to Ormos' first 260 K difference spectrum. The two spectra are superimposed with the glucose-embedded PM spectrum as a solid trace, and Ormos' difference spectrum as a dashed trace.

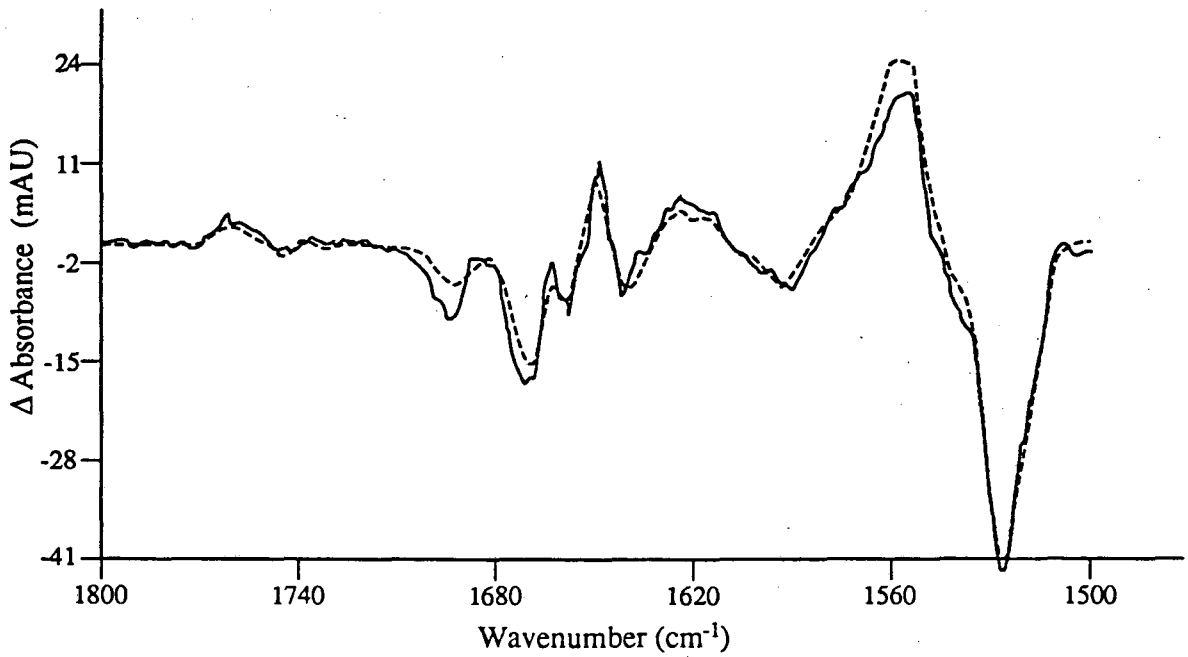
24
11
-2
-15
-28
-41
Δ Absorbance (mAU)
1800
1740
1680
1620
1560
1500
Wavenumber (cm-1)

XBL 922-4702

260 K spectra shows that in most aspects the glucose-embedded PM spectrum does not approximate the Ormos spectrum as well as the 240 K spectra approximate each other in the ethylenic region. The most noteworthy differences are, first, the deeper "well" at 1693 cm^{-1} and second, the decreased amplitude at 1555 cm^{-1} belonging to the glucose-embedded PM spectrum. A better approximation is obtained with other difference bands at 260 K. But, in no case is the fit strikingly good. As with the 240 K spectra superposition, the bands in the Amide I region show greater variation in peak amplitudes and are shifted slightly with respect to each other.

In the end, the reader must decide how closely the glucose-embedded PM spectra fit the spectra of Ormos (1991). A decision may depend on how one intends to use the results presented herein. Certainly, the spectra of glucose-embedded PM resemble those of Ormos recorded at both 240 K and 260 K. Thus, a confirmation of his results is provided. In particular, dramatic differences are confirmed in peak amplitudes of the conformational marker bands of the Amide I region, at the two temperatures. A likely scenario is that M_1 is trapped at 240 K, while M_2 is trapped at 260 K. But, are other intermediates present with the M substates? Can the differences noted between the glucose-embedded PM spectra and Ormos' spectra be interpreted in terms of Ormos' samples being "contaminated" by photocycle intermediates other than M? Such an interpretation is needed when discussing the reliability of conformational changes observed in M - bR difference Fourier maps made from glucose-embedded PM specimens.

Can one be confident that features observed in the difference Fourier maps of M_1 and M_2 represent factual structural differences between bR in the M states and quiescent bR? The answer to this question is, "yes". Because of the reported differences in the extent of conformational alterations upon M formation (Glaeser et al., 1986; Koch et al., 1991), it is not clear which M substate (or a mixture) was trapped in these two diffraction studies. My visible and FTIR spectroscopy results provide the key. The visible spectra show that 90 % or greater M can be trapped at low temperature. The implication being that one doesn't need to be concerned about other bR intermediates "contaminating" the difference Fourier maps, giving a smaller yield of M. The FTIR spectra show that M_1 can be trapped separately from M_2. Thus, one can be confident if the protocol for preparing specimens on EM grids and for isolating and trapping the M_1 and M_2 substates for electron diffraction studies is identical to the visible and FTIR protocols.

How Pure Are the M Substates?

Do the samples I used to record my FTIR difference spectra at 240 K and 260 K contain an appreciable amount of intermediates other than bR_{568} or M? According to the photocycle scheme presented by Varo and Lanyi (1991), the likely "contamination" would come from the L and N intermediates. Because the M_1 - M_2 step is irreversible, L would only contaminate the M_1 difference spectrum recorded at 240 K and N would only contaminate the M_2

difference spectrum recorded at 260 K, assuming that there is insufficient energy at 240 K for bR to overcome the barrier in the forward direction between M_1 and M_2.

There are two reasons for searching for the presence of L in my 240 K difference spectrum and for the presence of N in my 260 K difference spectrum. First, the values for the percent M formed were for measurements conducted 8 seconds after cessation of the actinic light (See Chapter 2, Methods.). However, the effective time resolution for my FTIR spectra is 15 seconds. The M-decay kinetics discussed in Chapter 4 indicate that the 7-second difference will not change the M concentration by much at 240 K. 96 % M remains 15 seconds after the actinic light has been terminated. But, at 260 K, M decay is significantly faster (Table 4.1). The M decay curve (Figure 4.2) gives a value of 83 % M at a time equal to 15 seconds after the light is terminated. As a result, the 260 K, M - bR difference spectrum may be perturbed by the presence of N. Second, both Rothschild and Lanyi have voiced a criticism (private communications) of the Ormos (1991) work. They believe that Ormos' 240 K sample may be contaminated with a significant concentration of L (even in the earliest-recorded spectrum). Furthermore, they claim that N may be a major contaminant in Ormos' 260 K, M_2 - bR samples. These criticisms are relevant to a discussion of my M - bR difference spectra, since I have used Ormos' work to guide my own. It is incumbent on me to determine how "pure" my M - bR spectra are.

FTIR difference spectra of L - bR have been published (Engelhard et al., 1985; Roepe et al., 1987; Gerwert et al., 1989; Gerwert et al., 1990). A number of difference bands in these spectra are present only when L is trapped. By comparing the published spectra of L - bR with Ormos' and my own 240 K, M - bR spectra, I am able to determine if the characteristic L-bands are present. The most notable band in the L - bR spectra is found at 1739 cm^{-1}; it has a strong, negative peak. This band has been tentatively assigned to the Asp-115 residue (Braiman et al., 1988; Gerwert et al., 1989). Small positive peaks border this band at 1748 cm^{-1}, assigned to Asp-96 (Gerwert et al., 1989) and 1729 cm^{-1}. It is uncertain if the 1729 cm^{-1}, 1739 cm^{-1} pair can be assigned to Asp-115 alone or if there is another carboxylic acid group contributing to these difference bands (Gerwert et al., 1989; Engelhard et al., 1985; Eisenstein et al., 1987). The bands at 1748, 1739 and 1729 cm^{-1} may represent changes in the protonation states of aspartic acid residues (Engelhard et al., 1985; Eisenstein et al., 1987; Braiman et al., 1991), or just as likely, represent changes in hydrogen bonding character. L also has a positive peak at 1540 cm^{-1}, which shows up as a shoulder on the strongly absorbing ethylenic positive-negative pair. In addition, L possesses strong positive peaks at 1190 cm^{-1} and 1400 cm^{-1}. But, since the N intermediate has bands at 1535 cm^{-1}, 1186 cm^{-1} and 1396 cm^{-1} (Pfefferle et al., 1991; Bousche et al., 1991), close to the L-bands, it is best not to use these three bands as L-marker bands.

My 240 K, M - bR spectra (See Figure 6.2), and those of Ormos, do not give any evidence that the L intermediate is present. Instead of a strong, negative peak centered at 1739 cm^{-1}, the spectra shown by Ormos have a small positive peak at 1738 cm^{-1} (Ormos, 1991; see Figure 1.). The 1738 cm^{-1} band has been assigned to Asp-212 (Braiman et al., 1988). In my 240 K spectra, the absence of a negative 1739 cm^{-1} peak is conspicuous; if there is a positive 1738 cm^{-1} peak, it is buried in the noise. Moreover, the presence of a strong, positive 1762 cm^{-1} band, which is used to characterize M (Pfefferle et al., 1991) speaks strongly that M is trapped with little if any L present.

FTIR difference spectra of N - bR have also been published (Pfefferle et al., 1991; Bousche et al., 1991). The bands that characterize N are positive peaks at 1755, 1535, 1396, 1303 and 1186 cm^{-1} and a negative peak at 1742 cm^{-1}. For comparison purposes, the positive 1755 cm^{-1} and negative 1742 cm^{-1} peaks are best, since they are distinct from the L and M difference bands in that wavenumber region. The 1755 cm^{-1} and 1742 cm^{-1} bands have been unequivocally assigned to Asp-85 and Asp-96, respectively, and represent protonation/deprotonation differences between bR_{568} and N. The 1535 cm^{-1} peak could also be used as an N-marker peak even though the amplitude of this peak is so much greater in the Pfefferle et al. (1991; see Figure 6.) results than that in the Bousche et al. (1991; see Figure 3.) results.

While there is a significant contribution to Ormos' (1991) 260 K, M - bR spectra from the N intermediate (becoming more pronounced as time lapses), there is much less N contribution in my 260 K, M - bR spectra (See Figure 6.3), as judged by the presence (or absence) of N-marker peaks. At the earliest time recorded, Ormos' 260 K difference spectra exhibits a 1758 cm^{-1} positive peak and a 1742 cm^{-1} negative peak. The 1758 cm^{-1} peak lies between the 1762 cm^{-1} M-peak and the 1755 cm^{-1} N-peak and shifts to 1755 cm^{-1} with time. The 1742 cm^{-1} peak has a smaller relative amplitude than that reported by either Bousche et al. (1991) or Pfefferle et al. (1991) under conditions where the percent N is enriched at the expense of M. The amplitude of the 1742 cm^{-1} band is as great as that of the 1755 cm^{-1} band in the published N - bR spectra. In Ormos' earliest 260 K, M - bR spectrum, the Δabsorbance at 1758 cm^{-1} is 2.3 mAU and at 1742 cm^{-1} is -1.5 mAU. A case can be made that Ormos' earliest 260 K difference spectrum has more N than M, as judged by two standards: 1) The 1758 cm^{-1} peak is closer to the N-marker peak position, at 1755 cm^{-1}, than it is to the M-marker peak position, at 1762 cm^{-1}. 2) The 1742 cm^{-1} peak amplitude is more than half that of the 1758 cm^{-1} peak. In contrast to the spectra shown by Ormos, my 260 K, M - bR difference spectra exhibit a 1762 cm^{-1} peak, a very small 1742 cm^{-1} peak and no 1535 cm^{-1} peak, although there is a shoulder at this position. I conclude that M predominates in the 260 K, M - bR spectra recorded with samples of PM embedded in glucose. This is corroborated by the kinetic studies of M decay which show that at least 83 % M remains 15 seconds after the actinic light source has been turned off.

Why don't samples of PM embedded in glucose and photoexcited at 260 K form the N intermediate as readily as do the no-glucose PM samples of Ormos (1991)? Two possibilities are worth considering. First, my thin films of glucose-embedded PM may not be as hydrated as the thin films of PM used by Ormos. It is recognized that M stability increases as the hydration level in thin films of PM decreases (Korenstein & Hess, 1977b; Varo & Lanyi, 1991). Pfefferle et al. (1991) report that when thin films of PM, with a water content of 50 % by weight (pH = 10) are illuminated with actinic light at 230 K, no N is formed; the sample is effectively trapped in the M state at close to 100 % occupancy. Only with well-hydrated (70 % water by weight) PM specimens do they obtain 80 % or greater concentration of N at 274 K. Ormos (1991) does not report the water content of his PM specimens, but claims that they are "fully hydrated". My specimens of PM embedded in glucose have a water content of 34 % by weight (Table 3.1). Relative to the Pfefferle et al. (1991) specimens, and most likely those of Ormos, my specimens are dehydrated; thus, my specimens stabilize M at the expense of N. Second, glucose embedment may affect N formation. Glucose embedment offers a more rigid environment surrounding the PM than does water. Perhaps, conformational changes in the M_2 - N step are inhibited by the surrounding medium. One, or both, of the two effects envisioned here may cause the M_2 - N reaction to be slowed at 260 K.

Extended C - T Model

In view of the results presented in this dissertation, with guidance from published results using molecular vibrational spectroscopy, I propose an extension of the C - T Model (Fodor et al., 1988) to explain how changes in bR's retinal induce changes in bR's protein conformation and vice versa. In proposing to extend the C - T Model, I am guided by the principle of mutual induced fit (Koshland, 1973). Both ligand and protein must change conformation in order to "handshake". At equilibrium, the protein conformation will always be optimized for the particular ligand that it binds. This does not mean that a protein can only change its conformation when going from one equilibrium state to another. There are allowed to be precursor conformations on the way to equilibrium. In this discussion, bound retinal is the ligand.

The transition from the T protein conformation to the C protein conformation is postulated to occur during either the L - M reaction (Fodor et al., 1988) or during the M_1 - M_2 reaction (Mathies et al., 1991; Ormos, 1991). However, it can be argued that the T - C transition occurs earlier in the photocycle, as early as the K - L reaction. When bR_{568} absorbs a photon, the retinal chromophore is isomerized from an all-trans configuration to a 13-cis configuration; the primary photoproduct being the K (or J) intermediate. Because of the new retinal configuration, the interaction between protein, still in the T state, and retinal ligand is strained, i.e. no longer optimal. Steric strain in the chromophore

binding pocket, as indicated by a twisted chromophore, has been observed in the J and K states (Braiman & Mathies, 1982; Earnest et al., 1986; Fodor et al., 1988; Fahmy et al., 1991). By measuring the Stokes HOOP intensities as a function of time, Doig et al. (1991) provide evidence that steric strain occurs in the J and KL species (but is reduced in the K state). It is unclear, however, if the KL state should be classified as a separate photointermediate, or as a mixture of the K and L intermediates. For this discussion, I use the photocycle scheme presented in Chapter 1, with the understanding that the reader may substitute the KL nomenclature for K.

The C state of bR must have a protein conformation that exerts minimal steric distortion on the cis retinal chromophore. In the jargon of mutual induced fit, the "handshake" is complete. A completed handshake may occur upon formation of the L intermediate, or just as likely, not until the M_1 intermediate has formed. Steric distortions in the chromophore binding pocket are reduced upon completion of the K - L reaction (Engelhard et al., 1985; Smith et al., 1985; Eisenstein et al., 1987). Recently published FTIR difference spectra, however, indicate that the steric strain on the retinal is not completely relaxed in the L state (Fahmy et al., 1991). As judged by the lowered intensity of the HOOP bands in both FTIR and resonance Raman, M - bR spectra, relaxation of the steric strain is complete upon M formation (Earnest et al., 1986; Braiman & Mathies, 1980). Based on steric strain evidence, I propose that the C conformation is not reached in the bR photocycle until the appearance of the M intermediate.

Difference FTIR spectra of L - bR give evidence that a significant protein conformational change has occured between the bR_{568} and L states, as judged by difference bands in the Amide I and II regions (Engelhard et al., 1985; Roepe et al., 1987; Gerwert et al., 1989; Gerwert et al., 1990; Fahmy et al., 1991). L - bR spectra exhibit a negative 1660 cm^{-1} peak and a strong, positive 1554 cm^{-1} peak. The 1554 cm^{-1} peak has been assigned as an Amide II band that monitors peptide backbone alterations. The magnitude of protein conformational change between L and bR and between M_1 and bR might be similar. Even though the 1660 cm^{-1} peak has a smaller relative amplitude (comparison is made with the ethylenic pair) in the L - bR spectra (Engelhard et al., 1985; Roepe et al., 1987; Gerwert et al., 1989; Gerwert et al., 1990) than in the M_1 - bR spectra (Ormos, 1991), the 1554 cm^{-1} peak appears to have a larger relative amplitude. This peak overlaps with the 1564 cm^{-1} ethylenic band in the M_1 - bR spectra, making it difficult to determine the peak amplitude, yet is distinct in the L - bR spectra.

These results provide the impetus for extending the C - T Model to include the conformational change observed upon L formation. Because the retinal is cis-distorted in K (Doig et al., 1991), but is cis-planar in L, there must be some local rearrangement of amino acid residues surrounding the chromophore binding pocket that alleviate the steric strain found in K. This means that the protein must relax between K and L so as to have a shape-of-the-binding-pocket in L which is a better fit for the cis-retinal than is the case

in K. This change in protein shape should rightly be called the T - C_1^+ conformational transition, since the protein is required to accommodate a change in the ligand, i.e. the protonated, 13-cis retinal. Doig et al. (1991) have postulated a retinal-induced, protein conformational change occuring between the K (KL) and L states.

The completely relaxed C state may not occur until the appearance of M_1 or even M_2. As bR progresses from L to M_1, another conformational change occurs. This change is manifest by the increased amplitude of the 1660 cm^{-1} peak and the decrease of the 1556 cm^{-1} peak in M_1 - bR spectra, relative to the same bands in the L - bR spectra (Roepe et al., 1987). During the L - M_1 transition, the Schiff base is deprotonated. This means that a new ligand is formed, i.e. 13-cis, deprotonated Schiff base chromophore; it is not the same ligand as the one bound in the L state. In this extended C - T Model, the deprotonation of the Schiff base is accompanied by movements of the peptide chain, producing the conformation C_1^0, formed in an integral step with deprotonation. This conformation is prerequisite to the conformational change occuring in the next step, M_1 - M_2. I call this conformation, C_2^0, representing an (irreversible) lower-energy state that is accessible, once the ligand is deprotonated, 13-cis retinal. The M_1 - M_2 conformation change is documented in this work and by Ormos (1991). Once again, the change in ligand structure has induced a change in protein fit. For most of the conformational changes detected by absorption spectroscopy (e.g. L and N states) the relevance to a functional role remains unclear. It should be

emphasized, however, that the C_1^0 to C_2^0 transition is a functionally important conformational change in that it controls the "reprotonation switch" (Fodor et al., 1988) allowing the regeneration of bR_{568}.

The succession of protein conformational states leading to the "reprotonation switch" must be reversed, but not necessarily in the same manner. The Schiff base is reprotonated in the M_2 - N reaction. Even though the chromophore is identical in L and N (Fodor et al., 1988; Ames & Mathies, 1990) and their visible absorption maxima are found at the same wavelength, i.e. 550 nm, the N intermediate must have a protein conformation different from L. Ames and Mathies (1990) report that L and N differ in the frequencies and intensities of certain resonance Raman bands, namely the methyl rock, the C-C and C=C stretching vibrations. These differences must be caused by different protein environments in L and N. In order to reset the pump, the protonated Schiff base needs to be near Asp-85. This requires a reversion to the T protein conformation, which happens concurrent with retinal reisomerization to the all-trans configuration during the N - O reaction. The protein in O has not yet relaxed to the T conformation characteristic of bR_{568} because the retinal is distorted (Smith et al., 1983). Complete relaxation to the initial T conformation occurs in the O - bR_{568} reaction. In this manner, the ion pumping apparatus and the chromophore-reset steps are coupled.

By the preceding arguments, bR should assume seven structurally distinct protein conformations in the course of its photocycle. These are T, T_1^s, C_1^+, C_1^0, C_2^0, C_2^+ and T_2^s where the *s* superscript indicates steric strain on the retinal and the subscripts differentiate between various C or T states. The salient features of the extended C - T Model, as discussed in the previous paragraphs, are summarized in the mini-table below. As per preceding arguments, the T to C transition may occur during the K to L reaction, or during the L to M_1 reaction; the former is listed in the table. A more detailed account of the mechanism of ion transport in bR, including a discussion of how the C - T Model elucidates the characterization of the reprotonation switch, as well as mediates the Schiff base connectivity to key residues in the chromophore binding pocket are included in Fodor et al. (1988) and Mathies et al. (1991).

"Extended C - T Model"

State	bR_{568}	K	L	M_1	M_2	N	O
Retinal	$trans^{(+)}$	$cis^{*(+)}$	$cis^{(+)}$	$cis^{(0)}$	$cis^{(0)}$	$cis^{(+)}$	$trans^{*(+)}$
Protein	T	T_1^s	C_1^+	C_1^0	C_2^0	C_2^+	T_2^s

The superscript on the retinal isomerization states indicates the protonation state of the Schiff base, and the asterisk indicates steric strain on the chromophore.

REFERENCES

Alshuth, T., Hildebrandt, P. & Stockburger, M. (1984) Structural and kinetic studies of bacteriorhodopsin by resonance Raman spectroscopy. *Spectroscopy of Biological Molecules* (ed. by C. Sandorfy & T. Theophanides), pp. 329-346. D. Reidel.

Ames, J., Fodor, S., Gebhard, R., Raap, J.,van den Berg, E., Lugtenburg, J. & Mathies, R. (1989) Bacteriorhodopsin's M412 intermediate contains a 13-cis, 14-s-trans, 15-anti-retinal Schiff base chromophore. *Biochemistry* 28, 3681-3687.

Ames, J. & Mathies, R. (1990) The role of back-reactions and proton uptake during the N-O Transition in bacteriorhodopsin's photocycle: A kinetic resonance Raman study. *Biochemistry* 29, 7181-7190.

Bagley, K., Balogh-Nair, V., Croteau, A., Dollinger, T., Ebrey, T., Eisenstein, L, Hong, M., Nakanishi, K. & Vittitow, J. (1985) Fourier-transform infrared difference spectroscopy of rhodopsin and its photoproducts at low temperature. *Biochemistry* 24, 6055-6071.

Bagley, K., Dollinger, G., Eisenstein, L., Singh, A. & Zimanyi, L. (1982) Fourier transform infrared difference spectroscopy of bacteriorhodopsin and its photoproducts. *Proc. Nat. Acad. Sci., U.S.A.* 79, 4972-4976.

Becher, B., Tokunaga, F. & Ebrey, T. (1978) Ultraviolet and visible absorption spectra of the purple membrane protein and the photocycle intermediates. *Biochemistry* 17, 2293-2300.

Bell, R. (1972) *Introductory Fourier Transform Spectroscopy.* Academic Press, London.

Birge, R. (1990) Nature of the primary photochemical events in rhodopsin and bacteriorhodopsin. *Biochimica et Biophysica Acta* 1016, 293-327.

Bousche, O., Braiman, M., He, Y.-W., Marti, T., Khorana, G. & Rothschild, K. (1991) Vibrational spectroscopy of bacteriorhodopsin mutants. *J. Biological Chemistry* 266, 11063-11067.

Braiman, M., Ahl, P. & Rothschild, K. (1987) Millisecond Fourier-transform infrared difference spectra of bacteriorhodopsin's M412 photoproduct. *Proc. Nat. Acad. Sci., U.S.A.* 84, 5221-5225.

Braiman, M., Bousche, O. & Rothschild, K. (1991) Protein dynamics in the bacteriorhodopsin photocycle: submillisecond Fourier transform infrared spectra of the L, M, and N photointermediates. *Proc. Nat. Acad. Sci., U.S.A.* 88, 2388-2392.

Braiman, M. & Mathies, R. (1980) Resonance Raman evidence for an all-trans to 13-cis isomerization in the proton-pumping cycle of bacteriorhodopsin. *Biochemistry* 19, 5421-5428.

Braiman, M. & Mathies, R. (1982) Resonance Raman spectra of bacteriorhodopsin's primary photoproduct: evidence for a distorted 13-cis retinal chromophore. *Proc. Nat. Acad. Sci., U.S.A.* 79, 403-407.

Braiman, M., Mogi, T., Marti, T., Stern, L., Khorana, G. & Rothschild, K. (1988) Vibrational spectroscopy of bacteriorhodopsin mutants: light-driven proton transport involves protonation changes of aspartic acid residues 85, 96, and 212. *Biochemistry* 27, 8516-8520.

Braiman, M. & Rothschild, K. (1988) Fourier transform infrared techniques for probing membrane protein structure. *Ann. Rev. Biophys. Biophys. Chem.* 17, 541-570.

Bray, G. & White K. (1966) *Kinetics and Thermodynamics in Biochemistry*. Second Ed. New York, NY, Academic Press.

Burden, R. & Faires, D. (1985) *Numerical Analysis*, Third Ed., PWS Publishers, Boston, MA.

Cao, Y., Varo, G., Chang, M., Ni, B., Needleman, R. & Lanyi, J. (1991) Water is required for proton transfer from aspartate 96 to the bacteriorhodopsin Schiff base. *Biochemistry* 30, 10972-10979.

Ceska, T. & Henderson, R. (1990) Analysis of high-resolution electron diffraction patterns from purple membrane labelled with heavy-atoms. *J. Mol. Biol.* 213, 539-560.

Curry, B., Palings, I., Pardoen, J., Lugtenberg, J. & Mathies, R. (1985) Vibrational analysis of retinal isomers. *Adv. Infrared Raman Spectroscopy* 12, 115-124.

Dencher, N., Dresselhaus, G., Zaccai, G. & Buldt, G. (1989) Structural changes in bacteriorhodopsin during proton translocation revealed by neutron diffraction. *Proc. Nat. Acad. Sci., U.S.A.* 86, 7876-7879.

Der, A., Toth-Boconadi, R. & Keszthelyi, L. (1989) Bacteriorhodopsin as a possible chloride pump. *FEBS Letters* 259, 24-26.

Doig, S., Reid, P. & Mathies, R. (1991) Picosecond time-resolved resonance Raman spectroscopy of bacteriorhodopsin's J, K, and KL intermediates. *J. Physical Chemistry* 95, 6372-6379.

Dollinger, G., Eisenstein, L., Lin, S., Nakanishi, K. & Termini, J. (1986) Bacteriorhodopsin: Fourier transform infrared methods for studies of protonation of carboxyl groups. *Biochemistry* 25, 6524-6533.

Dunn, R., McCoy, J., Simsek, M., Majumdar, A., Chang, S., RajBhandary, U. & Khorana, G. (1981) The bacteriorhodopsin gene. *Proc. Nat. Acad. Sci., U.S.A.* 78, 6744-6748.

Earnest, T. (1987) Fourier transform infrared and resonance Raman spectroscopic studies of bacteriorhodopsin. Ph. D. dissertation, Boston University, Boston, MA. 1-193

Earnest, T., Herzfeld, J. & Rothschild, K. (1990) Polarized Fourier transform infrared spectroscopy of bacteriorhodopsin. *Biophysical J.* 58, 1539-1546.

Earnest, T., Roepe, P., Braiman, M., Gillespie, J. & Rothschild, K. (1986) Orientation of the bacteriorhodopsin chromophore probed by polarized Fourier transform infrared difference spectroscopy. *Biochemistry* 25, 7793-7798.

Ebrey, T. & Nakanishi, K., eds. (1987) *Biophysical studies of retinal proteins.* Univ. of Illinois Press, Urbana, IL.

Eisenstein, L., Lin, S. & Dollinger, G. (1987) FTIR difference studies on apoproteins. Protonation states of aspartic and glutamic acid residues during the photocycle of bacteriorhodopsin. *J. American Chemical Society* 109, 6860-6862.

Engelhard, M., Gerwert, K., Hess, B., Kreutz, W. & Siebert, F. (1985) Light-driven protonation changes of internal aspartic acids of bacteriorhodopsin: An investigation by static and time-resolved infrared difference spectroscopy using [4-^{13}C]aspartic acid labeled purple membrane. *Biochemistry* 24, 400-407.

Engelman, D., Henderson, R., McLachlan, A. & Wallace, B. (1980) Path of the polypeptide in bacteriorhodopsin. *Proc. Nat. Acad. Sci., U.S.A.* 77, 2023-2027.

Fahmy, K., Siebert, F. & Tavan, P. (1991) Structural investigation of bacteriorhodopsin and some of its photoproducts by polarized

Fourier transform infrared spectroscopic methods-difference spectroscopy and photoselection. *Biophys. J.* 60, 989-1001.

Fodor, S., Ames, J., Gebhard, R., van den Berg, E., Stoeckenius, W., Lugtenberg, J. & Mathies, R. (1988) Chromophore structure in bacteriorhodopsin's N intermediate: Implications for the proton-pumping mechanism. *Biochemistry* 27, 7097-7101.

Gerwert, K., Hess, B. & Engelhard, M. (1990) Proline residues undergo structural changes during proton pumping in bacteriorhodopsin. *FEBS Letters* 261, 449-454.

Gerwert, K., Hess, B., Soppa, J. & Oesterhelt, D. (1989) Role of aspartate-96 in proton translocation by bacteriorhodopsin. *Proc. Nat. Acad. Sci., U.S.A.* 86, 4943-4947.

Gerwert, K. & Siebert, F. (1986) Evidence for light-induced 13-cis, 14-s-trans isomerization in bacteriorhodopsin obtained by FTIR difference spectroscopy using isotopically labelled retinals. *EMBO J.* 45, 805-811.

Gerwert, K., Souvignier, G. & Hess, B. (1990) Simultaneous monitoring of light-induced changes in protein side-group protonation, chromophore isomerization, and backbone motion of bacteriorhodopsin by time-resolved Fourier-transform infrared spectroscopy. *Proc. Nat. Acad. Sci., U.S.A.* 87, 9774-9778.

Glaeser, R., Baldwin, J., Ceska, T. & Henderson, R. (1986) Electron diffraction analysis of the M412 intermediate of bacteriorhodopsin. *Biophys. J.* 50, 913-920.

Glaeser, R., Downing, K. & Jap, B. (1991) What spectroscopy can still tell us about the secondary structure of bacteriorhodopsin. *Biophysical J.* 59, 934-938.

Glaeser, R. & Jap, B. (1984) The "Born energy" problem in bacteriorhodopsin. *Biophysical J.* 45, 95-97.

Goodman, J. (1968) *Introduction to Fourier Optics,* McGraw-Hill, New York, NY.

Griffiths, P. (1975) *Chemical Infrared Fourier Transform Spectroscopy.* John Wiley and Sons, New York, NY.

Harbison, G., Smith, S., Pardoen, J., Courtin, J., Lugtenburg, J., Herzfeld, J., Mathies, R. & Griffin, R. (1985) Solid-state 13C NMR detection of a perturbed 6-s-trans chromophore in bacteriorhodopsin. *Biochemistry* 24, 6955-6962.

Henderson, R. (1977) The purple membrane from Halobacterium halobium. *Annual Reviews of Biophysics and Bioengineering* 6, 87-109.

Henderson, R., Baldwin, J., Ceska, T., Zemlin, F., Beckmann, E. & Downing, K. (1990) Model for the structure of bacteriorhodopsin based on high-resolution electron cryo-microscopy. *J. Molecular Biology* 213, 899-929.

Henderson, R. & Unwin, N. (1975) Three-dimensional model of purple membrane obtained by electron microscopy. *Nature (London)* 257, 28-32.

Heyn, M., Westerhausen, J., Wallet, I. & Seiff, F. (1988) High-sensitivity neutron diffraction of membranes: location of the Schiff base end of the chromophore of bacteriorhodopsin. *Proc. Nat. Acad. Sci., U.S.A.* 85, 2146-2150.

Holz, M., Drachev, L., Mogi, T., Otto, H., Kaulen, A., Heyn, M., Skulachev, V. & Khorana, G. (1989) Replacement of aspartic acid-96 by asparagine in bacteriorhodopsin slows both the decay of the M intermediate and the associated proton movement. *Proc. Nat. Acad. Sci., U.S.A.* 86, 2167-2171.

Huang, K., Radhakrishnan, R., Bayley, H. & Khorana, G. (1982) Orientation of retinal in bacteriorhodopsin as studied by cross-linking using a photosensitive analog of retinal. *J. Biol. Chem.* 257, 13616-13620.

Hurley, J., Becher, B. & Ebrey, T. (1978) More evidence that light isomerises the chromophore of purple membrane protein. *Nature (London)* 272, 82.

Jap, B., Downing, K. & Walian, P. (1990) Structure of PhoE porin in projection at 3.5 Å resolution. *J. Structural Biol.* 103, 1-7.

Kalisky, O., Ottolenghi, M., Honig, B. & Korenstein, R. (1981) Environmental effects on formation and photoreaction of the M412 photoproduct of bacteriorhodopsin: implications for the mechanism of proton pumping. *Biochemistry* 20, 649-655.

Khorana, G. (1988) Bacteriorhodopsin, a membrane protein that uses light to translocate protons. *J. Biological Chemistry* 263, 7439-7442.

Khorana, G., Gerber, G., Herlihy, W., Grant, C., Anderess, R., Nihel, J. & Bieman, K. (1979) Amino acid sequence of bacteriorhodopsin. *Proc. Nat. Acad. Sci., U.S.A.* 5046-5049.

Koch, M., Dencher, N., Oesterhelt, D., Plohn, H., Rapp, G. & Buldt, G. (1991) Time-resolved X-ray diffraction study of structural changes associated with the photocycle of bacteriorhodopsin. *EMBO J.* 10, 521-526.

Korenstein, R. & Hess, B. (1977a) Hydration effects on cis-trans isomerization of bacteriorhodopsin. *FEBS Letters* 82, 7-11.

Korenstein, R. & Hess, B. (1977b) Hydration effects on the photocycle of bacteriorhodopsin in thin layers of purple membrane. *Nature (London)* 270, 184-186.

Koshland, D. (1973) Protein shape and biological control. *Scientific American* 229, 52-64.

Krimm, S. & Dwivedi, A. (1982) Infrared spectrum of the purple membrane: clue to a proton conduction mechanism? *Science* 216, 407-408.

Kühlbrandt, W. & Wang, D. (1991) Three-dimensional structure of plant light-harvesting complex determined by electron crystallography. *Nature (London)* 350, 130-134.

Lazarev, Y. & Terpugov, E. (1980) Effect of water on the structure of bacteriorhodopsin and photochemical processes in purple membrane. *Biochim. et Biophys. Acta* 590, 324-338.

Lewis, A., Spoonhower, R., Bogomolni, R., Lozier, R. & Stoeckenius (1974) Tunable laser resonance Raman spectroscopy of bacteriorhodopsin. *Proc. Nat. Acad. Sci., U.S.A.* 71, 4462-4466.

Lin, S. & Mathies, R. (1989) Orientation of the protonated retinal Schiff base group in bacteriorhodopsin from absorption linear dichroism. *Biophysical J.* 56, 653-660.

Lozier, R., Bogomolni, R. & Stoeckenius, W. (1975) Bacteriorhodopsin: a light-driven proton pump in Halobacterium halobium. *Biophysical J.* 15, 955-959.

Lozier, R., Niederberger, W., Bogomolni, R., Hwang, S. & Stoeckenius, W. (1976) Kinetics and stoichiometry of light-induced proton release and uptake from purple membrane fragments, Halobacterium halobium cell envelopes, and phospholipid vesicles containing oriented purple membrane. *Biochim. Biophys. Acta* 440, 545-556.

Lugtenburg, J., Muradin-Szweykowska, M., Heeremans, C., Pardoen, J., Harbison, G., Herzfeld, J., Griffin, R., Smith, S. & Mathies, R. (1986) Mechanism for the opsin shift of retinal's absorption in bacteriorhodopsin. *J. American Chemical Society* 108, 3104-3105.

Mathies, R., Cruz, B., Pollard, W. & Shank C. (1988) Direct observation of the femtosecond excited-state cis-trans isomerization in bacteriorhodopsin. *Science* 240, 777-779.

Mathies, R., Lin, S., Ames, J. & Pollard, T. (1991) From femtoseconds to biology: mechanism of bacteriorhodopsin's light-driven proton pump. *Annual Reviews of Biophysics and Biophysical Chemistry* 20, 491-518.

Mathies, R., Smith, S. & Palings, I. (1987) *Biological Applications of Raman Spectroscopy.* Wiley, New York, NY, pp. 59-108.

Mogi, T., Stern, L., Marti, T., Chao, B. & Khorana, G. (1988) Aspartic acid substitutions affect proton translocation by bacteriorhodopsin. *Proc. Nat. Acad. Sci., U.S.A.* 85, 4148-4152.

Motto, M., Sheves, M., Tsujimoto, K., Balogh-Nair, V. & Nakanishi, K. (1980) Opsin shifts in bovine rhodopsin and bacteriorhodopsin. Comparison of two external point-charge models. *J. American Chemical Society* 102, 7947-7949.

Muller, K., Butt, H., Bamberg, E., Fendler, K., Hess, B., Siebert, F. & Engelhard, M. (1991) The reaction cycle of bacteriorhodopsin: an analysis using visible absorption, photocurrent and infrared techniques. *Eur. Biophys. J.* 19, 241-251.

Nabedryk, E. & Breton, J. (1986) Polarized Fourier transform infrared (FTIR) difference spectroscopy of the M412 intermediate in the bacteriorhodopsin photocycle. *FEBS Letters* 202, 356-360.

Nakanishi, K., Balogh-Nair, V., Arnaboldi, M., Tsujimoto, K. & Honig, B. (1980) An external point-charge model for bacteriorhodopsin to account for its purple color. *J. American Chemical Society* 102, 7945-47.

Nakasako, M., Kataoka, M., Amemiya, Y. & Tokunaga, F. (1991) Crystallographic characterization by X-ray diffraction of the M-intermediate from the photo-cycle of bacteriorhodopsin at room temperature. *FEBS Letters* 292, 73-75.

Oesterhelt, D. & Stoeckenius, W. (1971) Rhodopsin-like protein from the purple membrane of Halobacterium halobium. *Nature New Biology* 233, 149-152.

Oesterhelt, D. & Stoeckenius, W. (1974) Isolation of the cell membrane of Halobacterium halobium and its fractionation into red and purple membrane. *Methods in Enzymology* (Ed. by S. Fleischer & L. Packer), Vol. 31, pp. 667-678. Academic Press, NY.

Organick, E. & Meissner, L. (1974) *Fortran IV*, Second Ed., Addison-Wesley, Reading, MA.

Ormos, P. (1991) Infrared spectroscopic demonstration of a conformational change in bacteriorhodopsin involved in proton pumping. *Proc. Nat. Acad. Sci., U.S.A.* 88, 473-477.

Ovchinnikov, Y., Abdulaev, N., Feigina, M., Kiselev, A. & Lobanov, N. (1979) The structural basis of the functioning of bacteriorhodopsin. *FEBS Letters* 100, 219-224.

Papadopoulos, G., Dencher, N., Zaccai, G. & Buldt, G. (1990) Water molecules and exchangeable hydrogen ions at the active centre of bacteriorhodopsin localized by neutron diffraction. *J. Molecular Biology* 214, 15-19.

Parker, F. (1983) *Applications of infrared, Raman, and resonance Raman spectroscopy in biochemistry.* Plenum Press, New York, NY.

Pfefferle, J., Maeda, A., Sasaki, J. & Yoshizawa, T. (1991) Fourier transform infrared study of the N intermediate of bacteriorhodopsin. *Biochemistry* 30, 6548-6556.

Pollard, T., Lee, S. & Mathies, R. (1990) Wave packet theory of dynamic absorption spectra in femtosecond pump-probe experiments. *J. Chemical Physics* 92, 4012-4029.

Roepe, P., Ahl, P., Das Gupta, S., Herzfeld, J. & Rothschild, K. (1987) Tyrosine and carboxyl protonation changes in the bacteriorhodopsin photocycle 1. M412 and L550 intermediates. *Biochemistry* 26, 6696-6707.

Rothschild, K. (1988) Infrared studies of bacteriorhodopsin. *Photochemistry and Photobiology* 47, 883-887.

Rothschild, K. & Clark, N. (1979a) Polarized infrared spectroscopy of oriented purple membrane. *Biophysical J.* 25, 473-488.

Rothschild, K. & Clark, N. (1979b) Anomalous amide infrared absorption of purple membrane. *Science* 204, 311-312.

Rothschild, K. & Marrero, H. (1982) Infrared evidence that the Schiff base of bacteriorhodopsin is protonated: bR570 and K intermediates. *Proc. Nat. Acad. Sci., U.S.A.* 79, 4045-4049.

Rothschild, K., Marrero, H., Braiman, M. & Mathies, R. (1984) Primary photochemistry of bacteriorhodopsin: comparison of Fourier transform infrared difference spectra with resonance Raman spectra. *Photochemistry and Photobiology* 40, 675-679.

Rothschild, K., Roepe, P., Ahl, P., Earnest, T., Bogomolni, R., Das Gupta, S., Mulliken, C. & Herzfeld, J. (1986) Evidence for a tyrosine protonation change during the primary phototransition of bacteriorhodopsin at low temperature. *Proc. Nat. Acad. Sci., U.S.A.* 83, 347-351.

Rothschild, K., Zagaeski, M. & Cantore, W. (1981) Conformational changes of bacteriorhodopsin detected by Fourier transform infrared difference spectroscopy. *Biochemical & Biophysical Research Communications* 103, 483-489.

Scherrer, P., Mathew, M., Sperling, W. & Stoeckenius, W. (1989) Retinal isomer ratio in dark-adapted purple membrane and bacteriorhodopsin monomers. *Biochemistry* 28, 829-834.

Sharkov, A., Pakulev, A., Chekalin, S. & Matveetz Y. (1985) Primary events in bacteriorhodopsin probed by subpicosecond spectroscopy. *Biochim. et Biophys. Acta* 808, 94-102.

Siebert, F., Mantele, W. & Kreutz, W. (1982) Evidence for the protonation of two internal carboxylic groups during the photocycle of bacteriorhodopsin. *FEBS Letters* 141, 82-87.

Smith, S., Myers, A., Mathies, R., Pardoen, J., Winkel, C., van den Berg, E., Lugtenberg, J. (1985) Vibrational analysis of the all-trans retinal protonated Schiff base. *Biophysical J.* 47, 653-664.

Smith, S., Pardoen, J., Mulder, P., Curry, B., Lugtenburg, J. & Mathies, R. (1983) Chromophore structure in bacteriorhodopsin's O640 photointermediate. *Biochemistry* 22, 6141-6148.

Stoeckenius, W. & Bogomolni, R. (1982) Bacteriorhodopsin and related pigments of Halobacteria. *Annual Review of Biochemistry* 52, 587-616.

Stoeckenius, W., Lozier, R. & Bogomolni, R. (1979) Bacteriorhodopsin and the purple membrane of Halobacteria. *Biochim. Biophys. Acta* 505, 215-278.

Subramaniam, S., Marti, T. & Khorana, G. (1990) Protonation state of Asp(Glu)-85 regulates the purple-to-blue transition in bacteriorhodopsin mutants Arg-82 - Ala and Asp-85 - Glu: the blue form is inactive in proton translocation. *Proc. Nat. Acad. Sci., U.S.A.* 87, 1013-1017.

Urey, H., Brickwedde F. & Murphy, G. (1932) A hydrogen isotope of mass 2 and its concentration. *The Physical Review* 40, 1-15.

Varo, G. & Keszthelyi, L. (1983) Photoelectric signals from dried oriented purple membranes of Halobacterium halobium. *Biophys. J.* 43, 47-51.

Varo, G. & Lanyi, J. (1990) Protonation and deprotonation of the M, N, and O intermediates during the bacteriorhodopsin photocycle. *Biochemistry* 29, 6858-6865.

Varo, G. & Lanyi, J. (1991) Distortions in the photocycle of bacteriorhodopsin at moderate dehydration. *Biophys. J.* 59, 313-322.

Xie, A., Nagle, J. & Lozier, R. (1987) Flash spectroscopy of purple membrane. *Biophysical J.* 51, 627-35.

Zimanyi, L., Keszthelyi, L. & Lanyi, J. (1989) Transient spectroscopy of bacterial rhodopsins with optical multichannel analyser. 1. Comparison of the photocycles of bacteriorhodopsin and halorhodopsin. *Biochemistry* 28, 5165-5172.

LAWRENCE BERKELEY LABORATORY
UNIVERSITY OF CALIFORNIA
TECHNICAL INFORMATION DEPARTMENT
BERKELEY, CALIFORNIA 94720